



AALBORG UNIVERSITY
DENMARK

Aalborg Universitet

Millimeter Wave Beam Management for 5G systems

A Link Level Study and Performance Enhancing Solutions

Fernandes, Filipa Santana da Silva

DOI (link to publication from Publisher):
[10.54337/aau528209643](https://doi.org/10.54337/aau528209643)

Publication date:
2023

Document Version
Publisher's PDF, also known as Version of record

[Link to publication from Aalborg University](#)

Citation for published version (APA):

Fernandes, F. S. D. S. (2023). *Millimeter Wave Beam Management for 5G systems: A Link Level Study and Performance Enhancing Solutions*. Aalborg Universitetsforlag. <https://doi.org/10.54337/aau528209643>

General rights

Copyright and moral rights for the publications made accessible in the public portal are retained by the authors and/or other copyright owners and it is a condition of accessing publications that users recognise and abide by the legal requirements associated with these rights.

- Users may download and print one copy of any publication from the public portal for the purpose of private study or research.
- You may not further distribute the material or use it for any profit-making activity or commercial gain
- You may freely distribute the URL identifying the publication in the public portal -

Take down policy

If you believe that this document breaches copyright please contact us at vbn@aub.aau.dk providing details, and we will remove access to the work immediately and investigate your claim.

MILLIMETER WAVE BEAM MANAGEMENT FOR 5G SYSTEMS

A LINK LEVEL STUDY AND PERFORMANCE
ENHANCING SOLUTIONS

BY
FILIPA SANTANA DA SILVA FERNANDES

DISSERTATION SUBMITTED 2023



AALBORG UNIVERSITY
DENMARK

Millimeter Wave Beam Management for 5G systems

A Link Level Study and Performance Enhancing Solutions

Ph.D. Dissertation
Filipa Santana da Silva Fernandes

Aalborg University
Department of Electronic Systems
Fredrik Bajers Vej 7B
DK-9220 Aalborg

Dissertation submitted: February 2023

PhD supervisor: Assoc. Prof. Carles Navarro Manchón
Aalborg University

Assistant PhD supervisors: Dr. Christian Rom
Nokia Aalborg
Head of Device Standardization Research Johannes Harrebek
Nokia Aalborg

PhD committee: Associate Professor Ming Shen (chairman)
Aalborg University, Denmark
Associate Professor Olga Muñoz Medina
Universitat Politècnica de Catalunya, Spain
Senior Research Engineer Luca Rose
Nokia Bell-Labs, France

PhD Series: Technical Faculty of IT and Design, Aalborg University

Department: Department of Electronic Systems

ISSN (online): 2446-1628

ISBN (online): 978-87-7573-749-9

Published by:
Aalborg University Press
Kroghstræde 3
DK – 9220 Aalborg Ø
Phone: +45 99407140
aauf@forlag.aau.dk
forlag.aau.dk

© Copyright: Filipa Santana da Silva Fernandes, except where otherwise stated.

Printed in Denmark by Stibo Complete, 2023

Curriculum Vitae

Filipa Santana da Silva Fernandes



Filipa Santana da Silva Fernandes received her B.Sc. and M.Sc. degrees in electrical and computer engineering from Instituto Superior Técnico (IST), University of Lisbon, Lisbon, Portugal, in 2016 and 2019, respectively. She is currently pursuing a Ph.D. degree in the Wireless Communication Networks section at Aalborg University in collaboration with Nokia at the Aalborg, Denmark office. Her research interests include beamforming solutions for beam management and user blockage modelling in handheld devices at mmWave frequencies.

Abstract

5G cellular networks rely on millimeter wave (mmWave)'s large spectrum availability to sustain data-hungry applications. 5G New Radio (NR) system operations have been enabled and optimized between 24.25 GHz and 71 GHz, while higher bands in the spectrum are already being explored for future releases. Unlocking mmWave's potential requires highly directional links to counteract its challenging propagation conditions, creating the beam alignment issue that motivates the current 3rd Generation Partnership Project (3GPP) beam management procedure. However, the constant emergence of new use cases, services and form factor designs may challenge this procedure's capabilities, especially when migrating to higher frequencies.

This thesis takes a critical look at the existing beam management framework to increase its ability to support the evermore stringent usage scenarios of 5G mmWave cellular systems. A limitation assessment is carried out by evaluating the link-level performance of beam management under operational conditions such as intra-cell mobility, propagation environment, beamforming architecture, device rotation and mmWave user hand blockage. Results reveal that mobility, device rotation and large angular spread channels are detrimental to beam alignment: beam measurements obtained through the current procedure can quickly become outdated in dynamic scenarios, leading to erroneous beam selection and performance degradation. Moreover, user blockage is shown to be a largely neglected hindrance to beam management, capable of compromising the device's original beam shape and further degrading performance. The severity of this effect is dependent on aspects such as hand grip type, antenna placement and device orientation, which are not captured by the current 3GPP user blockage model.

In addition, two different approaches are proposed to address the outdated measurement challenge. While one targets overhead and latency reduction of the procedure, minimizing the likelihood of outdated beam information, the other explores the outdated measurements in a data-driven solution to find the best beam pair. Both solutions offer an improvement of beam management performance with easy integration to the current NR standard.

Resumé

5G-mobilnetværk udnytter den store spektrum tilgængelighed ved millimeterbølge frekvenser for understøttelse af data tunge applikationer. 5G New Radio (NR) systemdrift er blevet optimeret mellem 24.25 GHz og 71 GHz, alt imens højere frekvensbånd i spektret bliver analyseret for fremtidige 3GPP opdateringer. Det kræver stærkt retningsbestemte signaler for at modvirke de udfordrende udbredelsesforhold og frigøre det fulde millimeterbølge potentiale, hvilket skaber det antennestråle justeringsproblem, der motiverer den nuværende 3rd Generation Partnership Project (3GPP) antennestråle håndteringsprocedure. Den konstante fremkomst af nye scenarier, tjenester og mobilt udstyrs design kan dog udfordre denne procedure, især ved migrering til højere frekvenser.

Denne afhandling tager et kritisk blik på den eksisterende antennestråle håndteringsprocedure med henblik på at øge evnen til at understøtte stadig mere stringente brugscenarier for 5G millimeterbølge cellulære systemer. Der udføres en begrænsningsvurdering ved at evaluere link-niveau antennestråle styringseffektivitet under operationelle forhold, såsom intra-celle mobilitet, udbredelsesmiljø, retningsbestemt stråleformende arkitektur, håndsæt rotation og millimeterbølge brugerhåndsblokering. Resultaterne afslører at mobilitet, håndset rotation og kanaler med stor vinkelspredning er problematiske for antennestrålejustering: resultater af antennestråle målinger udført med den nuværende procedure kan hurtigt blive forældede i dynamiske scenarier, hvilket fører til forkert valg af antennestråle og forringelse af ydeevnen. Derudover viser det sig at brugerblokering, der er i stand til at kompromittere enhedens originale stråleform og yderligere forringe ydeevnen, er et stort set overset problem for antennestrålestyring. Størrelsen af denne effekt afhænger af aspekter såsom håndgrebstype, antenneplacering og håndset orientering, som ikke fanges af den aktuelle 3GPP brugerblokeringsmodel.

Derudover foreslås to forskellige tilgange til at løse udfordringen med forældede måleresultater. Mens den ene adresserer procedure signalerings- og latensreduktion for minimering af sandsynligheden for forældet stråleinformation, undersøger den anden de forældede målinger i en datadrevet

løsning for at finde det bedste antennestråle par. Begge løsninger tilbyder en forbedring af antennestråle styringseffektiviteten med simpel integration i nuværende NR-standard.

Contents

Curriculum Vitae	iii
Abstract	v
Resumé	vii
Glossary	xiii
Acknowledgements	xvii
I Thesis Summary	1
1 Introduction	3
1 Background and Motivation	3
1.1 5G and the mmWave spectrum	3
1.2 Beam Management	5
2 Thesis Outline	6
2 Problem Statement	9
1 Research questions	9
2 Methodology	11
3 5G NR Beam management	13
1 Beam management framework	13
1.1 Beam management procedures	14
1.2 Beam acquisition and beam tracking	15
1.3 Beam management signalling and measurement	16
2 Beam management modelling assumptions	18
4 Beam management challenges	21
1 State-of-art	21
1.1 mmWave solutions prior to Release 15	22

1.2	mmWave solutions following Release 15	24
1.3	The need for a common evaluation framework	27
2	PhD project contributions	27
2.1	Publications and patents	28
2.2	Simulation tool	30
2.3	Main findings	32
2.4	Summary of Contributions	36
5	Final Remarks	39
1	Conclusions	39
2	Outlook	42
	References	43
	Appendix - Simulation Tool	53
II	Papers	61
A	Beam Management in mmWave 5G NR: an Intra-Cell Mobility Study	63
1	Introduction	65
2	BM Procedures	66
3	System Model	67
3.1	Depicted intra-cell scenario	67
3.2	Propagation channel model	68
3.3	Measurement model	69
4	Research Target and Key Performance Indicators (KPI)	71
5	Results and Discussion	73
5.1	Simulation Parameters	73
5.2	Performance results	73
6	Conclusions	79
	References	80
B	Improving Beam Management Signalling for 5G NR Systems using Hybrid Beamforming	83
1	Introduction	85
2	System Model	86
2.1	Network Layout	86
2.2	Signal Model	87
2.3	gNodeB BF Codebook	88
3	Signalling scheme	88
3.1	Current Scheme in 5G NR	89
3.2	Proposed Scheme	89
3.3	Scheme Comparison	90

Contents

4	Results and Discussion	90
4.1	KPIs	90
4.2	Comparison of SSB Schemes with Common Overhead	92
4.3	Scheme Performance for a High-Speed Scenario	94
5	Conclusions	96
	References	98
C	Hand Blockage Impact on 5G mmWave Beam Management Performance	101
1	Introduction	103
1.1	Related Works	105
1.2	Organization	106
2	System model	106
2.1	Channel model	107
2.2	Signal Model	108
2.3	Beamforming Codebook	112
3	Antenna and Hand blockage model	114
3.1	3GPP model	114
3.2	CST model	115
4	Model comparison	118
4.1	Antenna and blockage model comparison	118
4.2	Codebook comparison	121
5	BM performance evaluation	124
5.1	KPIs	126
5.2	Hand grip impact	127
5.3	Beam detection accuracy	131
5.4	Channel model impact	133
6	Conclusion	134
6.1	Outlook	135
	References	136
D	Machine Learning-based Millimeter Wave Beam Management for Dynamic Terminal Orientation	139
1	Introduction	141
2	System model	143
2.1	Channel model	143
2.2	Signal model	144
2.3	Beamforming codebooks	145
2.4	Beam management model	145
2.5	Device mobility and rotation model	146
3	UE beam selection	147
3.1	Max-measurement based beam selection	148
3.2	ML-measurement based beam selection	148

4	Results and Discussion	149
4.1	Performance criteria	149
4.2	Beam selection schemes	151
4.3	Beam management performance - Freespace	152
4.4	Beam management performance - realistic propagation scenarios	154
5	Conclusions	154
	References	156

Glossary

1G	1 st generation
2G	2 nd generation
3GPP	3 rd generation Partnership Project
4G	4 th generation
5G	5 th generation
6G	6 th generation
AoA	angle-of-arrival
AoD	angle-of-departure
AR	augment reality
AWGN	additive white Gaussian noise
BFR2	beyond FR2
BF	beamforming
BM	beam management
BT	beam tracking
CAD	computer-aided design
CDL	cluster-delay-line
CR1	coverage range 1
CR2	coverage range 2
CSI-RS	Channel State Information Reference Signals
CSI	Channel State Information

CST	Computer Simulation Technology
CTIA	Cellular Telecommunications and Internet Association
DL	downlink
DMRS	Demodulation Reference Signal
eMBB	enhanced Mobile Broadband
FR2	frequency range 2
FR	frequency range
GCS	global coordinate system
gNodeB	Next Generation Node Base Station
GoB	grid-of-beams
HAD	hybrid analog-digital
IA	initial access
IoT	Internet of Things
ISD	intersite distance
KPI	key performance indicators
L1	layer 1
L2	layer 2
LCS	local coordinate system
LOS	line-of-sight
LTE	Long Term Evolution
MAC	medium access control
MCS	modulation/coding scheme
MIMO	multiple-input-multiple-output
ML	machine learning
mMTC	Massive Machine Type Communications
mmWave	millimeter wave
MPE	maximum permissible exposure

Glossary

NLOS no line-of-sight

NN neural network

NR New Radio

OFDM Orthogonal Frequency-Division Multiplexing

PBCH Physical Broadcast Channel

PHY physical

PSS Primary Synchronization Signal

QuaDRiGa QUAsi Deterministic RadIo channel GenerAtor

RF radio frequency

RLF radio link failure

RRC Radio Resource Control

RRM Radio Resource Management

RSRP Reference Signal Received Power

RSS Received Signal Strength

SCS subcarrier spacing

SISO single-input-single-output

SNR signal-to-noise ratio

SS/PBCH Synchronization Signal/Physical Broadcast Channel

SSB Synchronization Signal Blocks

SSS Secondary Synchronization Signal

SS Synchronization Signal

TCI Transmission Configuration Indicator

ToS time-of-stay

TXRU transceiver units

UAV unmanned aerial vehicles

UE user equipment

ULA uniform linear array

UL uplink

UMa Urban Macro

UMi Urban Micro

UPA uniform planar array

URLLC Ultra-Reliable and Low-Latency Communications

VR virtual reality

WCN Wireless Communication Networks

WLAN wireless local area networks

WPAN wireless personal area networks

Acknowledgements

This thesis is the product of over three years of hard work, learning and personal growth. Through its many ups and downs I was fortunate to meet great people who played their own part in getting me to where I am today, writing these acknowledgments, and to whom I owe a huge thank you.

First and foremost, I would like to thank my supervisors for their commitment, thought-provoking debates and endless feedback that helped me become a better researcher. I'm grateful to Johannes Harrebek for helping me feel welcome in a new environment and for always facilitating opportunities for me to grow; to Christian Rom, for believing in my potential and encouraging me to dream big and bold; and especially to Carles Navarro Manchón for the guidance, unwavering support and for teaching me that not seeing the way forward doesn't always mean you are lost.

I would like to express my gratitude to my colleagues at AAU, in particular to Gilberto Berardinelli for helping me take my first steps into this project and for always offering great discussions. And a big thank you to the colleagues at Nokia, from which I must highlight Simon Svendsen, for always teaching me something new and for his help in making this thesis a reality; and the International Alliance, for all the coffee breaks, camaraderie and cheerful Friday breakfasts.

I would also like to thank the friends I managed to find in the middle of these very busy PhD years. To Pilar, Roberto, Melisa, Enric and Santiago - my fellow soldiers in battle who rode the highs and lows of the PhD with me - as well as Majken and Adriana: thank you for the many dinners, trips, board game and karaoke nights, bike rides to work, volleyball matches and heart-to-heart talks. You are all part of my happiest and fondest memories of Denmark that I will cherish forever. And, of course, to my dear Portuguese friends that are always cheering me on from afar, obrigada malta!

This would not have been possible if not for João, my biggest supporter, who dove head first with me into this adventure and never looked back. We traded Lisbon for this small and gloomy town but you have made all of our days here sunny and warm. Thank you for always having the right words to say, for the never ending laughs and late-night chocolate runs to Rema that

always turned a bad day into the best one. In the blink of an eye, almost 12 years have passed and here we are, celebrating yet another achievement together. Our 16-year old selves probably wouldn't have guessed where we are now but would definitely be proud of how much we have grown. I love you and can't wait for the adventures that are yet to come!

Finally, I would like to thank my family, for keeping me grounded and relentlessly rooting for me even when I didn't have the energy to text or call back. To my Aunts and Uncle for their love and encouragement. To my Grandmother, who mastered Whatsapp to keep in touch with her granddaughters abroad. To my Mom who is tired of seeing her daughter study for so many years but still celebrates every milestone with the same enthusiasm. To my big sister that shows me everyday that life is whatever you make of it. And lastly to my Dad, who taught me to stay curious and see less beaten paths as growth opportunities. Thank you for shaping me into who I am today.

Filipa Fernandes
Aalborg University, February, 2023.

Part I

Thesis Summary

Chapter 1

Introduction

1 Background and Motivation

The first wireless communication systems were pioneered in the 1900s thanks to visionary minds like Nikola Tesla, Jagdish Chandra Bose, Alexander Popov and Guglielmo Marconi [1]. Since then, the wireless industry has flourished into several sectors, one of the most impactful being dedicated to mobile communications. A continuous technology growth allied with consumer demand has already produced five evolutionary generations of mobile networks. What initially started in the 1980s as a mobile voice service in the 1st generation (1G) quickly extended towards the mobile broadband network we use today in the 4th generation (4G), supporting data-dominated applications that have shaped our modern world into a fast-paced always-connected society, even through a global pandemic [2, 3].

However 4G/Long Term Evolution (LTE) has rapidly reached its maturity stage, lacking the network flexibility, scalability and spectrum availability to continuously adapt to new emerging use cases. These limitations motivated the shift to the 5th generation (5G), envisioned as a forward-looking system that facilitates compatibility with previous and future generations of wireless deployments, all while enabling unprecedented data rates, connected devices and low latency applications [4].

1.1 5G and the mmWave spectrum

Up until now, all generations of wireless technologies have introduced major paradigm shifts in the wireless industry. 5G is no different in the sense that it aims to go beyond virtually connecting people to also interconnecting machines and devices, sustaining a tremendous amount of growth in connectivity and data traffic volume while offering higher data speeds, low latency and

a wider range of usage scenarios [5]. The targeted use cases are loosely categorized within the industry into 3 broad areas of service, according to its feasibility requirements [6]. Massive Machine Type Communications (mMTC) cater to massive Internet of Things (IoT) applications, where machines communicate autonomously to enable concepts like smart cities. Ultra-Reliable and Low-Latency Communications (URLLC) tend to small but critical data exchanges that support futuristic markets such as remote healthcare or autonomous vehicles. Finally, enhanced Mobile Broadband (eMBB) continues to focus on supporting the ever-growing demand for mobile broadband in cloud services, 8K streaming, and immersive experiences [7].

Currently, eMBB services are the most prevalent among everyday users, driving the first 5G commercial deployments through consumers' smartphones. Ericsson accurately predicted in [8] the average monthly usage per smartphone in 2022 would surpass 15 GB and the number of 5G mobile subscriptions to go over 1 billion. This trend shows no indication of slowing down in the future, as seen in Fig. 1.1, with predictions pointing at 4.4 billion 5G mobile subscriptions by the end of 2027.

To sustain the higher data rates and overall increased system capacity needed for these applications, an essential piece of the puzzle lies in securing sufficient bandwidth [9]. However, the current sub-6 GHz bands employed by LTE have become too crowded to enable this new wave of data-hungry use cases. Therefore, it is necessary to find additional room in the frequency spectrum for 5G.

The millimeter wave (mmWave) frequency band, spanning from 30 to 300 GHz, makes for a worthy candidate. Since it has remained for the most part unused, this range of frequencies can easily offer large amounts of bandwidth in a contiguous portion of the spectrum. While this seems like a straightforward solution, there is a reason why mmWave have been mostly overlooked in previous communication systems. At these high frequencies, propagation conditions are quite hostile and challenged by significant pathloss, atmospheric and rain absorption, low object penetration and weak diffraction around obstacles [10], [11]. Although these properties limit the applications of mmWave, technology has now evolved to circumvent some of these challenges and unleash its full potential for 5G.

An example of this is pathloss mitigation. Simply put, Friis' equation states that the received power between isotropic antennas in free space scales with the square of the waveform's wavelength, λ^2 [12]. Under the assumption of a fixed antenna electrical size, it is then clear that the received power is negatively impacted by an increase of frequency. In fact, migrating in the spectrum from a popular LTE band of 2.4 GHz to the 28 GHz mmWave band results in a free space power loss of around 21 dB. Considering the regulated transmission power and battery life of devices, increasing the transmit power would not be enough to counteract a loss of this magnitude. Therefore, to

1. Background and Motivation

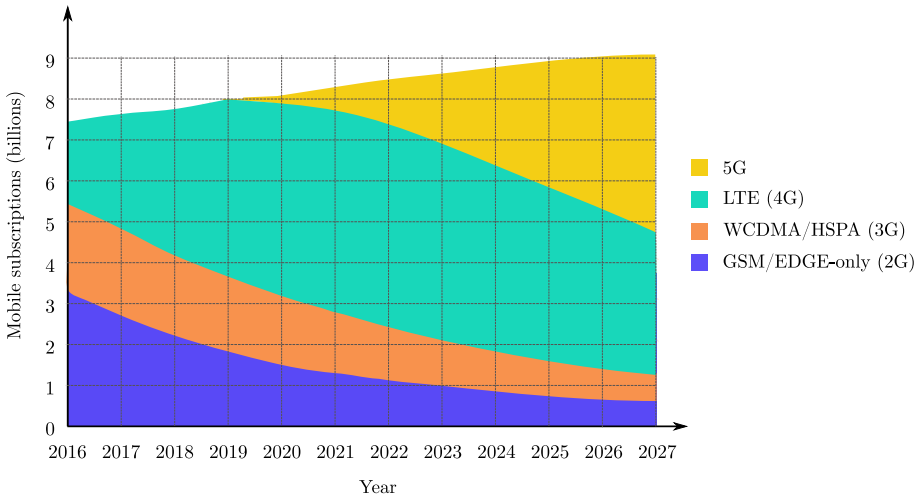


Fig. 1.1: Number of mobile subscriptions per technology: inspired by Ericsson’s 2022 Mobility Report [8].

maintain adequate coverage of the system, a gain increase must be pursued. To that end, large directional antenna arrays can be implemented to perform beamforming, where all the gain from each antenna element is constructively combined and focused in a particular direction. Since this technique produces narrow beam patterns, it is vital that the transmitter and receiver beam pair point towards each other to achieve adequate signal strength [13].

In mobile communications, where the device is not limited to a fixed location, the best beam pair combination not only has to be determined for each user but also has to be kept up to date to ensure seamless connectivity. The narrow nature of these beams allied with the user’s demanding mobility requirements creates a beam alignment issue between the base station and the user equipment (UE) beams, becoming one of the biggest challenges of mmWave communications for 5G. Therefore, in order to transition to mmWave and utilize its bandwidth, beam adaptation protocols must first be established to manage the crucial operations of beam pair link search and maintenance.

1.2 Beam Management

From the 2nd generation (2G) onwards, all wireless system have been established and deployed according to a set of standards driven by the 3rd generation Partnership Project (3GPP), a collaborative group of telecom organizations responsible for designing globally applicable specifications for new wireless technologies. Under the new global wireless standard for 5G’s

radio access technology, designated as 5G New Radio (NR), 3GPP has defined a range of mmWave frequencies, frequency range 2 (FR2), where operations are being optimized. FR2, which previously spanned from 24.25 GHz to 52.6 GHz, has now been extended to 71 GHz with even higher frequency bands also being currently explored in the spectrum for future releases of 5G and 6th generation (6G), as seen in Fig. 1.2 [14].

To resolve the issue of beam alignment, a set of layer 1 (L1) and layer 2 (L2) procedures has been established in NR, under the umbrella term of beam management, to acquire and maintain an optimal beam pair link between the Next Generation Node Base Station (gNodeB) and the UE out of a pre-defined set of beam combinations [15]. The wide bandwidths characteristic of mmWave combined with large antenna arrays and bit resolution requirements make it challenging to scale up the transceiver units (TXRU) required to achieve complete beamforming flexibility to make the beam selection process as swift as possible. To prevent it from becoming an overly complex and costly system, the current beam management process adopts an analog beamforming approach instead [4]. Analog beamforming relies on adjusting the antenna array's phase shifts to point the beam in different directions, requiring only one TXRU per desired beam. However, a single TXRU configuration comes with limitations such as the inability to multiplex signals in the spatial dimension. This is why the current beam management framework relies on sequentially sweeping, measuring and reporting a large number of potential beam pair candidates before determining the best selection. Moreover, due to the user's mobility, this monitoring must be repeated periodically to avoid a link drop, always ensuring the best connection for the user.

Although this method might be sufficient for the first deployments of mmWave services, it may not be adequate to meet consumer demand on new applications that require frequent beam switches like augmented reality (AR) and virtual reality (VR) systems, unmanned aerial vehicles (UAV) services, and new types of handset designs, such as foldable phones [16]. This problem will further aggravate in future deployments where the migration to higher frequencies is certain. Therefore, this thesis focuses on the important task of assessing what the limits of the current framework are and pinpointing areas of improvement to make fully fledged mmWave communications a reality.

2 Thesis Outline

This thesis is structured into 2 parts, Part I and Part II. First, Part I offers a summary of the work conducted during the PhD project. The remainder of Part I's content is organized as follows: Chapter 2 details the open problem at hand, the research questions posed and methodology used to tackle

2. Thesis Outline

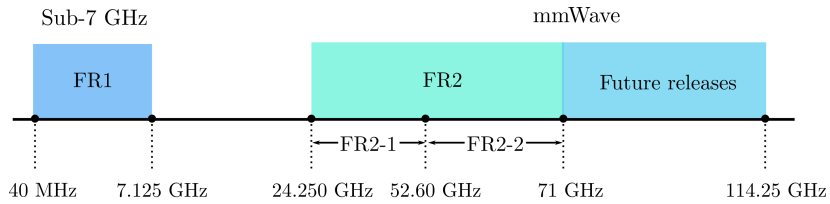


Fig. 1.2: Current 5G spectrum for Release 17.

it. Chapter 3 provides a description of the beam management framework as established in Release 15 and the specific procedures that are targeted in this work. Chapter 4 dives into the main challenges of beam management, the current state-of-art on circumventing them and as lists this PhD project's outcomes on that subject. Finally, Chapter 5 summarizes the contributions made and how they fit into the research questions posed. Additionally, an outlook on future research directions for this topic is provided. Part II concludes this thesis by presenting a compilation of the publications that resulted from the work detailed in Part I.

Chapter 2

Problem Statement

The motivation behind this work can be stated as

Future cellular networks will increasingly rely on the mmWave band to increase capacity. To circumvent these frequencies' challenging propagation conditions, highly directional beamforming is required to acquire and maintain beam alignment for an adequate link quality. The constant emergence of new use cases, services and form factor designs may challenge the capabilities of the current beam management procedure, threatening the feasibility of mmWave communications for 5G.

This thesis aims to mitigate such challenges by critically examining the vulnerabilities of the current beam management procedure and devising solutions that can be incorporated in the NR standard, thus ensuring the adaptability of 5G mmWave cellular systems to future demanding or disruptive use cases.

1 Research questions

Tackling this problem sparks several inquiries which are categorized into two main research questions: **RQ1** and **RQ2**. In order to improve a procedure's performance, one must first find its vulnerabilities. Therefore, **RQ1** ponders on potential limitations of the current beam management framework:

- **RQ1: What are the main vulnerabilities of the beam management procedure?**
 - **RQ1-a:** How robust is the current beam management procedure to high user mobility and device rotation?
 - **RQ1-b:** Is user blockage a hindrance to the current beam management procedure?

- **RQ1-c:** To what extent is the absence of line-of-sight (LOS) conditions a factor in beam management performance?

Mobility and intermittent LOS conditions are prevalent factors of beam management performance for outdoor urban environments. The users are likely to move through an inherently dynamic propagation environment at mmWave frequencies, where a user's connection can quickly degrade just by turning a building's corner. It is important to assess how well the current procedure handles such challenges to pinpoint any potential aspects to be improved upon. Additionally, and considering that a large portion of eMBB applications are enabled through handheld devices, it is worthwhile investigating how disruptive the user's influence, manifested through blockage or device rotation, could be to the beam alignment process. Although its effects are known to be detrimental for mmWave antennas' spherical coverage, the study of user blockage impact on beam management performance is not widespread in current literature [17–19]. Similarly, the user could also subject the device to sudden and frequent rotations during use, further disturbing the delicate alignment of mmWave's narrow beams. These questions naturally lead to a reflection, expressed in **RQ2**, on the type of solutions that could help overcome such challenges:

- **RQ2: What changes are required in the current BM framework to improve mmWave communications?**
 - **RQ2-a:** Could such changes be introduced within the current beam management implementation?
 - **RQ2-b:** Would the improvement of the current beam management procedure require additional information available to the device?

If changes to the current procedure are necessary, it is relevant to contemplate whether improvements could be achieved through enhancements built upon the current signalling and measurement framework or if significant changes to the NR standard would be required. While the standard is meant to evolve throughout different 3GPP Releases to support new features and functionalities, incremental changes that stand on pre-existing implementations are easier to introduce and ensure backward compatibility with older devices and infrastructure. Moreover, with the foreseen challenges, relying solely on measurements to secure narrow beam alignment may not suffice and additional data such as positioning or orientation of the user terminal might need to be extracted from sensors and integrated into the beam management procedure.

Finally, it bears mentioning that beam management is a growing and vast topic that encompasses several areas of study. However, due to the time-limitation of a PhD project, not all research avenues can be pursued. Instead,

2. Methodology

this work focuses on a subset of beam management challenges perceived to be amongst the most likely to jeopardize beam alignment and investigates them in depth, offering a well-balanced study on mmWave beam management performance.

2 Methodology

All publications listed in this body of work result from research carried out according to the following scientific approach:

1. **Problem definition and research questions:** An extended literature survey is conducted to deepen knowledge on the topic of beam management for 5G NR and pinpoint the main research problems of interest. Specifically, ponder on the potentially vulnerable procedures of beam management for which performance could suffer from more demanding use cases and applications.
2. **Formulation of hypothesis solution or study proposal:** To answer the research questions at hand and pose a potential study or solution, depending on the nature of the research question.
3. **System modelling:** To investigate the hypothesis made, a high detail system model is employed including 3GPP compliant beam management signalling, intra-cell user mobility, variable propagation environments, different beamforming architectures, device rotation and mmWave user hand blockage. Since such signalling and propagation details become too complex to model analytically, a self-developed 3D geometric link-level simulation tool is adopted based on the Monte Carlo method. Further details on the simulator structure are provided in the Appendix.
4. **Result processing and analysis:** After collecting the results from the simulator, numerical evaluations are employed using appropriate key performance indicators (KPI) to depict beam alignment performance such as Reference Signal Received Power (RSRP), Received Signal Strength (RSS), beam time-of-stay (ToS), beam misalignment probability and beam misalignment loss. These metrics are used to assess a link's performance degradation or enhancement when studying the impact of an identified procedure vulnerability or when testing a solution's effectiveness for beam management.
5. **Conclusion and dissemination of results:** The work developed is compiled and shared in a peer-reviewed community through scientific publications targeting high-impact journals and conferences. Moreover,

presentations are given in project-related meetings in Nokia and the Wireless Communication Networks (WCN) section.

Chapter 3

5G NR Beam management

This chapter delves into the details of 5G NR's beam management process introduced in Section 1.2 of Chapter 1. To contextualize this project, Section 1 describes the current beam management framework supported by 3GPP and Section 2 narrows down the scope of this research by specifying which procedures and system assumptions are explored in the course of this project.

1 Beam management framework

In 5G mobile networks user mobility is categorized into inter-cell and intra-cell mobility. Inter-cell mobility, remaining true to its definition in legacy networks, pertains to cell-level mobility where UEs are moving between coverage areas of different cells. To ensure the connection is maintained, handovers are performed based on cell quality measurements handled by the Radio Resource Management (RRM) mobility procedure, which relies on the upper Radio Resource Control (RRC) layer [20] , [7].

Intra-cell mobility refers instead to beam-level mobility within the cell [21]. As previously established, FR2 communications require narrow beams, which entails larger codebooks must be employed to meet the cell's coverage requirements. In an intra-cell mobility scenario, the best serving beam for a non-static UE may change quite often. In order for a user to experience seamless connection when moving through the cell, timely beam alignment between the transmitter and receiver narrow beams must be provided at all times. That is handled by beam management, which takes place solely in L1 and L2, without resorting to higher layers. This thesis focus mainly on intra-cell mobility and its associated beam management procedures.

1.1 Beam management procedures

The following beam management procedures are supported in the standard to handle intra-cell mobility [15]:

- **Beam sweeping:** the gNodeB or the UE cover the cell's spatial area using a set of beams transmitted or received in pre-specified directions and time intervals.
- **Beam measurement:** the gNodeB or the UE evaluate quality of received beamformed signals, typically through L1-RSRP measurements, on a per beam basis.
- **Beam determination:** the gNodeB or the UE identify their own best beam for transmission or reception based on measurements.
- **Beam reporting:** the UE periodically reports measurement-based information on beamformed signals.
- **Beam switching:** the gNodeB or UE switch between available beams to maintain beam alignment.
- **Beam failure detection:** the UE, while monitoring the quality of the serving beam pair, identifies sudden interruption of the communication link.
- **Beam failure recovery:** The UE attempts to recover from a rapid interruption of connectivity after a beam failure is declared by indicating the failure to the gNodeB, along with a new suitable beam.

There are three distinct downlink (DL) processes of operations to obtain the best beam pair selection. While not specified in the standard, these are colloquially referred to as P1, P2 and P3 in technical discussions and reports:

- P1: initial process dedicated to gNodeB beam selection. Broad beams are typically used to sweep the angular space and a coarse serving direction is chosen based on measurements from a broad-beam UE.
- P2: second process to refine P1's beam selection using narrower gNodeB beams, still employing a broad-beam at the UE.
- P3: final process of beam alignment for UEs equipped to support beamforming. After beam selection at the gNodeB side, the transmit beam is fixed so the UE can refine its broad-beam by sweeping through its own narrow beams.

These processes, represented in Fig. 3.1 are meant to secure a beam pair selection that is suitable for both transmission and reception. This assumption stands on the concept of beam correspondence, which states that the best transmit beam for the gNodeB or the UE is also its best receive beam.

1. Beam management framework

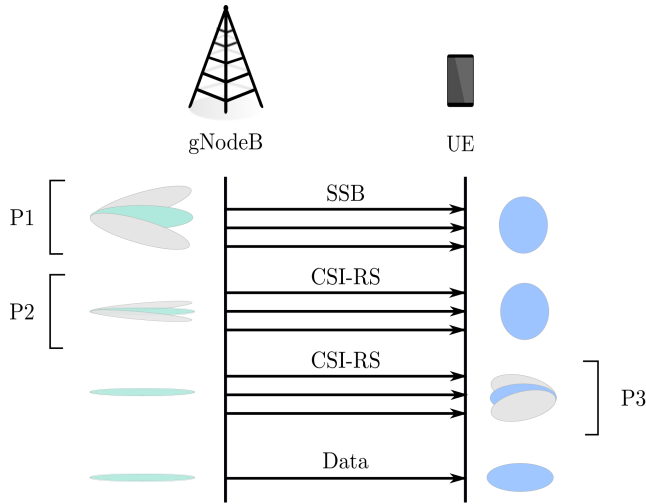


Fig. 3.1: Beam management processes.

1.2 Beam acquisition and beam tracking

According to the definition of beam management in [15], the procedures above are used both for acquiring and maintaining a beam pair link. Therefore, two types of beam alignment can be envisioned: beam acquisition and beam maintenance or tracking [22]. Beam acquisition occurs when the UE is not yet connected or has lost connection, for example, after an unsuccessful beam failure recovery attempt. In other words, beam acquisition is the starting point of the beam management process where the best initial beam pair is acquired with little to no prior knowledge on cell quality information. For this reason, initial beam alignment must be achieved through a P1-P2-P3 process of sweeping and measuring the available beam pair combinations. Beam tracking takes place after beam acquisition, when the UE has already in place a physical link connection to a gNodeB associated to a serving beam pair. Consequently, the network must periodically monitor that connection and assess whether its quality triggers a beam switching procedure or even a beam failure recovery procedure. Since a link is already established, the network usually has access to information that allows it to select a subset of beam candidates most likely to replace the current serving beam once the link quality deteriorates, reducing the beam alignment search space.

In summary, while beam tracking is an on-going process that relies on all the beam management procedures listed, beam acquisition is successfully completed after a beam pair link is secured, employing only a fraction of those procedures, as illustrated in Fig. 3.2.

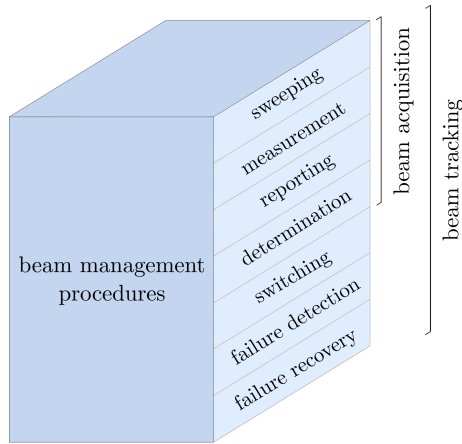


Fig. 3.2: Beam management procedures for beam acquisition and beam tracking.

1.3 Beam management signalling and measurement

Beam management measurements rely mostly on two types of DL signals: Synchronization Signal/Physical Broadcast Channel (SS/PBCH) Blocks and Channel State Information Reference Signals (CSI-RS) [23].

SS/PBCH

SS/PBCH Blocks, typically shortened to Synchronization Signal Blocks (SSB), are a pivotal part of NR, being broadcasted periodically for UE measurement purposes. A single SSB, spanning 4 Orthogonal Frequency-Division Multiplexing (OFDM) symbols in time and 240 subcarriers in frequency, is composed of both synchronization signals and broadcast channels, as seen in Fig. 3.3. The Primary Synchronization Signal (PSS) and Secondary Synchronization Signal (SSS) are carried in the SSB as two 127-long pseudo random binary m-sequences employed for initial synchronization and cell identification. The Physical Broadcast Channel (PBCH), associated with the Demodulation Reference Signal (DMRS), contains system control information the UE requires to communicate with the network.

During the beam sweeping procedure these SSBs are transmitted in groups, known as SSBursts, according to a numerology-dependent transmission pattern. In FR2 an SSBurst can contain up to 64 SSBs, as displayed in Fig. 3.3 [24]. Each SSB is mapped to a unique gNodeB beam so that the UE can decode it, measure that beam's power level and report its L1-RSRP value back to the gNodeB for beam determination. This is done through SS-RSRP, which is defined as the linear average over the power contributions in Watt of the resource elements that carry a SSS [25]. For beam acquisition, SSBs are

1. Beam management framework

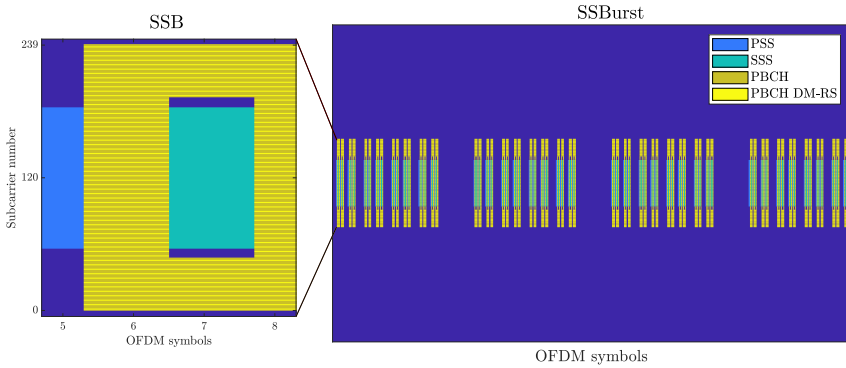


Fig. 3.3: SSB structure and SSBurst transmission pattern.

usually employed during P1, where broader beams are considered.

CSI-RS

CSI-RS's are UE-specific signals transmitted by the gNodeB to monitor DL radio channel conditions. These NR signals are extremely flexible, allowing for 18 different time-frequency allocation configurations tailored to a multitude of applications such as Channel State Information (CSI) acquisition, RRM or beam management. In the latter, CSI-RS can only be configured through 3 distinct configurations to be used, similarly to SSBs, in L1-RSRP measurements for beam candidate selection. This is achieved using CSI-RSRP, which is the linear average over the power contributions in Watt of the resource elements of the antenna port(s) that carry CSI-RS configured for RSRP measurements within the considered measurement frequency bandwidth in the configured CSI-RS occasions.

In the context of beam acquisition, CSI-RS's are associated with narrower beams and, therefore, are employed in both P2 and P3. However, their configuration differs in a higher layer parameter titled "repetition" which displays a binary "on" or "off" state. This parameter is only set for CSI-RSs configured for L1-RSRP and it clues in the UE on which assumptions it can make regarding the DL beamforming configuration on the gNodeB side. In P2, "repetition" is "off", entailing that the beamforming applied to each CSI-RS resource at the gNodeB may vary. Therefore, the UE takes that information as an indication to maintain the same spatial filtering until P2 is complete. In P3 however, this parameter is set to "on", meaning that the UE can assume that no beam sweeping is performed on the gNodeB side and, therefore, is free to sweep through its own beams for beam refinement.

2 Beam management modelling assumptions

Beam management is an essential building block of NR system design for mmWave. However, due to the complex nature of this process and the range of use cases it is meant to serve, modelling it within a simulation tool can become an increasingly complex task. Therefore, in order to create a 3GPP-compliant yet attainable evaluation framework, this thesis imposes some beam management model stipulations tightly inspired by the process described above.

Firstly, a standalone mmWave system is assumed, where all control and measurement message exchanges are delivered without any errors through an ideal control channel. Furthermore, this work relies on the principle of beam correspondence by assuming the best beam pair link for both transmission and reception is always obtained directly through DL measurements. Moreover, the topic of beam management is further scoped down to focus on the beam acquisition stage, along with the procedures associated with it: beam sweeping, beam measurement, beam reporting and beam determination. The beam reporting procedure, as well as any other uplink (UL) operations such as Random Access, are assumed to display ideal signaling, with no errors or delays. Regarding P1, P2 and P3 in beam acquisition, it is worth highlighting that these stages are merely conceptual and the standard does not mandate that all of them be put to use at once. Furthermore, the relationship previously described between P1 and P2 beamwidths is also not specified in the standard, despite being a widespread practice in the industry. Therefore, this work adopts a variation of these stages, employing mostly P1 and P3 as represented in Fig. 3.4. The beam acquisition process in this work is kicked off in P1 with beam sweeping on the gNodeB side. The beams used to carry the SSBs required in this phase are intentionally configured to have a narrow beamwidth. This is meant to circumvent the need to perform P2 and achieve gNodeB beam refinement already in P1. These signals are received at the UE using either a single omnidirectional beam or several directional broad beams, depending on the UE model employed. The UE then decodes and measures SS-RSRP in each SSB in order to report those L1-RSRP values back to the gNodeB for beam determination. In P3 the gNodeB employs the beam previously determined in P1 to transmit CSI-RS resources to the UE, which performs narrow beam sweeping on its end to received each of them. The UE then decodes and measures CSI-RSRP for each of its beams to determine which is the best beam candidate. Once P1 and P3 have taken place, it is assumed that beam acquisition has been successfully completed and DL data transmission can occur. All publications in this thesis follow this beam management framework with different levels of complexity on the simulation tool, as is further explained in Section 2.2 of Chapter 4.

2. Beam management modelling assumptions

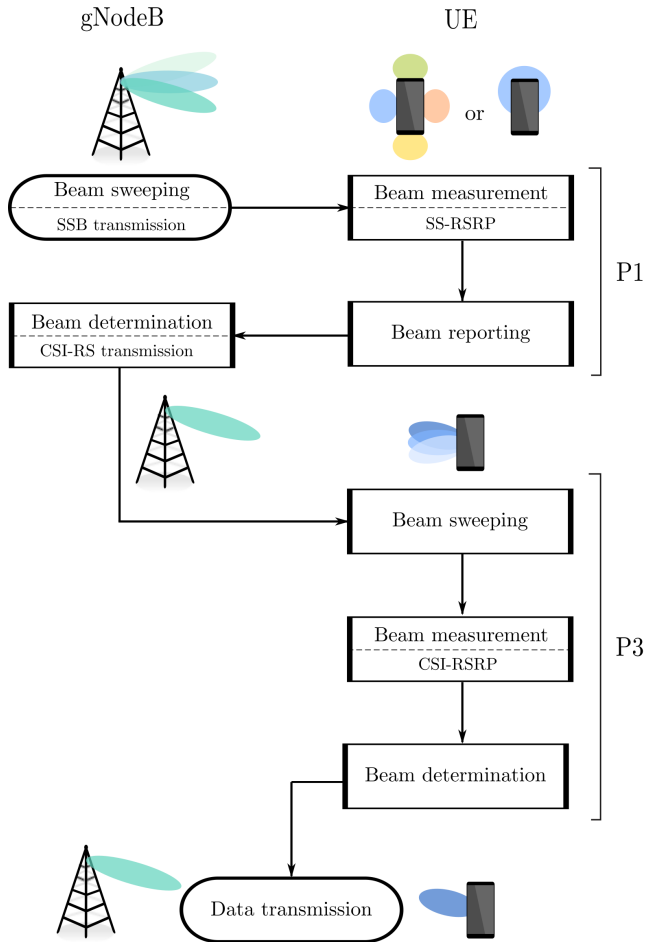


Fig. 3.4: General beam management framework adopted in the thesis.

Chapter 4

Beam management challenges

This chapter focuses on the challenges of the current 5G NR's beam management framework, which is the main subject of this PhD project. First, Section 1 describes the evolution of research for mmWave mobile communications over the years, the main challenges identified in this front and the solutions proposed in the literature to mitigate these issues. Section 2 details this PhD thesis's contributions towards extending the state-of-art knowledge of beam management performance at a link level.

1 State-of-art

The use of mmWave technologies was first researched for wireless applications outside cellular networks, mostly on the 60GHz frequency band [26]. Prior to its inclusion in the NR standard with Release 15 and Release 16 [27], mmWave had been integrated into other standards of wireless communications, namely IEEE 802.15.3c and IEEE 802.11ad. These standards set the protocols and requirements of mmWave usage for wireless personal area networks (WPAN) and wireless local area networks (WLAN), respectively [28], [29]. In this medium the issue of beam alignment was already prevalent, sparking countless studies and proposals to overcome this challenge and achieve multi-gigabit connections for indoor short-range and static environments [30–34]. Ultimately, this trend made its way to cellular communications, where beam alignment challenges would be dealt with by a set of procedures later referred by 3GPP as beam management.

This section presents a detailed survey of the research investigations done on mmWave for cellular communications, which includes generic

mmWave studies prior to its introduction in Release 15 (Section 1.1) and 3GPP-compliant studies following Release 15 (Section 1.2).

1.1 mmWave solutions prior to Release 15

The use of mmWave for cellular networks has been in the academic limelight for several years now, with its potential and feasibility being heavily explored in works such as [35–43]. Here, researchers strived to identify bands of interest and use cases, envision possible network architectures compatible with legacy equipment, test circuitry limitations and assess mmWave suitability for propagation through exhaustive measurement campaigns. These studies confirmed that mmWave could be employed to significantly improve system capacity for outdoor urban environments with a limited range but its challenging propagation conditions would demand the usage of beamforming technology to enable future mmWave commercial deployments.

Once established that mmWave was a viable solution, research interest shifted towards designing a cell search procedure for this new range of frequencies. In LTE networks, initial cell discovery employs either omnidirectional¹ or fixed antenna patterns, while beamforming operations and user-specific directional transmissions are reserved for communications after the UE is linked to a cell. However, mmWave without beamforming displays a very small coverage range due its challenging propagation conditions. Therefore, considering an analogous approach for mmWave would create a disparity between the discoverable coverage area of the cell and the actual supportable coverage area with high gain beamforming, as exemplified in Fig. 4.1. In other words, a distant user could sustain high data rates at mmWave, assuming the correct beamforming direction is known, but would fail to connect due to the limited coverage area that an omnidirectional initial cell search at these frequencies can offer, as showcased in [44]. In order to circumvent this issue, the authors ponder on a few possible solutions involving cooperation with legacy cells. Since their coverage range is significantly larger than mmWave, this could be leveraged to track the user's proximity to the mmWave cell: once close enough, the LTE cell would inform both the mmWave cell and the UE of where to steer their directional signals. Alternatively, the initial cell discovery procedure could be accomplished by the LTE cell at lower frequencies so that data transmission could then ensue in the mmWave band.

This is further explored in [45–48], where different directional cell search procedures are conceived based on periodical synchronization signal transmissions. These transmissions can be either omnidirectional, like in LTE, or

¹Transmissions are inherently directional due to the directive antenna radiation patterns employed in sectorized cellular layouts. However, in the context of this section the term "omnidirectional" refers to non beamformed communications.

1. State-of-art

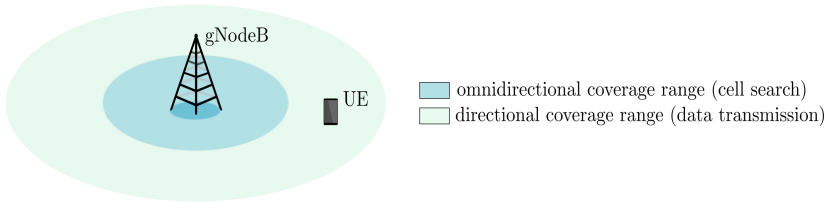


Fig. 4.1: Coverage drawback of mmWave omnidirectional cell search: the UE is out of range to establish a link to the cell, despite being able to reach high data rates with beamforming [45].

directional, scanning the angular space in hopes of aligning with a user. This is done by scanning random directions in each signal iteration or following a deterministic sequential pattern. Results indicate that omnidirectional transmission of the synchronization signals offers a more reliable signal level and a significantly smaller delay than its directional counterpart. Although the narrow directional beams provide higher gain values, they also often find themselves misaligned with the UE, leading to low signal strength levels. Instead, the omnidirectional approach maintains a weak but constant power reception. While the authors acknowledge the need for directional beams in the initial cell discovery process, it is clear that exhaustive beam acquisition procedures with analog beamforming, as assumed in [49], are accurate but very unpractical. Low-resolution digital beamforming is proposed to enable the simultaneous transmission of these periodic signals. This expedites the beam acquisition process while supposedly keeping a reasonable power consumption on the equipment. However, it is worth noting that digital beamforming requires as many TXRUs as antenna elements which can become quite costly and complex for mmWave, due to the sizeable arrays and large bandwidths.

As a result, more sophisticated solutions are pursued to prevent the delays and overhead of an exhaustive beam acquisition process. In [50] two beam search protocols are proposed based on the link's modulation/coding scheme (MCS). If a fixed MCS is imposed, then an interactive protocol is activated where the search is interrupted once a beam presents sufficient power to sustain acceptable link performance. Therefore, the protocol potentially forfeits the best possible link in exchange for an overhead reduction, speeding up the search process. If an adaptive MCS is used, however, no beam combinations can be discarded. To circumvent this, the authors propose an iterative method that progressively sectorizes the angular space to narrow down the optimal beam direction.

A similar hierarchical approach is taken in [51], presented as a multi-phase hierarchical procedure for beam acquisition, where a UE determines the best transmit and receive beams by first receiving the directional periodic signals with wide beams followed by successively narrower beams until ade-

quate beam alignment is reached. As described in [52], a converse approach can also be adopted for gNodeB beam refinement instead. The authors also employ the use of hybrid beamforming, boasting similar results to digital beamforming while using a less complex, costly and power consuming implementation. A variation of this iterative technique is proposed in [53] to further reduce the beam search time. A two-step beam acquisition procedure is envisioned where the gNodeB performs wide beam search in step 1 and the UE reverse training in step 2 according to the best beam decided in the previous step.

Furthermore, the papers in [54–56] propose mmWave network performance evaluation frameworks for these beam sweeping based cell discovery methods, making sure to include important aspects such as random access delay, blockage, pilot orthogonality and pilot re-usage, impact of beamwidth and cell density, beamforming architectures and several signal broadcasting schemes.

The literature on this topic also includes methods that go beyond beam sweeping and measurement for beam acquisition. A technique is proposed in [57] for a low-complexity beam selection process that does not rely on explicit channel estimation. This is achieved with compressive sensing, a signal processing technique used to recover signals with lower sampling rates than required by Nyquist’s Law [58]. The authors exploit the sparsity of scattering environments characteristic of mmWave channels to select analog beamformers through compressive sensing, resulting in a much smaller cell discovery overhead. Furthermore, using context information such as terminal positioning orientation, user spatial distribution or channel gain predictions can greatly improve the cell discovery process. Having access to this kind of additional information, even with some level of inaccuracy, helps restrict the search space, reducing significantly the overhead and latency of the procedure [59–62]. Such data could come from sensors in the device, external positioning systems like GPS, or through out-of band information obtained with sub-6 GHz communication systems [63, 64]. This data-driven approach can be further exploited by using it in machine learning (ML) implementations: [65] leverages vehicles’ positions and sizes to fast track beam selection in mobility scenarios.

1.2 mmWave solutions following Release 15

Based on the existent literature, 3GPP defined 5G NR’s beam management framework as described in Section 1 of Chapter 3. The beam acquisition portion is built on an iterative measurement and reporting approach that sweeps through a pre-defined codebook of analog beams, without relying on channel estimation. While this method is defined in the standard, details regarding antenna array sizes, beamwidths or beam codebook sizes are left open for

1. State-of-art

each vendor to configure on a use case basis [66]. While this straightforward solution has performed adequately for initial 5G deployments, new emerging use cases and applications keep pushing the needed capabilities beyond the current procedures, driving the need to improve on this baseline. Having the user on the move through a busy urban area while using a data-hungry application should be a perfectly plausible use case scenario for 5G mmWave services. However, a combined scenario of user mobility, fast multi-panel device rotation and blockage can make the task of narrow beam alignment quite elusive. In this context, the beam sweeping-based approach becomes prone to erroneous beam decisions, since the latency of the process prevents it from obtaining timely beam information to keep up with the dynamic nature of the environment [16, 67].

Several works in the literature propose alternative solutions to improve the capabilities of the current 3GPP-defined beam management framework by targeting overhead and latency reduction. Compressive sensing is once again explored in works such as [68], to determine the number of SSB-based measurements needed to find a ‘dominant’ channel cluster. Since the search space is reduced, beams pointing away from said cluster are skipped in the beam sweeping process, saving resources and speeding the beam alignment process. The authors in [69] rely on hybrid analog to digital beamformers to design a multi-level beam codebook for uplink beam acquisition based on flat top beams. These beams display nearly constant gain values through a large angular span around the direction of transmission that can be exploited for a hierarchical, and therefore more time-efficient, beam sweeping procedure.

These solutions still assume an autonomous search method, where beam acquisition is mostly based on signal exchanges between the gNodeB and the UE. However, the vast majority of solutions in modern literature strays away from the current standard implementation by additionally exploiting any kind of context information that can be made available to the network or the UE. Despite it not being a new concept, data-driven solutions have been revisited in recent works with a more up-to-date system modelling for 5G which includes complex mobility patterns, directional antennas, multi-panel UEs and device rotation.

In [64] a non-standalone deployment scenario is envisioned, where spatial information is extracted from sub-6 GHz bands to establish mmWave links. This out-of-band information reveals to the network a coarse direction for the sub-6 GHz dominant propagation direction, which is spatially congruent with mmWave frequencies. The mmWave beam weights are then defined based on this side information, narrowing down the beam search space and reducing its corresponding overhead. Positioning-based methods are also quite popular in the literature to manage the latency of the beam search procedure. In [70] positioning information is gathered for users already connected to the network, as well as their beam selection indexing.

The target UE and other users in its vicinity will display highly correlated downlink channels, which means that their optimal beam selection is likely to be similar. This information can then be used to restrict the number of candidate beams, leading to faster beam acquisition. Furthermore, [71] relies on past users to statistically identify usual directions of arrival in the cell. Once this data is acquired, beam acquisition can be significantly accelerated by searching more often that angular space, instead of uniformly sweeping the beams through the cell's coverage range.

The authors in [67] propose to instead collect the UE's orientation information obtained with device integrated sensors. This data, along with the usual SS-RSRP measurements would then be fused through a particle filter to improve the robustness of beam prediction against frequent and unpredictable rotation patterns, such as AR/VR use cases. While not particularly targeting the reduction of the beam sweeping latency, having access to this side information is shown to reduce losses from sub-optimal beam selection, which even aids the UE's battery life. As predicted in [72], many solutions in the literature resort to ML to tackle this challenge, a trend that is also seen in 3GPP for Release 18 [73]. Orientation is again leveraged in [74], along with SS-RSRP, to train a recurrent neural network (NN) for best UE beam determination. While under a genie gNodeB beam assumption, this solution produces better results than the conventional beam sweeping-based strategy and the solution presented in [67], particularly for high mobility and fast rotation environments. Additionally, the authors in [75] propose a beam acquisition technique that relies on both location and orientation to propose a deep neural network based solution for indoor beam alignment. This data produces alignment probability values for different beam pairs, which are used to create a smaller beam candidate list, reducing the overhead and delay of the procedure. This work is extended in [76] to different designs of multi-panel devices. This approach decreases beam acquisition overhead by recommending a subset of candidate beams/panels to be tested. This not only improves the latency of the process but it also identifies which panels are not in use and, therefore, can be turned off, making it a power-efficient solution.

Blockage is also a major challenge of beam alignment for mmWave communications. At these frequencies, obstacles such as surrounding buildings, people or vehicles can be enough to disrupt or even interrupt narrow beam alignment. Not only that, but the user himself can bring about the same effect just by the way he grips the device or by placing its body between the UE and a gNodeB [77]. This effect is known as self-blockage and works such as [78–80] have attempted to mitigate it by proposing environment-aware codebooks that take into consideration aspects such as the type of hand grip, the application being used and the device's orientation to adjust beam weights on the UE side and minimize the blockage effects. While these

2. PhD project contributions

techniques are shown to boost the spherical coverage of mmWave terminals, its impact on link-performance has been scarcely investigated.

1.3 The need for a common evaluation framework

Despite the multitude of ingenious solutions available in the literature, there is a common denominator in most of these works that prevents them from being compared: a lack of a common evaluation framework for beam management performance. As exemplified in Table 4.1, every work seemingly dedicates a different level of detail to their system model, depending on what the focus of the topic is. This results in studies with very accurate modelling

Table 4.1: System modeling discrepancies in current literature for beam management solutions.

Publication	gNodeB model	UE model	UE mobility	UE rotation	channel model
[68]	single panel	single panel	no	no	3GPP UMi
[70]	single panel	single panel	no	no	LOS/NLOS (2D)
[71]	single panel	omni	data-traffic model	no	3GPP NLOS urban
[74]	isotropic antenna	multi-panel	random waypoint	yes	ray tracing urban
[76]	directional panel	multi-panel	no	yes	ray-tracing indoor

of certain components, such as a ray-tracing propagation environments that, to contain the complexity of the model, simplify other parts of the system like the signalling framework or the antenna patterns considered. This aspect makes it difficult to compare solutions since their performance might be impacted by modelling choices done by the authors. Additionally, if the modelling does not follow the NR standard, it is also difficult to assess its adequacy for future 5G deployments.

With that in mind, this work aims to fill that gap by using a consistent 3GPP-based evaluation framework for all proposed solutions. The simulation tool developed follows the 5G NR specifications for channel modeling, physical layer signals, measurement framework, device design and intra-cell mobility. While some assumptions are defined to keep the study's scope manageable, this thesis presents a body of work that results from a balanced level of detail for a system model built around the standard that future 5G deployments will be based on.

2 PhD project contributions

The work conducted in this PhD project has resulted in two main outcomes:

- Four peer-reviewed publications, briefly motivated and described in Section 2.1, covering different aspects of beam management link-level performance.

- A link-level simulation tool, described shortly in Section 2.2, developed for this project with configurable features such as the network layout, beamforming architecture, signalling, user mobility, device rotation, propagation channel, device modelling and user hand blockage.

The main findings extracted from these studies are compiled in Section 2.3, while Section 2.4 concludes this chapter with a summary of the PhD project's contributions.

2.1 Publications and patents

The main findings of this PhD project are compiled in the following scientific publication list:

Paper A: F. Fernandes, C. Rom, J. Harrebek and G. Berardinelli, "Beam Management in mmWave 5G NR: an Intra-Cell Mobility Study", *IEEE 93rd Vehicular Technology Conference (VTC2021-Spring)*, April 2021.

Paper B: F. Fernandes, C. Rom, J. Harrebek and C. Navarro Manchón, "Improving Beam Management Signalling for 5G NR Systems using Hybrid Beamforming", *IEEE Wireless Communications and Networking Conference (WCNC 2022)*, April 2022.

Paper C: F. Fernandes, C. Rom, J. Harrebek, S. Svendsen and C. Navarro Manchón, "Hand Blockage Impact on 5G mmWave Beam Management Performance", *IEEE Access*, vol. 10, pp. 106033 - 106049, October 2022.

Paper D: F. Fernandes, S. Rezaie, C. Rom, J. Harrebek and C. Navarro Manchón, "Machine Learning-based Millimeter Wave Beam Management for Dynamic Terminal Orientation", **submitted to 2023 IEEE 97th Vehicular Technology Conference: VTC2023-Spring**.

Additionally, a patent was successfully disclosed related to the work pursued in the thesis:

Patent Application 1: C. Rom, B. Vejlggaard, S. Svendsen, S. Carporal del Barrio, F. Fernandes, "Apparatus for transmitting and/or receiving radio frequency signals and method of operating such apparatus", *Published*: January 2023, Nokia Technologies.

This project first focuses on identifying the vulnerabilities and limitations of the current 3GPP-defined beam management procedures. Therefore, **Paper A** results from an initial assessment of beam management's sensitivity to UE mobility, propagation environment, and L1 filtering parametrization. This sensitivity study focuses on how such operational conditions can affect

2. PhD project contributions

the gNodeB's ToS on a beam². This is an important aspect of beam management since the frequency of beam switching must come from a delicate compromise between avoiding too frequent beam switches, along with the resource waste that comes with it, and preventing power deterioration from over-staying a serving beam. **Paper C** carries on the limitation analysis by assessing the impact of user hand blockage on beam management performance for handheld devices when compared to free space. Human influence is an infamous challenge of mmWave propagation, since mmWave signals are known to not easily penetrate objects, including the human body. Since many eMBB applications rely on handheld devices, it is crucial to assess how this affects beam alignment in a realistic context. This work characterizes human blockage through a high-detail electromagnetic model of a directional multi-panel UE with three different types of handgrips.

The knowledge gathered on the vulnerability assessment stage of the project is used to propose alternative solutions to enhance beam management performance. **Paper B** proposes to parallelize the beam sweeping procedure to improve beam selection on the gNodeB side. Using a hybrid beamforming architecture, and relying on the low cross correlation of synchronization signals, simultaneous SSB transmission is enabled to reduce beam alignment overhead and latency. This is particularly useful in high-mobility scenarios where beam information becomes outdated quicker, leading to erroneous beam determination. **Paper D** expands the analysis of outdated beam information to include UE beam selection. It investigates the feasibility of using the measurements made outdated by high-mobility and fast rotation of handheld devices to train a NN capable of inferring the device's rotation pattern and thus predicting the best UE beam.

Finally, it is important to highlight that all publications are based on three modelling assumptions established when defining the scope of this PhD project:

- **Assumption 1:** This body of work assumes a standalone 5G mmWave system configuration, without legacy network integration, operating in FR2's 28 GHz band with a subcarrier spacing of 120 KHz.
- **Assumption 2:** Since beam management occurs within the cell, all studies are conducted at link-level considering a single cell. Moreover, to contain the complexity of the problem at hand, a single user assumption is taken.
- **Assumption 3:** Studies are conducted with an urban propagation environment in mind, such as Urban Micro (UMi) or Urban Macro (UMa),

²A beam's ToS expresses the period of time during which a beam remains as the best serving beam, providing high link quality.

with a cell radius between 100 m and 200 m, to mimic a city street or an open square, which are typical scenarios for mmWave eMBB services.

2.2 Simulation tool

The results presented in all the publications are generated through a Monte Carlo-based simulation tool tailored specifically to assess beam management performance. The simulation tool used was developed by the student during the course of this project (see Appendix for additional details). It is constructed as a link-level evaluation framework for beam management with its main focus on the physical layer domain, to recreate the signalling exchanges and measurements that take place during this process. Shortly put, the gNodeB is modelled to be static, while the UE is characterized as a handheld device travelling linearly in the cell at different speeds, depicting both pedestrian and vehicular mobility scenarios.

Over the span of three years, the simulation tool has been subject to numerous enhancements to reach its current maturity level. However, a clear distinction can be made between implementation stages when it comes to system model complexity. Ultimately, two distinct levels of simulator capabilities can be identified: **Level 1** and **Level 2**.

Level 1

This corresponds to the first stage of development of the simulation tool. At this stage only P1 is implemented, thus only simulating SSB transmissions. The gNodeB is modelled as a single panel of directional antenna arrays equipped with a uniform linear array (ULA), which limits the beamforming to the azimuth domain. Additionally, two different beamforming architectures are considered on the gNodeB side: analog and hybrid, represented in Fig. 4.2. The left side depicts the classical analog beamforming architecture which current beam management procedures for mmWave are based on. The alternative hybrid analog-digital (HAD) beamforming architecture used in this project is shown on the right. This architecture employs both baseband and analog beamforming with a reduced number of TXRU to spatially multiplex up to N_{RF} streams of information. The UE is simply portrayed as a single isotropic antenna. It's linear trajectories can take any direction within the cell, but the device orientation remains the same at all times. Additionally, the available channel environments are mostly LOS-based profiles.

Level 2

In this stage significant improvements on system level detail are introduced to the simulation tool. Although the single panel assumption is kept on the

2. PhD project contributions

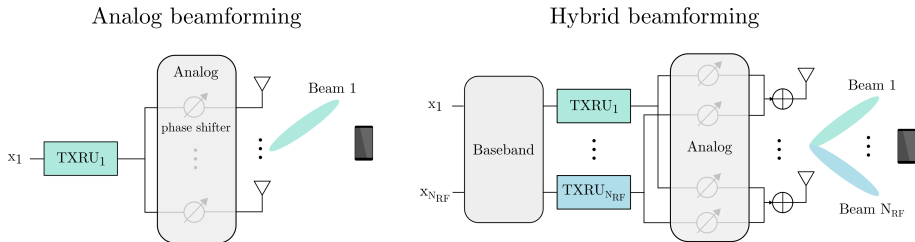


Fig. 4.2: gNodeB beamforming architectures adopted in this project: analog beamforming architecture (left) and HAD fully-connected beamforming architecture (right).

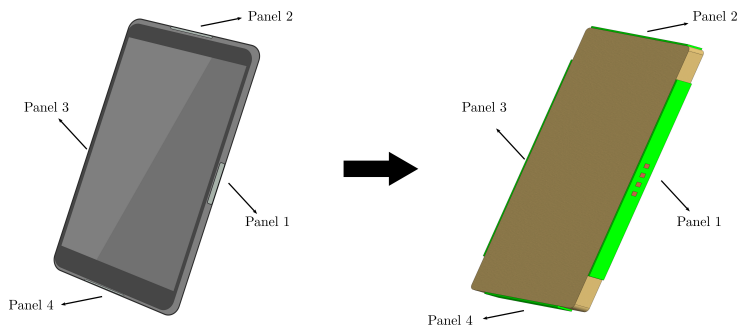
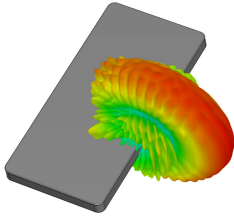


Fig. 4.3: Multi-panel UE design. The screen, glass, plastic case and other components are omitted on the right to highlight the ULA panel placement considered in this project.

gNodeB side, uniform planar array (UPA)s are made available for grid-of-beams (GoB) designs with both elevation and azimuth steering, producing more realistic cell coverage scenarios. On the UE side a more accurate model is included with a multi-panel design, each equipped with directional ULAs, as represented in Fig. 4.3. Since receiver beamforming is integrated, the signalling framework is also completed with configurable CSI-RS transmission to enable P3. To account for user influence, UE rotation is also introduced for all axis of rotation. Initially, this rotation was assumed to be constant throughout a trajectory but, at a later development stage, became feasible on a mid-trajectory basis. User blockage is incorporated as a high-detail electromagnetic model with several different human hand grips, as exemplified in Fig. 4.4. The propagation environments supported include LOS, no line-of-sight (NLOS) and LOS probability [81]. An analog beamforming assumption is kept on the UE side.

The main disparity between these two levels, summarized in Table 4.2, pertains to the model complexity on the UE side. Since Level 1 focuses solely on P1, an omnidirectional model for the UE is sufficient. Level 2, however focuses on P3 integration which requires a more complex UE design, device rotation, introduction of UE-specific signals (CSI-RS) and user blockage.

Free Space Scenario



Right Hand Grip Scenario

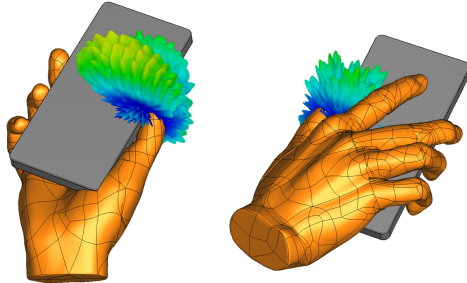


Fig. 4.4: Radiation pattern of a smartphone-integrated antenna array beam both in a free space scenario and a user hand grip scenario.

Table 4.2: Simulation tool capabilities.

Feature	System model Complexity	
	Level 1	Level 2
gNodeB design	1 panel - ULA	1 panel - UPA
gNodeB antenna model	directional [82]	
gNodeB BF architecture	analog/HAD fully-connected	
DL signalling	SSBs	SSB, CSI-RS
Channel environments	LOS variations	LOS, NLOS, mixed
UE design	1 antenna element	multi-panel - ULA
UE antenna model	isotropic	directional [82]
UE BF architecture	analog	
UE mobility	linear trajectories, pedestrian and vehicular speeds	
UE user influence	none	device rotation, user hand blockage

2.3 Main findings

This work initially focuses on uncovering the vulnerabilities of the beam management procedure introduced by 3GPP in Release 15.

Vulnerability analysis

Throughout the studies done in **Papers A-D** it becomes clear that the current approach described in Chapter 3 can be prone to errors in the beam alignment process. These errors, designated as beam misdetections throughout this body of work, do in fact occur under stress factors such as user mobility, device rotation, user blockage and challenging propagation environments.

2. PhD project contributions

Mobility and device rotation: Results indicate that even in predominantly LOS environments with low mobility and slow device rotation misdetections are recorded between 10% to 60% of the time³. Despite more frequent than expected in this close to static scenario, such misdetections are attributed to sub-optimal connections, using beams adjacent to the optimal one, which still provides a good enough link budget for communications. This is common in scenarios where the user is positioned within the coverage area of two adjacent beams that happen to overlap. Naturally, these are not the beam misdetections that threaten the performance of beam management, having little impact on beam alignment performance. Results show that beam misdetections tend to increase in scenarios where a user moves fast through the cell while also rotating the device at a fast pace. In environments where the UE's position and orientation keep changing, the best beam at the time of measurement may no longer be the best one once the sweeping, measurement and reporting cycle is complete, potentially leading to outdated beam information for beam selection. In these scenarios, the performance degradation incurred can become quite large and must be subject to improvements.

It is also evident that mobility and device rotation are two independent processes that affect beam management performance differently. Results indicate that, for slow UE rotation, high speed mobility does not cause additional misdetections on the UE side but increase the number of misdetections on the gNodeB side. In turn, for fast rotating UEs the number of beam misdetection at the UE increases considerably, regardless of speed. Introducing high speed mobility for fast rotating UE's causes increased beam misdetections only on the gNodeB side. In summary, mobility appears to have a larger impact on the gNodeB beam selection while device rotation seems to mostly affect the UE's beam selection. This can be explained by the beamwidths employed on each side of the link, since this work considers a gNodeB antenna array size 16 times larger than the size of the UE panel array, where space constraints are more restrictive. As a result, the narrower beams on the gNodeB side become outdated quicker in high mobility scenarios. The UE beams are wider, thus its beam information will remain accurate for longer, even in high mobility scenarios. However, once fast UE rotation is introduced, this beam information will quickly become outdated as well. Therefore, mobility and device rotation should be taken as two separate but equally important challenges that require distinct solutions to improve the robustness of beam management.

³It is worth noting that beam misdetections are heavily dependent on the type of beam management procedure adopted, beam codebook choices, antenna array sizes and the network layout. Therefore, the wide range of beam misdetection percentages recorded throughout the different publications can be explained by small configuration adjustments done to the simulation environment of each paper. These results should not be taken as absolute values outside this project's limited simulation environment but rather as relative values to compare the effects of each stress factor tested.

User hand blockage: Human blockage is studied in this work through the user's hand grip on the device. The studies conducted in **Paper C** show that the user's hand alone can destroy the original well-behaved shape of the UE panels' radiation patterns. Once a hand is in close proximity to a UE panel, very little energy is able to penetrate the user's skin, mostly slipping through the spaces between the user's fingers or getting reflected on the user's palm. It is also quite clear that each UE panel experiences the blockage source differently. Depending on how the user grips the device, some panels may remain undisturbed while others may even experience different blockage levels on each antenna element of the same panel. Essentially, hand grip blockage can very drastically alter the originally intended UE panel codebook and is highly dependent on factors such as hand grip type, grip tightness and panel placement.

The employed hand grip blockage does negatively affect beam management performance but not as drastically as expected. Its biggest impact occurs for double hand grip scenarios in predominantly LOS environments where the lack of a good alternative path to the blocked panel causes the biggest deterioration to a connection. In other cases, even when a panel is seemingly blocked by the user's hand, it is still possible to sustain a sub-optimal connection with an irregular-shaped beam. However it is still important to model this effect since the beam shape may not behave as theoretically expected leading to unexpected performance degradation or link failure.

It is also worth mentioning that these findings are not reflected in the current 3GPP model in [81] for human blockage which assumes a fixed blockage region with the same flat 30 dB attenuation applied to all panels. This results in harsher power losses over a limited angular region while the rest of the angular space remains unaltered. Consequently, the model in question exhibits overly pessimistic results when compared to this work's beam management performance analysis with hand grip blockage.

Propagation conditions: This project focuses mostly on 3GPP compliant propagation environments for urban scenarios, which include LOS, NLOS and mixed propagation conditions. It is now quite clear that increased angular spread of the channel hurts beam management performance. NLOS conditions display the harshest propagation conditions with very low received power levels. This causes a considerable increase of beam misdetections when compared to LOS, since the measurement-based beam management procedure struggles to find the best beam when all beams display similar low performance. However it is also observed that the effects of human blockage in environments without a clear dominant path are less severe. In NLOS conditions the second best path to a blocked panel is much closer to the best than in LOS, making the blockage effect appear less damaging.

2. PhD project contributions

Enhancement proposals

Results indicate that improvements are necessary to the currently available beam management framework to adequately support challenging conditions such as high speeds, user blockage or device rotation. The procedure must be precise to meet the link budget requirements of mmWave communications but also swift enough to keep up with all the dynamic changes in the environment. The solutions proposed in this body of work focus primarily on mitigating the effects of out of date beam information due to the procedure's inability to collect timely measurements in dynamic scenarios. Two proposals are presented in **Paper B** and **Paper D** to improve beam alignment performance, one implemented on the gNodeB side and the other on the UE side.

Parallelization of SSB transmission: The feasibility of simultaneously transmitting spatially multiplexed SSBs using low-cross correlation signals and HAD beamforming is investigated in **Paper B**. Results confirm that parallelizing the beam sweeping portion of beam management is feasible with small adjustments to the pre-existing signalling framework and can successfully improve beam management performance. Since it overlaps the SSB resources in time and frequency, this solution allows for the use of larger codebooks with a significantly lower overhead, improving coverage and thus beam alignment performance. Moreover, this strategy is shown to be particularly helpful in high-speed mobility scenarios since it reduces the latency of the beam sweeping and measurement stages, making it less likely for the beam determination stage to be done based on outdated beam information.

ML processing of outdated beam information: Instead of preventing outdated beam measurements, the solution in **Paper D** explores the potential of leveraging them in a deep NN to predict the best beam selection for a UE under dynamic orientation conditions. Results indicate that this approach can successfully infer the UE's orientation, and thus select its best beam, solely through RSRP measurements, without requiring any context information like other works in the literature. This solution is the most useful in dominant LOS environments with fast rotating UEs. In NLOS environments it is shown to lose efficacy, likely due to the significantly lower received signal strength recorded in environments with larger angular spread, making all the RSRP measurements closer in terms of power and hence more difficult for the NN to distinguish. Therefore, further investigation would be needed to take this solution from a proof-of-concept study to reality.

2.4 Summary of Contributions

The publications listed in Section 2.1 offer two types of contributions to the current state-of-art towards a robust beam management procedure for mmWave: **Vulnerability analysis** and **Enhancement proposals**. As hinted above, the research conducted in this thesis follows an incremental approach on the considered system model. Initially, a simple but 3GPP compliant beam management framework was designed for the first research problem (**Paper A**), unencumbered by excessive modelling details that could disguise the performance effects of each evaluated component like speed or angular spread. Once the target areas became clearer and the impact level of each component was gauged, the modelling gradually expanded to include details relevant to the research problems tackled in the thesis. In other words, the implementation levels described above can directly be mapped to each scientific paper in the publication list: While **Paper A** and **Paper B** result from **Level 1**, the simplest stage of the simulator's development, **Paper C** and **Paper D** are a product of the most mature stage of development of the simulator, **Level 2**⁴.

Fig. 4.5 displays a summary of the contributions' categorization and the main findings of this project. This body of work offers a solid contribution to the topic of mmWave beam management for 5G NR by not only identifying some of its most prominent challenges but also proposing solutions to improve its performance.

⁴It is important to note that mapping a paper to a certain system complexity level does not necessarily imply that all the available features are utilized. As an example, **Paper C** employs the user hand blockage and device rotation features in Level 2 while **Paper D** focuses solely on the device rotation feature.

2. PhD project contributions

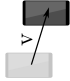

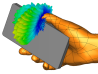
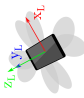
Contribution Type	
Vulnerability analysis	Enhancement proposal
<p>Paper A: intra-cell mobility affects beam management performance</p>  <ul style="list-style-type: none"> ◦ Narrow beams → small ToS (frequent beam switches). ◦ Large speed & angular spread → reduced ToS. ◦ Trade-off: extend ToS vs. performance degradation. 	<p>Paper B: Parallelization of SSB transmission with HAD beamforming</p>  <ul style="list-style-type: none"> ◦ Beam sweeping is vulnerable to mobility. ◦ Outdated beam measurements → beam misalignment. ◦ Parallelizing SSB transmissions: reduced procedure latency and overhead.
<p>Paper C: user hand grip affects beam management performance</p>  <ul style="list-style-type: none"> ◦ User's hand → UE codebook beam shape distortion. ◦ Blockage severity dependent on the type of hand grip. ◦ 3GPP self-blockage model: does not capture these effects. 	<p>Paper D: ML processing of outdated beam measurements</p>  <ul style="list-style-type: none"> ◦ Multi-panel UEs → increased beam alignment complexity. ◦ Dynamic device orientation → outdated beam measurements. ◦ NN training with outdated measurements: accurate UE beam selection prediction for LOS scenarios.
Level 1	
Level 2	
System Model Complexity	

Fig. 4.5: Contribution categorization and summary of main findings.

Chapter 5

Final Remarks

1 Conclusions

This project takes a critical look at the current 3GPP beam management framework for mmWave, setting out to uncover the vulnerabilities of the current process, as well as its potential for enhancements in challenging propagation environments.

Vulnerability study

As initially conjectured in this project's research questions, there are identifiable stress factors that jeopardize beam management's performance such as user mobility, device rotation, user blockage and difficult propagation conditions. The limitations of the current sweeping and measurement-based procedure are clearly highlighted in scenarios of both high mobility and fast device rotation. In such dynamic environments the beam information collected through sequential measurements quickly becomes outdated before beam selection can take place, resulting in beam misalignments between the gNodeB and UE, ultimately leading to significant performance degradation.

Additionally, it is shown that user-induced human blockage, which to date has been mostly neglected in beam management studies, is capable of destroying the original directive nature of UE beams. This is an important finding since the originally designed UE codebook may be compromised just by how the user grips the device during a video call or while gaming, making beam alignment even more challenging. Results show that hand grip blockage does have a negative impact on beam alignment, particularly in LOS scenarios with a dual hand grip, but not as significant as expected in other tested cases. This suggests that an irregular beam shape caused by a blocked panel may still be able to uphold a connection and that loosing the beam shape

due to blockage doesn't always equate to losing the beam's gain. However one must consider that the effect of the user's head and torso is not captured in this study, which may cause additional signal degradation. Moreover, this work does not explore maximum permissible exposure (MPE)-triggered power backoff on the UE side. If a panel is blocked by the user's body, a power backoff may be required for UL communications in order to meet MPE requirements. Therefore, even if a blocked panel is capable of providing a good connection, it may still need to comply with this safety limitation, further degrading the performance shown in the studies performed in this work. The impact of hand grip blockage on beam management performance is also compared with its 3GPP counterpart, exposing this model's inadequacy for properly depicting human blockage in link-level beam management evaluations. While such a model may be more than fitting for system-level studies, where a highly detailed blockage modelling may lead to excessive computational load, it is crucial to establish an additional, more nuanced model of human blockage on a per-panel basis that can be used to design solutions capable of circumventing human blockage challenges.

Furthermore, it becomes evident that increased angular spread of the channel manifests negatively in beam management performance. In other words, beam misdetections tend to increase significantly in urban environments when transitioning from a predominantly LOS environment to a NLOS environment, where power often drops drastically to the point of certain link failure. However, such results also raise a valid concern on how realistic the current 3GPP channel model is for mmWave. The 3GPP channel models detailed in both [81] and [83] are based on legacy sub-6 GHz results with some modifications to fit the spectrum beyond 6 GHz until 100 GHz. This approach has been challenged in the literature by works such as [84] that claim, among other modelling details, that the number of clusters in the 3GPP model are unrealistically large for both LOS and NLOS conditions, without actual real-life measurements to support it. This suggests that the vulnerability studies of mmWave beam management conducted in this work could look considerably different if instead a model with a lower number of clusters had been used to characterize NLOS conditions.

In conclusion, the current 5G beam management framework is capable of providing sub optimal, yet acceptable, link level performance for a large portion of the time. However, the occasions where the procedure does underperform can lead to significant link quality degradation and should be improved upon. Furthermore, future 5G and 6G releases will continue to explore higher frequencies which are accompanied by larger codebooks with even narrower beams. This will make the system even more vulnerable to the stress factors studied in this work, making the current beam management implementation impractical.

1. Conclusions

Enhancement proposals

A large portion of time was invested during this project to develop solutions that could mitigate the problems identified during the vulnerability assessment stage. Both solutions presented in this thesis take different approaches to the outdated measurement issue and are shown to successfully improve performance while still being able to be introduced in the current procedure without major changes to the NR standard.

It is worth mentioning that the feasibility of the solution proposed in **Paper B** stands on the assumption that the parallel transmission of SSBs is done with orthogonal signals to allow for proper decoding of the overlapped SSBs at reception. Therefore, this work considers that each SSB sent in parallel must be associated to an unique PSS and SSS combination, which are low cross-correlated sequences. While other signal coding alternatives can be pursued to meet such a requirement, this is out of scope for this paper, which aims instead to investigate whether such an approach would be possible or even effective in improving beam management performance.

Additionally, both solutions are shown to improve beam management performance without the assistance of any additional information sources. However, the usage of context information was explored during **Paper D**, particularly for the NLOS scenario where the efficacy of the proposed solution was reduced. While not included in this publication due to a page limitation, positioning and orientation-aided alternatives were investigated, yielding little to no gain over the baseline solution. However the dataset size employed was approximately the same as in this study, which is notably smaller than the dataset sizes taken in [67] and [74]. This further shows that there is a trade-off between data load/complexity and beam alignment performance when it comes to ML-based solutions for beam management that must be carefully considered on a scenario basis. Therefore, the answer to the research question posed in **RQ2-b** remains incomplete at the end of this project, requiring further investigation efforts.

Something that is left unexplored due to a time limitation is the impact of user blockage in the efficacy of ML-based solutions like the one proposed in **Paper D**. One could argue that the countless different grips that may be used to handle the device would make it impossible for a NN to accurately anticipate the best UE beam, since the beams would continuously change shape in close to unpredictable ways. Furthermore, it is important to acknowledge that models will always have limitations and developing realistic depictions of user mobility, device rotation, user influence and NLOS conditions in urban environments may become unfeasible. Perhaps the best option may be to collect as much data as possible from the environment and rely on data-driven approaches to ensure the feasibility of mmWave communications in future deployments.

Finally, it bears mentioning that the conclusions drawn from this project are limited to the complexity of the model employed. As an example, factors such as interference or vehicular blockage were not explored, due to the project's time restrictions, but could also be relevant to assess the feasibility of narrow beam alignment in urban environments. Therefore, this is a topic that still welcomes further investigation.

2 Outlook

Since its introduction in Release 15, mmWave has established a prominent role in the NR standard, making beam management a flourishing topic with several promising research avenues left to explore [85]. In fact, following this project, the student can pinpoint certain areas of interest that could be pursued in future studies:

- **System-level studies:** Firstly, the study conducted in this thesis should be extended to a system-level study that includes multiple cells and users. Additionally, other types of blockage like buildings and vegetation should be considered, which are shown to also hinder mmWave propagation. This would extend the beam management scope to include issues such as beam tracking and handovers between cells, allowing to assess how the issues found in this thesis regarding mobility, device rotation and user blockage would impact a full system level network performance.
- **User blockage:** This project concludes that user blockage will be a significant hindrance for mmWave communications in handheld devices. While this work explores the user hand impact on beam management performance, future work is required on characterizing the rest of the user's body blockage and finding mitigating solutions for this issue. These could include distributed antennas over the device to make reception more robust to a user's hand grip, developing ML-based algorithms for panel switching, among others.
- **TeraHertz communications:** The issue of beam alignment gets carried into 6G with the transition to Terahertz frequencies, a crucial step to continue to support the ever increasing number of data-hungry users in future deployments. Among other new challenges, many of the same problems discussed in this work will be encountered and likely heightened, due to the razor-sharp beams created by the colossal sizes of antenna arrays used to overcome the limited transmission range issues [86–88]. This is a new topic that requires attention and possibly new innovative solutions to unlock its potential, some of which include intelligent reflective surfaces and deep-learning methods [89].

- **Potential of ML:** 6G is currently being envisioned to integrate localization and sensing information with mobile communication functionalities [90–92]. In other words, it may be possible to employ infrastructure-mounted sensors to aid, among other applications, beam management for vehicular mmWave communications [93]. This unprecedented access to copious amounts of context information could be exploited through data-driven solutions like ML not only to reduce beam alignment overhead but also to potentially predict user blockage or anticipate NLOS conditions.

References

- [1] A. F. Molisch. *Wireless Communications*. John Wiley & Sons, 1st edition, 2005.
- [2] H. Holma and A. Toskala, editors. *LTE-Advanced 3GPP solutions for IMT-Advanced*. John Wiley & Sons, 1st edition, 2012.
- [3] B. K. Wiederhold. "Using Social Media to Our Advantage: Alleviating Anxiety During a Pandemic". *Cyberpsychology, Behavior, and Social Networking*, 23(4):197 – 198, 2020.
- [4] M. Enescu, editor. *5G New Radio: A Beam-based Air Interface*. John Wiley & Sons, 1st edition, 2020.
- [5] Qualcomm. "Making 5G NR a reality: Leading the technology inventions for a unified, more capable 5G air interface". White paper, 2016.
- [6] ITU-R. "IMT Vision – Framework and overall objectives of the future development of IMT for 2020 and beyond". Rec. ITU-R M.2083-0, International Telecommunication Union (ITU), 2015.
- [7] M. Kottkamp, A. Pandey, A. Roessler, R. Stuhlfauth, and D. Raddino. *5G New Radio - Fundamentals, Procedures, Testing Aspects*. Rohde & Schwarz GmbH & Co. KG, 4th edition, 2019.
- [8] Ericsson. "Ericsson Mobility Report". White paper, June 2022.
- [9] Qualcomm and Nokia. "Making 5G NR a reality: Addressing the Strong Mobile Broadband". White paper, 2017.
- [10] J. G. Andrews, S. Buzzi, W. Choi, S. V. Hanly, A. Lozano, A. C. K. Soong, and J. C. Zhang. "What Will 5G Be?". *IEEE Journal on Selected Areas in Communications*, 32(6):1065 – 1082, 2014.

- [11] I. A. Hemadeh, K. Satyanarayana, M. El-Hajjar, and L. Hanzo. "Millimeter-Wave Communications: Physical Channel Models, Design Considerations, Antenna Constructions, and Link-Budget". *IEEE Communications Surveys & Tutorials*, 20(2):870 – 913, 2018.
- [12] H. T. Friis. "A Note on a Simple Transmission Formula". *Proceedings of the I.R.E. and Waves and Electrons*, 34(5):254 – 256, 1946.
- [13] T. S. Rappaport, R. W. Heath, R. C. Daniels, and J. N. Murdock. *Millimeter Wave Wireless Communications*. Pearson, 1st edition, 2021.
- [14] 3GPP. NR; Base Station (BS) radio transmission and reception (Release 17). Tech. Spec. 38.104, V17.6.0 2022.
- [15] 3GPP. Study on new radio access technology Physical layer aspects (Release 14). Tech. Rep. 38.802, V14.2.0 2017.
- [16] Y. Heng, J. G. Andrews, J. Mo, V. Va, A. Ali, B. L. Ng, and J. C. Zhang. "Six Key Challenges for Beam Management in 5.5G and 6G Systems". *IEEE Communications Magazine*, 59(7):74 – 79, 2021.
- [17] K. Zhao, J. Helander, D. Sjoberg, S. He, T. Bolin, and Z. Ying. "User Body Effect on Phased Array in User Equipment for the 5G mmWave Communication System". *IEEE Antennas and Wireless Propagation Letters*, 16:864 – 867, 2016.
- [18] K. Zhao, C. Gustafson, Q. Liao, S. Zhang, T. Bolin, Z. Ying, and S. He. "Channel Characteristics and User Body Effects in an Outdoor Urban Scenario at 15 and 28 GHz". *IEEE Transactions on Antennas and Propagation*, 65(12):6534 – 6548, 2017.
- [19] K. Zhao, S. Zhang, Z. Ho, O. Zander, T. Bolin, Z. Ying, and G. F. Pedersen. "Spherical Coverage Characterization of 5G Millimeter Wave User Equipment With 3GPP Specifications". *IEEE Access*, 7:4442 – 4452, 2018.
- [20] 3GPP. NR; NR and NG-RAN Overall description; Stage-2 (Release 17). Tech. Spec. 38.300, V17.1.0 2022.
- [21] C. Johnson. *5G New Radio in Bullets*. Independently published, 1st edition, 2019.
- [22] M. Giordani, M. Polese, A. Roy, D. Castor, and M. Zorzi. "A Tutorial on Beam Management for 3GPP NR at mmWave Frequencies". *IEEE Communications Surveys and Tutorials*, 21(1):173 – 196, 2019.
- [23] 3GPP. NR; Physical channels and modulation (Release 17). Tech. Spec. 38.211, V17.2.0 2022.

References

- [24] 3GPP. NR; Physical layer procedures for control (Release 16). Tech. Spec. 38.213, V16.6.0 2021.
- [25] 3GPP. NR; Physical layer measurements (Release 17). Tech. Spec. 38.215, V17.2.0 2022.
- [26] P. Smulders. "Exploiting the 60 GHz Band for Local Wireless Multi-media Access: Prospects and Future Directions". *IEEE Communications Magazine*, 40(1):140 – 147, 2002.
- [27] A. Ghosh, A. Maeder, M. Baker, and D. Chandramouli. "5G Evolution: A View on 5G Cellular Technology Beyond 3GPP Release 15". *IEEE Access*, 7:127639 – 127651, 2019.
- [28] T. Baykas, C.-S. Sum, Z. Lan, J. Wang, M. A. Rahman, , and H. Harada. "IEEE 802.15.3c: The First IEEE Wireless Standard for Data Rates over 1 Gb/s". *IEEE Communications Magazine*, 49(7):114 – 121, 2011.
- [29] T. Nitsche, C. Cordeiro, A. B. Flores, E. W. Knightly, E. Perahia, and J. C. Widmer. "IEEE 802.11ad: Directional 60 GHz Communication for Multi-Gigabit-per-Second Wi-Fi". *IEEE Communications Magazine*, 52(12):132 – 141, 2014.
- [30] Y. Ming Tsang, Ada S. Y. Poon, and S. Addepalli. "Coding the Beams: Improving Beamforming Training in mmWave Communication System". *2011 IEEE Global Telecommunications Conference - GLOBECOM 2011*, pages 1 – 6, 2011.
- [31] R. R. Choudhury and N. H. Vaidya. "Deafness: a MAC problem in ad hoc networks when using directional antennas". *Proceedings of the 12th IEEE International Conference on Network Protocols*, pages 1 – 10, 2004.
- [32] J. Wang, Z. Lan, C.-W. Pyo, T. Baykas, C.-S. Sum, M. A. Rahman, J. Gao, R. Funada, F. Kojima, H. Harada, and S. Kato. "Beam Codebook Based Beamforming Protocol for Multi-Gbps Millimeter-Wave WPAN Systems". *IEEE Journal on Selected Areas in Communications*, 27(8):1390 – 1399, 2009.
- [33] S. Singh, F. Ziliotto, U. Madhow, E. M. Belding, and M. Rodwell. "Blockage and Directivity in 60 GHz Wireless Personal Area Networks: From Cross-Layer Model to Multihop MAC Design". *IEEE Journal on Selected Areas in Communications*, 27(8):1400 – 1413, 2009.
- [34] K. Chandra, R. V. Prasad, I. G. M. M. Niemegeers, and A. R. Biswas. "Adaptive Beamwidth Selection for Contention Based Access Periods in Millimeter Wave WLANs". *2014 IEEE 11th Consumer Communications and Networking Conference (CCNC)*, pages 458 – 464, 2014.

- [35] Z. Pi and F. Khan. "An Introduction to Millimeter-Wave Mobile Broadband Systems". *IEEE Communications Magazine*, 49(6):101 – 107, 2011.
- [36] S. Sun, T. S. Rappaport, R. W. Heath, A. Nix, and S. Rangan. "MIMO for Millimeter-Wave Wireless Communications: Beamforming, Spatial Multiplexing, or Both?". *IEEE Communications Magazine*, 52(12):110 – 121, 2014.
- [37] W. Roh, J.-Y. Seol, J. Park, B. Lee, J. Lee, Y. Kim, J. Cho, K. Cheun, and F. Aryanfar. "Millimeter-Wave Beamforming as an Enabling Technology for 5G Cellular Communications: Theoretical Feasibility and Prototype Results". *IEEE Communications Magazine*, 52(2):106 – 113, 2014.
- [38] T. S. Rappaport, S. Sun, R. Mayzus, H. Zhao, Y. Azar, K. Wang, G. N. Wong, J. K. Schulz, M. Samimi, and F. Gutierrez. "Millimeter Wave Mobile Communications for 5G cellular: It will work!". *IEEE Access*, 1:335 – 349, 2013.
- [39] T. S. Rappaport, J. N. Murdock, and F. Gutierrez. "State of the Art in 60-GHz Integrated Circuits and Systems for Wireless Communications". *Proceedings of the IEEE*, 99(8):1390 – 1436, 2011.
- [40] J. N. Murdock, E. Ben-Dor, Y. Qiao, J. I. Tamir, and T. S. Rappaport. "A 38 GHz Cellular Outage Study for an Urban Outdoor Campus Environment". *2012 IEEE Wireless Communications and Networking Conference (WCNC)*, pages 3085 – 3090, 2012.
- [41] T. S. Rappaport, F. Gutierrez, E. Ben-Dor, J. N. Murdock, Y. Qiao, and J. I. Tamir. "Broadband Millimeter-Wave Propagation Measurements and Models Using Adaptive-Beam Antennas for Outdoor Urban Cellular Communications". *IEEE Communications Magazine*, 61(4):1850–1859, 2013.
- [42] H. Zhao, R. Mayzus, S. Sun, M. Samimi, J. K. Schulz, Y. Azar, K. Wang, G. N. Wong, F. Gutierrez, and T. S. Rappaport. "28 GHz Millimeter Wave Cellular Communication Measurements for Reflection and Penetration Loss in and around Buildings in New York City". *2013 IEEE International Conference on Communications (ICC)*, pages 5163 – 5167, 2013.
- [43] T. Bai and R. W. Heath. "Coverage and Rate Analysis for Millimeter-Wave Cellular Networks". *IEEE Transactions on Wireless Communications*, 14(2):1100 – 1114, 2015.
- [44] Q. C. Li, H. Niu, G. Wu, and R. Q. Hu. "Anchor-booster based heterogeneous networks with mmWave capable booster cells". *2013 IEEE Globecom Workshops (GC Wkshps)*, pages 93 – 98, 2013.

References

- [45] C. N. Barati, S. A. Hosseini, S. Rangan, P. Liu, T. Korakis, S. S. Panwar, and Theodore S. Rappaport. "Directional Cell Discovery in Millimeter Wave Cellular Networks". *IEEE Transactions on Wireless Communications*, 14(12):6664 – 6678, 2015.
- [46] C. N. Barati, S. A. Hosseini, S. Rangan, P. Liu, T. Korakis, and S. S. Panwar. "Directional Cell Search for Millimeter Wave Cellular Systems". *2014 IEEE 15th International Workshop on Signal Processing Advances in Wireless Communications (SPAWC)*, pages 120 – 124, 2014.
- [47] C. N. Barati, S. A. Hosseini, M. Mezzavilla, P. Amiri-Eliasi, S. Rangan, T. Korakis, S. S. Panwar, and M. Zorzi. "Directional Initial Access for Millimeter Wave Cellular Systems". *2015 49th Asilomar Conference on Signals, Systems and Computers*, pages 307 – 311, 2015.
- [48] C. N. Barati, S. A. Hosseini, M. Mezzavilla, T. Korakis, S. S. Panwar, S. Rangan, and M. Zorzi. "Initial Access in Millimeter Wave Cellular Systems". *IEEE Transactions on Wireless Communications*, 15(12):7926 – 7940, 2016.
- [49] C. Jeong, J. Park, and H. Yu. "Random Access in Millimeter-Wave Beamforming Cellular Networks: Issues and Approaches". *IEEE Communications Magazine*, 53(1):180 – 185, 2015.
- [50] J. Kim and A. F. Molisch. "Fast Millimeter-Wave Beam Training with Receive Beamforming". *Journal of Communications and Networks*, 16(5):512 – 522, 2014.
- [51] V. Desai, L. Krzymien, P. Sartori, W. Xiao, A. Soong, and A. Alkhateeb. "Initial beamforming for mmWave communications". *2014 48th Asilomar Conference on Signals, Systems and Computers*, pages 1926 – 1930, 2014.
- [52] M. Giordani, M. Mezzavilla, C. N. Barati, S. Rangan, and M. Zorzi. "Comparative analysis of initial access techniques in 5G mmWave cellular networks". *2016 Annual Conference on Information Science and Systems (CISS)*, pages 1 – 6, 2016.
- [53] L. Wei, Q. C. Li, and G. Wu. "Exhaustive, Iterative and Hybrid Initial Access Techniques in mmWave Communications". *2017 IEEE Wireless Communications and Networking Conference (WCNC)*, pages 1 – 6, 2017.
- [54] A. Alkhateeb, Y.-H. Nam, Md. S. Rahman, J. Zhang, and R. W. Heath. "Initial Beam Association in Millimeter Wave Cellular Systems: Analysis and Design Insights". *IEEE Transactions on Wireless Communications*, 16(5):2807 – 2821, 2017.

- [55] Y. Li, J. G. Andrews, F. Baccelli, T. D. Novlan, and C. J. Zhang. "Design and Analysis of Initial Access in Millimeter Wave Cellular Networks". *IEEE Transactions on Wireless Communications*, 16(10):6409 – 6425, 2017.
- [56] Y. Li, J. Luo, M. H. Castañeda Garcia, R. Böhnke, R. A. Stirling-Gallacher, W. Xu, and G. Caire. "On the Beamformed Broadcasting for Millimeter Wave Cell Discovery: Performance Analysis and Design Insight". *IEEE Transactions on Wireless Communications*, 17(11):7620 – 7634, 2018.
- [57] J. Choi. "Beam Selection in mm-Wave Multiuser MIMO Systems Using Compressive Sensing". *IEEE Transactions on Communications*, 63(8):2936 – 2947, 2015.
- [58] M. Rani, S. B. Dhok, and R. B. Deshmukh. "A Systematic Review of Compressive Sensing: Concepts, Implementations and Applications". *IEEE Access*, 6:4875 – 4894, 2018.
- [59] M. Giordani, M. Mezzavilla, and M. Zorzi. "Initial Access in 5G mmWave Cellular Networks". *IEEE Communications Magazine*, 54(11):40–47, 2016.
- [60] A. Capone, I. Filippini, V. Sciancalepore, and D. Tremolada. "Obstacle Avoidance Cell Discovery using mm-waves Directive Antennas in 5G Networks". *2015 IEEE 26th Annual International Symposium on Personal, Indoor, and Mobile Radio Communications (PIMRC)*, pages 2349 – 2353, 2015.
- [61] W. Abbas and M. Zorzi. "Context Information Based Initial Cell Search for Millimeter Wave 5G Cellular Networks". *2016 European Conference on Networks and Communications (EuCNC)*, pages 1–6, 2016.
- [62] I. Filippini, V. Sciancalepore, F. Devoti, and A. Capone. "Fast Cell Discovery in mm-Wave 5G Networks with Context Information". *IEEE Transactions on Mobile Computing*, 17(7):1538 – 1552, 2018.
- [63] N. González-Prelcic, A. Ali, V. Va, and R. W. Heath. "Millimeter-Wave Communication with Out-of-Band Information". *IEEE Communications Magazine*, 55(12):140 – 146, 2017.
- [64] A. Ali, N. González-Prelcic, and R. W. Heath. "Millimeter Wave Beam-Selection Using Out-of-Band Spatial Information". *IEEE Transactions on Wireless Communications*, 17(2):1038 – 1052, 2018.
- [65] A. Klautau, P. Batista, N. González-Prelcic, Y. Wang, and Robert W. Heath. "5G MIMO Data for Machine Learning: Application to Beam-Selection Using Deep Learning". *2018 Information Theory and Applications Workshop (ITA)*, pages 1 – 9, 2018.

References

- [66] L. Wei, Q. C. Li, and G. Wu. "Initial Access Techniques for 5G NR: Omni/Beam SYNC and RACH designs". *2018 International Conference on Computing, Networking and Communications (ICNC)*, pages 249 – 253, 2018.
- [67] A. Ali, J. Mo, B. L. Ng, V. Va, and J. C. Zhang. "Orientation-Assisted Beam Management for Beyond 5G Systems". *IEEE Access*, 9:51832 – 51846, 2021.
- [68] I. Ayakin and M. Krunz. "Efficient Beam Sweeping Algorithms and Initial Access Protocols for Millimeter-Wave Networks". *IEEE Transactions on Wireless Communications*, 19(4):2504 – 2514, 2020.
- [69] G. C. Alexandropoulos, I. Vinieratou, M. Rebato, L. Rose, and M. Zorzi. "Uplink Beam Management for Millimeter Wave Cellular MIMO Systems with Hybrid Beamforming". *2021 IEEE Wireless Communications and Networking Conference (WCNC)*, pages 1–7, 2021.
- [70] S. Tomasin, C. Mazzucco, D. De Donno, and F. Cappellaro. "Beam-Sweeping Design Based on Nearest Users Position and Beam in 5G mmWave Networks". *IEEE Access*, 8:124402 – 124413, 2020.
- [71] H. Soleimani, R. Parada, S. Tomasin, and M. Zorzi. "Fast Initial Access for mmWave 5G Systems with Hybrid Beamforming Using On-line Statistics Learning". *IEEE Communications Magazine*, 57(9):132 – 137, 2019.
- [72] Y.-N. R. Li, B. Gao, X. Zhang, and K. Huang. "Beam Management in Millimeter-Wave Communications for 5G and Beyond". *IEEE Access*, 8:13282 – 13293, 2020.
- [73] "Study on Artificial Intelligence (AI)/Machine Learning (ML) for NR Air Interface". - RP-213599, 3GPP TSG RAN Meeting #94e, May 2022.
- [74] K. N. Nguyen, A. Ali, J. Mo, B. L. Ng, V. Va, and J. C. Zhang. "Beam Management with Orientation and RSRP using Deep Learning for Beyond 5G Systems". *2022 IEEE International Conference on Communications Workshops (ICC Workshops)*, pages 133 – 138, 2022.
- [75] S. Rezaie, C. Navarro Manchón, and E. De Carvalho. "Location- and Orientation-Aided Millimeter Wave Beam Selection Using Deep Learning". *ICC 2020 - 2020 IEEE International Conference on Communications (ICC)*, pages 1 – 6, 2020.
- [76] S. Rezaie, J. Morais, E. de Carvalho, A. Alkhateeb, and C. Navarro Manchón. "Location- and Orientation-aware Millimeter Wave Beam Selection for Multi-Panel Antenna Devices". *arXiv:2203.11714v1*, pages 1–5, 2022.

- [77] V. Raghavan, S. Noimanivone, S. K. Rho, B. Farin, P. Connor, R. A. Motos, Y. C. Ou, K. Ravid, M. A. Tassoudji, O. H. Koymen, and J. Li. "Hand and Body Blockage Measurements With Form-Factor User Equipment at 28 GHz". *IEEE Transactions on Antennas and Propagation*, 70(1):607 – 620, 2022.
- [78] A. Alammouri, J. Mo, B. L. Ng, J. C. Zhang, and J. G. Andrews. "Hand Grip Impact on 5G mmWave Mobile Devices". *IEEE Access*, 7:60532 – 60544, 2019.
- [79] J. Mo, B. L. Ng, S. Chang, P. Huang, M. N. Kulkarni, A. Alammouri, J. C. Zhang, J. Lee, and W.-J. Choi. "Beam Codebook Design for 5G mmWave Terminals". *IEEE Access*, 7:98387 – 98404, 2019.
- [80] V. Raghavan, R. A. Motos, M. A. Tassoudji, Y.-C. Ou, O. H. Koymen, and J. Li. "Mitigating Hand Blockage with Non-Directional Beamforming Codebooks", 2021. arXiv:2104.06472v1 [cs.IT].
- [81] 3GPP. Study on channel model for frequencies from 0.5 to 100 GHz (Release 17). Tech. Rep. 38.901, V17.0.0 2022.
- [82] 3GPP. Study on new radio access technology: Radio Frequency (RF) and co-existence aspects (Release 14). Tech. Rep. 38.803, V14.3.0 2022.
- [83] 3GPP. Study on channel model for frequency spectrum above 6 GHz (Release 15). Tech. Rep. 38.900, V15.0.0 2018.
- [84] T. S. Rappaport, S. Sun, and M. Shafi. "Investigation and Comparison of 3GPP and NYUSIM Channel Models for 5G Wireless Communications". *2017 IEEE 86th Vehicular Technology Conference (VTC-Fall)*, pages 1 – 5, 2017.
- [85] J. Bang, H. Chung, J. Hong, H. Seo, J. Choi, and S. Kim. "Millimeter-Wave Communications: Recent Developments and Challenges of Hardware and Beam Management Algorithms". *IEEE Communications Magazine*, 59(8):86–92, 2021.
- [86] Y. Chen and C. Han. "Razor-sharp Narrowbeam Communications and Management for Terahertz Wireless Networks". *2021 Computing, Communications and IoT Applications (ComComAp)*, pages 335–340, 2021.
- [87] W. Attaoui, K. Bouraqia, and E. Sabir. "Initial Access Beam Alignment for mmWave and Terahertz Communications". *IEEE Access*, 10:35363–35397, 2022.
- [88] H.-J. Song and N. Lee. "Terahertz Communications: Challenges in the Next Decade". *IEEE Transactions on Terahertz Science and Technology*, 12(2):105–117, 2022.

References

- [89] P. Wang, J. Fang, and W. Zhang. "Fast Beam Training and Alignment for IRS-Assisted Millimeter Wave/Terahertz Systems". *IEEE Transactions on Wireless Communications*, 21(4):2710–2724, 2022.
- [90] A. Ali, N. González-Prelcic, R. W. Heath, and A. Ghosh. "Leveraging Sensing at the Infrastructure for mmWave Communication". *IEEE Communications Magazine*, 58(7):84–89, 2020.
- [91] T. Wild, V. Braun, and H. Viswanathan. "Joint Design of Communication and Sensing for beyond 5G and 6G Systems". *IEEE Access*, 9:30845–30857, 2021.
- [92] H. Wymeersch, D. Shrestha, C. Morais de Lima, V. Yajnanarayana, B. Richerzhagen, M. F. Keskin, K. Schindhelm, A. Ramirez, A. Wolfgang, M. Francis de Guzman, K. Haneda, T. Svensson, R. Baldemair, and S. Parkvall. "Integration of Communication and Sensing in 6G: a Joint Industrial and Academic Perspective". *2021 IEEE 32nd Annual International Symposium on Personal, Indoor and Mobile Radio Communications (PIMRC)*, pages 1–7, 2021.
- [93] W. Chen, L. Li, Z. hen, T. Quek, and S. Li. "Enhancing THz/mmWave Network Beam Alignment With Integrated Sensing and Communication". *IEEE Communications Letters*, 26(7):1698–1702, 2022.
- [94] S. Jaeckel, L. Raschkowski, K. Börner, and L. Thiele. "QuaDRiGa: A 3-D Multicell Channel Model with Time Evolution for Enabling Virtual Field Trials". *IEEE Transactions on Antennas Propagation*, 62(6):3242 – 3256, 2014.
- [95] Dassault Systemes. CST Microwave Studio.
- [96] MathWorks. 5G Toolbox.

Appendix - Simulation Tool

This project employs a link-level Monte Carlo-based simulation tool built by the student with a focus on DL beam management performance. It focuses mainly on the physical layer domain, recreating the DL signalling transmissions and measurements that take place during beam alignment. This MATLAB-based simulation tool requires functionalities from three different tools to achieve this: QUAsi Deterministic RadIo channel GenerA-tor (QuaDRiGa), MATLAB[®] and CST Microwave Studio[®]. The tool is also configurable, supporting several tunable parameters such as network layout, beamforming architecture, signalling, user mobility, device rotation, propagation channel, device modelling and user blockage.

System model and Tooling

Fig. 1 illustrates the considered mmWave system in this project, where beam alignment takes place between the gNodeB and a single user using a handheld device. The gNodeB is modelled as a static single panel of N_t patch antennas at height h_t and the UE can be modeled at height h_r as either a single omnidirectional antenna or a multi-panel device. For the latter, each of the I panels at the UE is equipped with an array of N_r patch antennas and placed on each side of the form factor.

The user can be static or move through the cell limited by mobility bounds r and R . The UE position is defined according to the global coordinate system (GCS) represented in Fig. 1. The UE's orientation can remain constant or change along the user's trajectory, following a local coordinate system (LCS) (x_L, y_L, z_L) . As illustrated in Fig. 2, the LCS is obtained from any 3D rotation with respect to the GCS, (x_G, y_G, z_G) , over three distinct angles: the bearing angle α , the downtilt angle β and the slant angle γ . This set of angles represents three elemental rotations about the z , y and x axes, respectively [81].

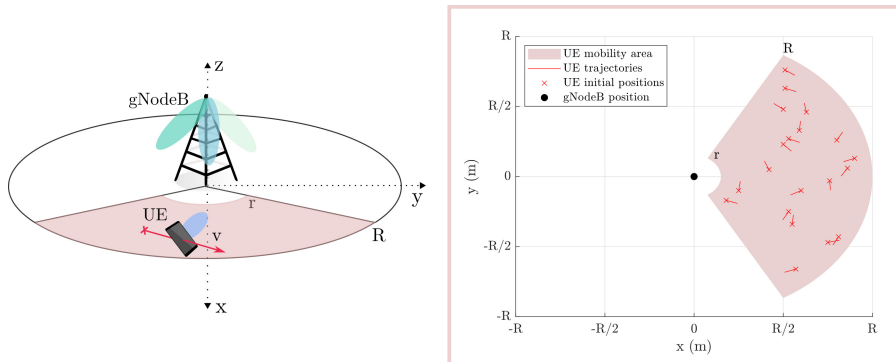


Fig. 1: Simulation tool's system model.

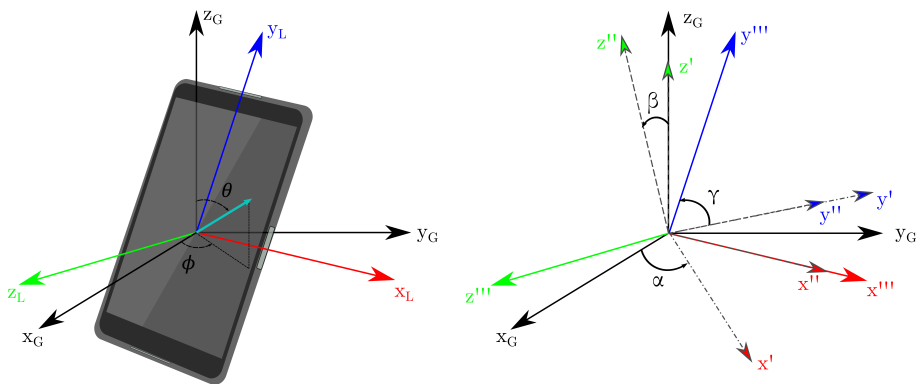


Fig. 2: Spherical coordinates in the GCS (left) and LCS transformation (right) with respect to the GCS through 3 sequential rotations: α, β, γ . Inspired by illustration from Fig. D.2 in Paper D.

Channel model

The mmWave DL channel response for the i th UE panel is modelled for a frequency-time resource element (s, k) as

$$\mathbf{H}^i(s, k) = \sum_{l=1}^{L(k)} g_l(k) \mathbf{a}_r^i(\boldsymbol{\varphi}_{r,l}^i(k)) \mathbf{a}_t^H(\boldsymbol{\varphi}_{t,l}(k)) e^{-j2\pi\tau_l(k)f_s}, \quad (1)$$

where $L(k)$, $g_l(k)$, $\tau_l(k)$ are the time-varying total number of multipath components of the channel, the path l 's complex gain and its delay values at time k , respectively. Additionally, f_s denotes the s th subcarrier frequency. The transmitter and i th receiver panel array responses are expressed in \mathbf{a}_t and \mathbf{a}_r^i for a path l 's time-varying angles of departure, $\boldsymbol{\varphi}_t$, and arrival, $\boldsymbol{\varphi}_r^i$. These angles, expressed in elevation and azimuth (θ, ϕ) , are given by

$$\boldsymbol{\varphi}_{r,l}^i(k) = (\theta_{r,l}^i(k), \phi_{r,l}^i(k)), \quad (2)$$

$$\boldsymbol{\varphi}_{t,l}(k) = (\theta_{t,l}(k), \phi_{t,l}(k)). \quad (3)$$

The array response for a gNodeB or UE array panel of size $N = N_x N_y N_z$ is written as

$$\mathbf{a}(\theta, \phi) = \tilde{\mathbf{a}}(\theta, \phi) \odot \mathbf{g}_{ae}(\theta, \phi) \quad (4)$$

where $\mathbf{g}_{ae} \in \mathbb{C}^N$ denotes each antenna element's linear gain, \odot the Hadamard product and $\tilde{\mathbf{a}}$ is described as

$$\tilde{\mathbf{a}}(\theta, \phi) = \frac{1}{\sqrt{N}} \mathbf{a}_z(\theta) \otimes \mathbf{a}_y(\theta, \phi) \otimes \mathbf{a}_x(\theta, \phi) \quad (5)$$

where \otimes expresses the Kronecker product, with $\mathbf{a}_x \in \mathbb{C}^{N_x}$, $\mathbf{a}_y \in \mathbb{C}^{N_y}$ and $\mathbf{a}_z \in \mathbb{C}^{N_z}$ given by

$$\mathbf{a}_x(\theta, \phi) = [1, e^{j\pi \sin \theta \cos \phi}, \dots, e^{j\pi(N_x-1) \sin \theta \cos \phi}]^T \quad (6)$$

$$\mathbf{a}_y(\theta, \phi) = [1, e^{j\pi \sin \theta \sin \phi}, \dots, e^{j\pi(N_y-1) \sin \theta \sin \phi}]^T \quad (7)$$

$$\mathbf{a}_z(\theta) = [1, e^{j\pi \cos \theta}, \dots, e^{j\pi(N_z-1) \cos \theta}]^T. \quad (8)$$

This work assumes perfect subcarrier orthogonality conditions, where the maximum channel delay response is within the cyclic prefix duration and the channel response remains constant during a full OFDM symbol.

Signal model

The received signal at any UE panel i in a single frequency-time resource element is given by

$$\mathbf{y}^i(s, k) = \mathbf{w}^{iH}(k) \mathbf{H}^i(s, k) \mathbf{F}(s, k) \mathbf{x}(s, k) + \mathbf{w}^{iH}(k) \mathbf{n}^i(s, k), \quad (9)$$

where $\mathbf{H}^i(s, k) \in \mathbb{C}^{N_r \times N_t}$ expresses the channel matrix between the gNodeB and the i th UE panel, as denoted in (1). $\mathbf{F}(s, k) \in \mathbb{C}^{N_t \times N_{RF}}$ describes the gNodeB beamforming matrix, where each column contains a set of analog phase shifts $\mathbf{f}_{\psi_t} \in \mathbb{C}^{N_t}$ for a TXRU to transmit a beam ψ_t with a constant modulus of $\frac{1}{\sqrt{N_t}}$. These beams are employed to spatially filter the transmitted signals in the vector $\mathbf{x}(s, k) \in \mathbb{C}^{N_{RF}}$, which expresses the N_{RF} transmitted signals in the frequency resource (s, k) , with a symbol variance of $\frac{1}{\sqrt{N_{RF}}}$. These signals, that can be either SSBs or CSI-RSs, are received at the UE with a beam defined by the analog phase shifts in the beamforming vector $\mathbf{w}^i(k) \in \mathbb{C}^{N_r}$ with a constant modulus of $\frac{1}{\sqrt{N_r}}$. The receiver noise is modelled as a complex additive white Gaussian noise (AWGN) vector with variance σ_n^2 and given by $\mathbf{n}^i(s, k) \in \mathbb{C}^{N_r} \sim \mathcal{CN}(\mathbf{0}, \sigma_n^2 \mathbf{I})$.

Table 1: 3GPP gNodeB and UE antenna modelling.

Parameter	gNodeB	UE
$\theta_{3\text{ dB}}$	65°	90°
$\phi_{3\text{ dB}}$		
SLA_v	30 dB	25 dB
A_m		
$\max\{G_{ae}\}$	8 dBi	5 dBi

Beamforming codebook models

For beam sweeping at the gNodeB, a directional beamforming codebook is adopted, dividing the cell's sector coverage into angular regions. These beams belong to a finite pre-defined set of N_T vectors $\mathcal{C}_t = \{\mathbf{f}_{\psi_t} | \psi_t = 1, \dots, N_T\}$ which is referred to henceforth as the gNodeB codebook. The array steering vector for a transmit beam ψ_t pointing towards $(\theta_{\psi_t}, \phi_{\psi_t})$ is defined in the ψ_t^{th} vector of the codebook as

$$\mathbf{f}_{\psi_t} = \mathbf{a}_t(\theta_{\psi_t}, \phi_{\psi_t}). \quad (10)$$

Each UE panel produces a finite set of N_R vectors $\mathcal{C}_r^i = \{\mathbf{w}_{\psi_r} | \psi_r = 1, \dots, N_R\}$, constituting the UE panel codebook. In any of the panels the array steering vector for a receive beam ψ_r directed towards $(\frac{\pi}{2}, \phi_{\psi_r})$ is expressed as

$$\mathbf{w}_{\psi_r} = \mathbf{a}_r\left(\frac{\pi}{2}, \phi_{\psi_r}\right). \quad (11)$$

Antenna element model

This project models the gNodeB and UE antenna elements to be patch antennas, as described in Table 1 [82]. The obtained antenna radiation pattern describes $G_{ae}(\theta, \phi)$ used in (4) in linear units. Many models typically assume that $g_{ae}(\theta, \phi)$ values are interchangeable between antenna elements of the same panel. In reality, each antenna element from a common UE panel displays their own unique $g_{ae}(\theta, \phi)$ matrix, which is influenced by factors such as antenna placement in the form factor, spacing between antenna elements or close proximity to the user's body, as will be further explained in the CST section.

UE mobility and UE rotation model

This simulation tool models time-varying UE mobility and UE rotation as two independent processes in time. The user is assumed to move linearly through the cell sector with constant speed v depicting both pedestrian and

vehicular mobility scenarios. It's initial position and trajectory direction follow a uniform distribution in the xy plane within the sector's region, with the user's height fixed in the z-axis. The UE's orientation, described through (α, β, γ) , is drawn from a uniform random distribution, with a variable range of values. Time-varying device rotation scenarios use a filtered random walk model to update the UE's orientation smoothly along its trajectory. Therefore, the UE's orientation at time sample t for α is expressed as

$$\alpha_t = \frac{1}{M} \sum_{m=0}^{M-1} \bar{\alpha}_{t-m}, \quad (12)$$

where M is described as the filter's length and $\bar{\alpha}_t$ as the filter inputs obtained from the following random walk model

$$\bar{\alpha}_t = \bar{\alpha}_{t-1} + \mathcal{N}(0, \sigma^2), \quad (13)$$

with σ representing the random walk's standard deviation and $\bar{\alpha}_0 \sim \mathcal{U}[0^\circ, 360^\circ]$. The same procedure is applied to obtain β_t and γ_t , with all angles wrapped within $[0^\circ, 360^\circ]$.

This set of angles creates a different LCS for each UE orientation, which means the angle-of-arrival (AoA) coordinates obtained from QuaDRiGa in the GCS must be converted to the current LCS by

$$\theta_{t,l}(\alpha, \beta, \gamma; \theta, \phi) = \arccos((\cos \beta \cos \gamma \cos \theta + (\sin \beta \cos \gamma \cos(\phi - \alpha) - \sin \gamma \sin(\phi - \alpha) \sin \theta)) \quad (14)$$

$$\begin{aligned} \phi_{t,l}(\alpha, \beta, \gamma; \theta, \phi) = \arg((\cos \beta \sin \theta \cos(\phi - \alpha) - \sin \beta \cos \theta) + \\ j(\cos \beta \sin \gamma \cos \theta + (\sin \beta \sin \gamma \cos(\phi - \alpha) + \cos \gamma \sin(\phi - \alpha)) \sin \theta)) \quad (15) \end{aligned}$$

These values are ultimately used to update the $\phi_{r,l}^i$ values in (1) over time.

Measurement model

The received signal is measured for RSRP, defined as the linear average over the power contributions of the resource elements carrying reference signals. the RSRP measurement for a beam pair (ψ_t, ψ_r^i) over \mathcal{V} , a resource data set containing the reference signals in question, is computed as

$$RSRP(\psi_t, \psi_r^i) = \frac{1}{|\mathcal{V}|} \sum_{(s,k) \in \mathcal{V}} |\mathbf{w}_{\psi_r^i}^H \mathbf{H}^i(s,k) \mathbf{f}_{\psi_t} + \mathbf{w}_{\psi_r^i}^H \mathbf{n}^i(s,k)|^2. \quad (16)$$

The simulator supports both SSB-based measurements through SS-RSRP and CSI-RS measurements through CSI-RSRP measurements [25].

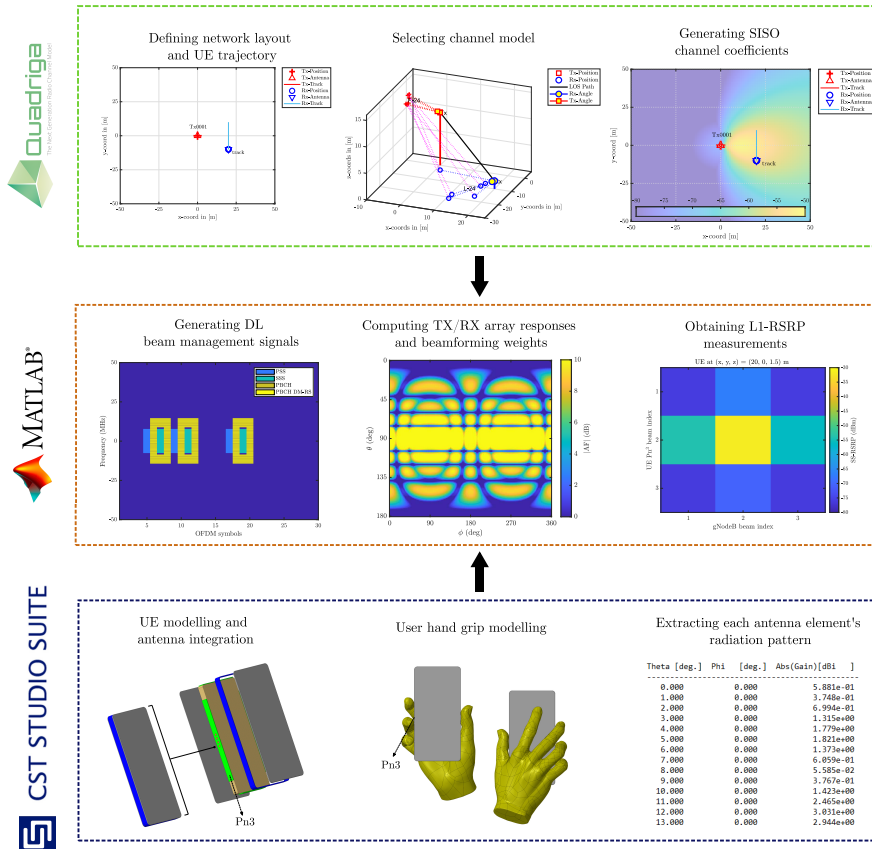


Fig. 3: Graphical representation of the link-level simulator used in this PhD project.

Tooling

In order to implement the system model described above, three different tools were required. As described in Figure 3, QuaDRiGa is responsible for channel response generation, CST is employed to model and characterize user hand blockage and finally MATLAB[®] is used for 3GPP compliant signalling generation and measuring for beam management, being the main implementation tool of this simulator.

QuaDRiGa

QuaDRiGa is a 3D geometry-based stochastic channel model generator that creates realistic radio channel impulse responses for mobile network sim-

ulations. This tool, popular among standardization bodies, is able to create channel responses with a continuous time evolution, spatially correlated large and small-scale-fading and supports several 3GPP-compliant propagation scenarios [94]. QuaDRiGa is used in this project to generate the channel coefficients of a link between the gNodeB and the UE according to the desired channel model, gNodeB position, UE speed and trajectory¹. This tool generates the gain and delay values for each multipath component, as well as the angle-of-departure (AoD) and AoA (in the GCS) that are employed in (1). It is worth mentioning that, for the simulations done in **Paper C** and **Paper D**, QuaDRiGa is employed to generate solely single-input-single-output (SISO) channel responses, which are then used to compute the originally intended multiple-input-multiple-output (MIMO) channel responses in MATLAB[®]. This relies on the assumption that the delay difference between antenna elements of the same array is negligible and that the AoD/AoA barely change among the antenna elements of an array, since the spacing between them (about 0.0429 m between the extremity antennas of a 8-element array with $\frac{\lambda}{2}$ spacing at 28 GHz) is so much smaller than the typical distance between the gNodeB and UE (usually around 15 m). This alternative approach is appealing due to its flexibility, since the same coefficients can be re-used for any arbitrary array geometry. Furthermore, relying on a smaller SISO prevents large running simulation times for coefficient generation, as well as storage issues, since both these factors significantly increase as bigger antenna array sizes are considered.

CST

Computer Simulation Technology (CST) is a 3D electromagnetic solver commonly used to design, analyze and optimize electromagnetic components and systems [95]. This project opted for this tool to introduce user hand blockage in the beam management study by modelling and simulating the UE form factor, all the antennas integrated in each panel and also a human hand gripping the device. The model of the UE's form factor can include components such as the glass, the metal chassis and the plastic case. Several different hand grips can be simulated in CST to portray different usage scenarios. This can be done by importing them to the tool as computer-aided design (CAD) models publicly available from sources such as Cellular Telecommunications and Internet Association (CTIA). The UE antennas in CST are designed to resemble 3GPP's antenna model described in [82]. However CST simulations record certain phenomena like antenna coupling, an-

¹This strategy is adopted for **Paper B-Paper D**. However, at an earlier stage of development of the simulator, pertaining to **Paper A**, a cluster-delay-line (CDL) channel model is used instead with a 3GPP-based channel profile from [81].

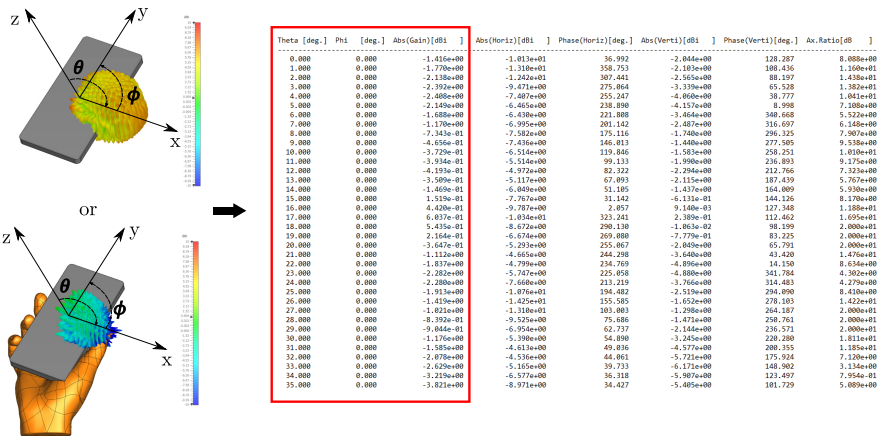


Fig. 4: Excerpt of an ASCII file containing $G_{ae}(\theta, \phi)$ values for one of the antenna elements in UE Panel 3. The same file structure is common to both freespace and blockage scenarios.

tenna mismatch, rippling and reflections caused by the metal structure and the user's hands, which make each antenna element's radiation pattern completely unique, providing a more realistic depiction of the antenna's behavior.

As an output, CST provides the unique individual radiation patterns of each antenna element, $G_{ae}(\theta, \phi)$, in the format of ASCII files, as highlighted in Fig. 4, which are then used in (4) to compute the UE array response². This is a versatile tool that can support an extensive level of modelling detail. While not explored in this project, CST can simulate a user's full body, including features such as muscle and bone. Furthermore, the form factor models can be designed in the tool to also account for more specific details of the phone such as microphone, camera and other sensors, making this tool very well suited to extend the studies conducted in this thesis.

MATLAB

This simulator is built in MATLAB[®], where the data from QuaDRiGa and CST are used as inputs to simulate and evaluate beam management performance. Besides generating the procedure's DL signalling for sweeping and measuring using the 5G Toolbox[™] [96], MATLAB[®] is used to compute the MIMO channel responses, the received signal at the UE and measure KPIs such as RSRP, misdetection probability or misalignment loss.

²It is important to reiterate that the CST radiation patterns have been provided by Nokia. This thesis' contribution focuses on incorporating these realistic antenna element radiation patterns from CST in the MATLAB-based simulation tool for beam management performance evaluation

Part II

Papers

Paper A

Beam Management in mmWave 5G NR: an Intra-Cell Mobility Study

F. Fernandes, C. Rom, J. Harrebek and G. Berardinelli

The paper has been published in the
IEEE 93rd Vehicular Technology Conference (VTC2021-Spring)

© 2021 IEEE

The layout has been revised.

Abstract

5th Generation (5G) millimeter wave (mmWave) communications rely on directive and narrow beams to circumvent its challenging propagation conditions. Therefore, Medium Access Control (MAC)-based Beam Management (BM) becomes essential to secure adequate beam alignment between the User Equipment (UE) and the Next Generation Node Base Station (gNodeB) beams. For dynamic environments, this can be challenging, potentially compromising control procedures such as Beam Tracking (BT) under the current 5G New Radio (NR) deployments for FR2. This paper presents a sensitivity study on the stability of the gNodeB selected beam - measured by the beam's time-of-stay (ToS) - and the resulting link quality under different operational conditions with respect to UE mobility, propagation environment and operational bands. Results show that the suitability of 5G NR BM procedures can be significantly affected by UE angular speed, channel's angular spread and availability of channel-adaptive BM parametrization.

1 Introduction

An integral part of the 5G NR focus has been to explore the mmWave frequency spectrum, since it allows for large amounts of bandwidth allocation and thus, unprecedented data rates [1]. The 3GPP has defined in [2] the mmWave frequency range (FR), FR2, comprised between 24.25 GHz and 52.6 GHz, where NR system operations have been enabled and optimized. These high frequencies, however, display increasingly challenging propagation conditions, with significant pathloss, environment absorption, low penetration through objects and weak diffraction around corner edges of obstacles.

In order to mitigate these effects, antenna arrays are used to create high gain directional beams at the UE and the gNodeB. As a result, the signal's range is extended and the beams can be steered away from obstruction sources. Unfortunately, such directive beams are also narrow and beam alignment between the UE and the gNodeB beams becomes imperative to maintain link quality. This task can be challenging for fast-varying channels with UE mobility, negatively impacting the performance of control procedures such as beam tracking (BT), designed to ensure an ubiquitous connection through beam switching.

There are several proposals in the literature on how to perform fast and robust BT. While [3] proposes a multi-connectivity solution using both mmWave 5G cells and legacy non-beamformed sub-6 GHz cells, [4] develops a tracking scheme that alternates periodic beam refinements with sparser refresh procedures. Other solutions for BT aiming at reducing overhead and beam misalignment in high-speed UE mobility scenarios are presented in [5], [6], and [7]. Moreover, ML solutions are described in [8] and [9],

where beam alignment is achieved through strategies of shared situational awareness between connected vehicles and the use of the UE's location and orientation. Most of these solutions, however, have been proposed at a time where the 3GPP standard for NR was not released and, therefore, have yet to be reassessed in the context of 5G NR.

3GPP introduces BT in [10] as one of the medium access control (MAC)-based beam management (BM) procedures to maintain beam alignment for DL and UL transmission/reception. These procedures perform signaling-based beam selection, first at the gNodeB and then at the UE, through beam sweeping, measurement, determination and reporting operations. Studies are conducted in [11], [12] and [13], obeying the current 5G NR standard, to evaluate accuracy, responsiveness and overhead of different BM frameworks, as well as analyze 5G NR system-level network deployment choices.

Once the best gNodeB beam is established, the UE beam must be determined before the deterioration of the link triggers a gNodeB beam switch. In other words, to perform BM, the period of time during which a gNodeB beam provides high link quality, the beam's ToS, must be large enough to accommodate the subsequent UE beam selection process. This requirement can be difficult to secure depending on the propagation environment, UE speed and frequency range. A sensitivity analysis on this beam timing aspect of 3GPP-defined BM has not been conducted in the context of challenging mmWave environment conditions.

This paper evaluates the behavior of the average gNodeB beam ToS, in an intra-cell context, under three scenario variables: user mobility, dynamic radio channel characteristics and increasing operational frequencies. Under the ToS constraint, it is investigated whether unhindered BM can take place without compromising link quality. This assessment is made for the FR2 operational frequency of 28 GHz and also the beyond FR2 (BFR2) frequency of 60 GHz, as part of the new range of mmWave frequencies explored by 3GPP [14].

The remainder of this paper is organized as follows: Section 2 describes the current BM procedure set in the standard that is evaluated in this paper. Section 3 details the proposed system model for simulations. Section 4 states the research target of the paper and presents the study's performance metrics. Section 5 analyzes the performance results for FR2 and BFR2 and, finally, Section 6 concludes the paper and elaborates on future work.

2 BM Procedures

3GPP defines BM in [15], under the assumption of UL/DL beam correspondence, as three supported DL procedures, P1, P2 and P3, represented in Figure A.1. P1 is dedicated to gNodeB beam selection. The gNodeB performs an

3. System Model

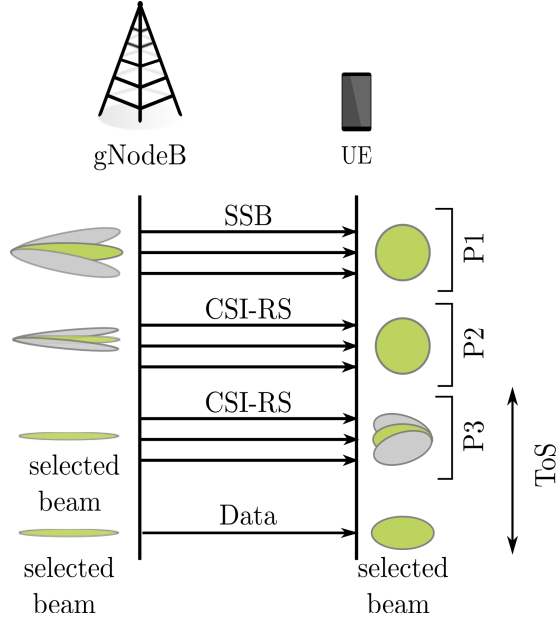


Fig. A.1: Downlink 3GPP BM procedure.

angular beam scan, where each beam is associated with a different SSB [16]. The UE measures each beam's RSRP level and reports the best measurements back to the gNodeB for the beam selection. As shown in Fig. A.1, a refinement of the P1 gNodeB beam is performed in P2, using CSI-RS. After the P2 gNodeB beam is set, the UE (assuming beamforming capabilities) sweeps through its beams in P3 to establish the best narrow beam that aligns with the gNodeB selected beam, also using CSI-RS. A simplified BM model is adopted in this study, where P1 and P2 are merged into a single gNodeB beam refinement stage. To achieve a target DL gain through beam alignment, the selected gNodeB beam must remain unaltered until the P3 stage is completed.

3 System Model

3.1 Depicted intra-cell scenario

This section presents the system model under evaluation. Fig. A.2 depicts an intra-cell BT scenario, where a UE in connected mode travels in a circular motion around the gNodeB with a radius of travel R , linear speed v and angular displacement of $\Delta\phi$, making for a travel period $T = \frac{\Delta\phi \times R}{v}$ seconds.

On the gNodeB side, a ULA of N_{gNodeB} isotropic antenna elements is considered. On the UE side, a multi-panel broad beam scanning configuration is

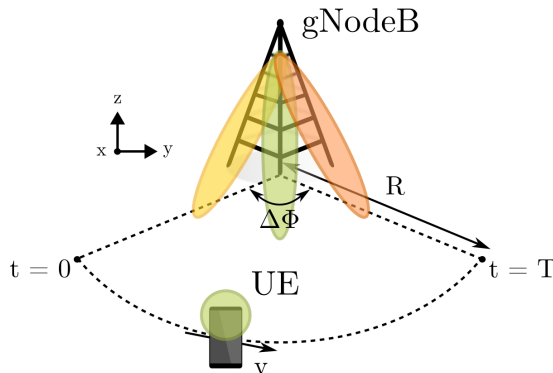


Fig. A.2: Intra-cell simulation model.

assumed, where the AoA modeling of a multi panel solution with simultaneously active panels resembles an omnidirectional antenna. To emulate this, the UE beam is modeled with a single isotropic antenna element in simulations, $N_{UE} = 1$.

The gNodeB transmits N_{SSB} beams with a periodicity of T_{SS} ms. While traveling, the UE collects N RSRP samples from each incoming SSBurst. After proper filtering, the UE reports these measurements back to the gNodeB to determine whether a beam switch is required. Regarding the beam switching commands from the gNodeB to the UE, ideal signaling is considered, with no errors or delays.

In this study, several UE angular speeds are tested by varying R and v . This simulation model is implemented in MATLAB[®] supported by functions in 5G Toolbox[™].

3.2 Propagation channel model

The 3GPP-defined channel model CDL is used for the simulations. This is a 3D link-level fading channel model whose properties are extensively detailed in [17]. Three distinct channel profiles are evaluated, CDL-D, CDL-D3 and CDL-D5, spatially represented in Fig. A.3 according to their clusters' azimuth AoD. The radius size of each cluster is proportional to its relative power level.

CDL-D is a LOS CDL profile, with a single dominant cluster, indicated in Fig. A.3a by the larger size of cluster 1. To broaden this study's performance analysis, two other CDL-D based profiles are customized, CDL-D3 and CDL-D5. In these profiles, the clusters' positioning and power levels are manipulated to obtain, respectively, three and five dominant clusters to recreate a progressively wider angular spread environment, as highlighted in Fig. A.3b and Fig. A.3c. This channel model does not include blockage but accounts for the Doppler effect inflicted by the UE movement. It is assumed

3. System Model

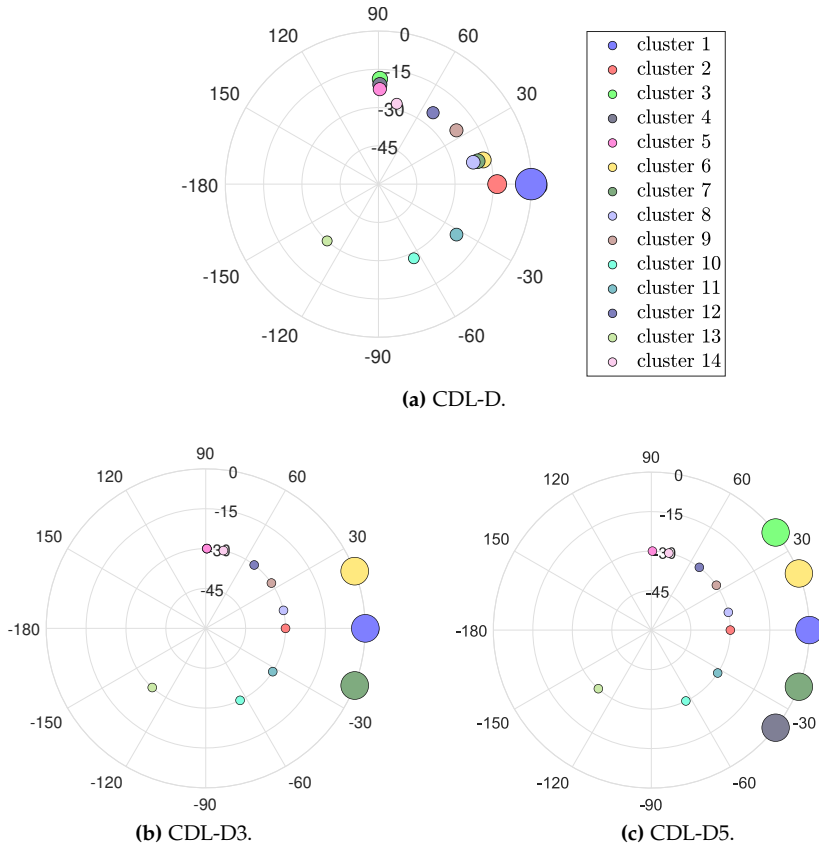


Fig. A.3: AoD representation of CDL clusters (some share the same power level and AoD, becoming therefore, overlapped).

that the UE's travel path is within acceptable coverage range. Therefore, since it does not affect the ToS assessment, pathloss and noise are neglected in this paper.

3.3 Measurement model

In this paper, the UE performs SSB-based RSRP measurements. RSRP is defined as the linear average over the power contributions (in [W]) of the resource elements that carry cell-specific reference signals within the considered measurement frequency bandwidth [18].

In an ideal scenario, free of fast-fading variations, the beam choice for each time sample n would fall under the beam with the highest instantaneous RSRP. However, in a realistic scenario, depicted in the left-hand side of Fig. A.4, this solution would cause a beam ping-pong effect. In the transition

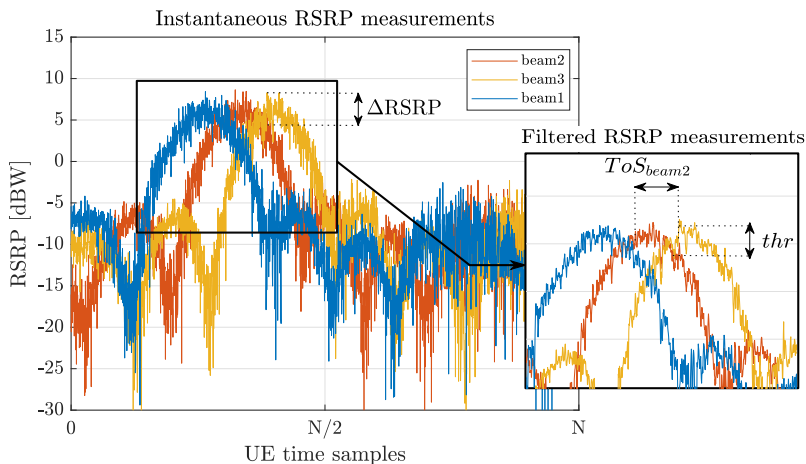


Fig. A.4: UE's instantaneous and filtered RSRP measurements for three beams.

between two beams, the values reported by the UE would cause the beam selection to bounce back and forward between beam 1 and 2 or 2 and 3 due to small, fast-fading-induced power variations.

To mitigate this, the measurements are filtered prior to the reporting and beam selection stage. This work employs L1 filtering combined with an additional recursive filter and a power threshold criterion to minimize unnecessary beam switching during the beam selection process, as seen in the right-hand side window in Fig. A.4.

L1 filtering

Although L1 filtering is required by 3GPP's measurement model, its exact configuration is implementation dependent [19]. A moving average filter is adopted with a sliding window dimension L_f . The L1 filtered RSRP measurement for the n^{th} time sample is given by

$$RSRP_{L1}[n] = \frac{\sum_{i=0}^{L_f-1} RSRP_{\text{measurement}}[n-i]}{L_f}, \quad (\text{A.1})$$

where $RSRP_{\text{measurement}}$ is the physical (PHY) layer RSRP measurement recorded at the UE.

4. Research Target and Key Performance Indicators (KPI)

Additional filtering

After L1 filtering, the RSRP values can be computed via a recursive filter as follows:

$$RSRP[n] = (1 - \alpha)RSRP[n - 1] + \alpha RSRP_{L1}[n], \quad (\text{A.2})$$

where $RSRP_{L1}[n]$ stands for the latest received L1 filtered results and $\alpha = 0.5^{k/4}$, with filter coefficient k .

Power threshold criterion

The power-based criterion is used in the gNodeB beam selection process to dictate when a beam switch occurs. The best beam choice is based on the filtered RSRP measurements. Therefore, a beam switch is only triggered, for a time sample n , when the filtered RSRP value of the new beam exceeds the filtered RSRP value of the current best beam by a threshold, thr . This is represented in the right-hand side of Fig. A.4. The UE perceives beam 2 as the best beam for as long as its filtered power level is less than thr dB below beam 3's filtered power level, extending ToS_{beam2} . The parameters L_f , α and thr constitute the BM parametrization and can take on several values which, collectively, impact the instantaneous RSRP measurements reported by the UE and, consequently, BM performance.

4 Research Target and Key Performance Indicators (KPI)

In a mobility scenario, it is possible that the ToS per gNodeB beam may fall short to accommodate the UE beam refinement portion of the BM procedure. In this case, the procedure must resume by keeping a broad UE beam which, given mmWave propagation conditions, affects coverage, throughput and may even cause radio link failure (RLF). Therefore, this paper investigates whether P3 can take place during BT before a gNodeB beam switch occurs.

One of the factors that can impact this evaluation is BM parametrization. For certain configurations, the BM parametrization can alter the perceived gNodeB beam ToS enough to either impede or enable the UE beam refinement stage. However, the latter would come at the cost of power loss. In the right-hand side of Fig. A.4, the ToS for beam 2 is stretched beyond the crossover point between beams due to parametrization, although the quality of the connection progressively worsens as the power level associated with beam 2 decreases. This incurred power loss is designated in this paper as

$\Delta RSRP$. For a certain n , $\Delta RSRP$ is defined as the power gap between the instantaneous RSRP value of the highest power beam before filtering, $RSRP_{bf}$, and the instantaneous RSRP value of the best beam after filtering, $RSRP_{af}$.

Considering this trade-off, a ToS increase through parametrization is only beneficial if the corresponding $\Delta RSRP$ does not deteriorate the link's quality to a level comparable to a broad UE beam configuration. Both ToS and $\Delta RSRP$ are selected as KPIs for this study and a balance must be maintained between the two through the selection of L_f , α and thr . This paper assumes that an optimal BM parametrization maximizes ToS while keeping $\Delta RSRP$ low enough to avoid link deterioration. Since ToS varies per gNodeB beam and $\Delta RSRP$ varies along T , a statistical measure is defined for both KPIs. \overline{ToS} is introduced as the average ToS per beam for a particular (R, v) simulation scenario, calculated by

$$\overline{ToS}_{(R,v)} = \frac{\sum_{j=1}^{N_{SSB}} ToS_{Bj}}{N_{SSB}}, \quad (\text{A.3})$$

where ToS_{Bj} is the ToS of gNodeB beam j and N_{SSB} is the number of gNodeB transmitted SSB beams. Similarly, $\overline{\Delta RSRP}$ conveys the average $\Delta RSRP$ along the UE's travel period T given by

$$\overline{\Delta RSRP}_{(R,v)} = \frac{\sum_{n=1}^N RSRP_{bf}[n] - RSRP_{af}[n]}{N_{(R,v)}}, \quad (\text{A.4})$$

where N represents the total number of RSRP samples registered by the UE. According to each (R, v) scenario, N is an integer that varies as per

$$N_{(R,v)} = \left\lfloor \frac{T}{T_{SS}} \right\rfloor + 1, \quad (\text{A.5})$$

where $\lfloor \cdot \rfloor$ denotes the floor function. Achieving proper BM parametrization is a function of the operational scenario which cannot be known beforehand. In a real-life scenario, the UE, commanded by the gNodeB, is likely to adopt a default (suboptimal) BM parametrization. It is therefore crucial to gauge the sensitivity of \overline{ToS} and $\overline{\Delta RSRP}$ to BM parametrization under challenging operation conditions. For this, a new metric is introduced, RG , that tracks how wide the range of \overline{ToS} and $\overline{\Delta RSRP}$ values are for all parametrizations. This is calculated as

$$RG_{KPI} = \max KPI - \min KPI, \quad (\text{A.6})$$

where KPI is either \overline{ToS} or $\overline{\Delta RSRP}$.

5 Results and Discussion

Subsection 5.1 reports the simulation parameters featured in the study. Subsection 5.2 presents the simulation results with the purpose of (i) assessing how sensitive \overline{ToS} and $\overline{\Delta RSRP}$ are to parametrization in 5.2; (ii) identifying the (R, v) scenarios for which BM is not feasible, given an optimal parametrization, in 5.2.

5.1 Simulation Parameters

Table A.1 summarizes all scenarios, BM parametrization and channel model configurations used in the simulations.

The UE's travel radius R assumes 10 values between 20 m and 200 m. The upper bound of R corresponds to the intersite distance (ISD) established in [17] for UMi open area scenarios. Similarly, the UE's travel speed v takes on 10 values between 3.6 km h^{-1} , for a pedestrian user, and 120 km h^{-1} , for a user in a fast moving vehicle. The UE measures RSRP levels with the same periodicity $T_{SS} = 20 \text{ ms}$ as the gNodeB transmits Synchronization Signal (SS) Bursts, while traveling with an angular displacement of $\Delta\phi = 120^\circ$. Regarding BM parametrization, L_f , k and thr take on, respectively, three, four and five discrete values. Their combination generates 60 parametrizations that are employed in this study. For the CDL channel model, two operational frequencies are considered: the FR2 frequency of 28 GHz and BFR2 frequency of 60 GHz. Besides sharing the same subcarrier spacing (SCS) = 120 kHz configuration and $N_{UE} = 1$, the frequencies adopt different N_{gNodeB} and N_{SSB} at the gNodeB. While in FR2 the gNodeB panel has eight antennas elements transmitting 16 SSBs per burst, in BFR2, to compensate for poorer propagation conditions, these numbers are doubled. Finally, CDL-D, CDL-D3 and CDL-D5 are considered, making for 300 different (R, v, CDL) scenarios under evaluation.

5.2 Performance results

KPIs sensitivity to BM parametrization

The 60 parametrizations evaluated generate 60 \overline{ToS} and $\overline{\Delta RSRP}$ values for all 300 evaluated (R, v, CDL) scenarios. Fig. A.5 displays these values for six illustrative FR2 CDL-D scenarios. Here, three speed values, $v = 3.6 \text{ km h}^{-1}$, $v = 55 \text{ km h}^{-1}$ and $v = 120 \text{ km h}^{-1}$, are analyzed for two radiuses, $R = 20 \text{ m}$, in Fig. A.5a, and $R = 100 \text{ m}$, in Fig. A.5b.

The blue curves represent each parametrization's \overline{ToS} , sorted by increasing order. For a scenario SC , a parametrization index of $i_{SC} = 1$ corresponds

Table A.1: Simulation Parameters.

Scenario		
R [m]	$20 < R < 200$, step size=20	
v [km h ⁻¹]	$3.6 < v < 120$, step size=13	
T_{SS} [ms]	20	
$\Delta\phi$ [°]	120	
BM parametrization		
L_f	$1 < L_f < 3$, step size=1	
k	$1 < k < 4$, step size=1	
thr [dB]	$1 < thr < 3$, step size=0.5	
Channel model		
FR	FR2	BFR2
f [GHz]	28	60
SCS [kHz]	120	
N_{gNodeB}	8	16
N_{SSB}	16	32
N_{UE}	1	
CDL profile	CDL-D/CDL-D3/CDL-D5	

to the (L_f, k, thr) combination with the lowest \overline{ToS} while $i_{SC} = 60$ corresponds to the highest \overline{ToS} of said scenario. The orange curves depict the corresponding $\overline{\Delta RSRP}$ to the sorted \overline{ToS} values. It should be stressed that the parametrization associated with a common i_{SC} index between scenarios is not necessarily the same.

Fig. A.5 confirms an intuitive trend regarding \overline{ToS} and (R, v) . For a fixed v , \overline{ToS} increases hand in hand with R , as can be seen through the \overline{ToS} curves for $v = 3.6 \text{ km s}^{-1}$, in Fig. A.5a and Fig. A.5b. Since the radius of travel increases, for the same speed, the UE observes each beam for a longer period of time, increasing ToS. Moreover, for a fixed R , \overline{ToS} tends to decline as v increases. In Fig. A.5b, the maximum attainable \overline{ToS} value for $v = 3.6 \text{ km s}^{-1}$ is around 13.9 s while $v = 120 \text{ km s}^{-1}$ does not go over 432 ms. The UE is moving progressively faster and, therefore, needs to update its gNodeB beam more often, reducing the ToS per beam.

Sorting the results by increasing \overline{ToS} reveals the consistent behavior of $\overline{\Delta RSRP}$. For all displayed scenarios, as \overline{ToS} increases through parametrization, $\overline{\Delta RSRP}$ values tend to grow as well, confirming the trade-off effect described in section 4. However, this $\overline{\Delta RSRP}$ increase is significantly more noticeable for smaller radiuses, especially at high speeds. In Fig. A.5a, the $v = 120 \text{ km s}^{-1}$ curve reaches higher values than the same curve in Fig. A.5b, despite the UE's traveling speed being the same for both scenarios. This can be explained by the fact that a small R , combined with high v , makes for a small number of samples N . With a reduced N , it is possible that some parametrizations are too aggressive, resulting in big filtering-induced power losses.

5. Results and Discussion

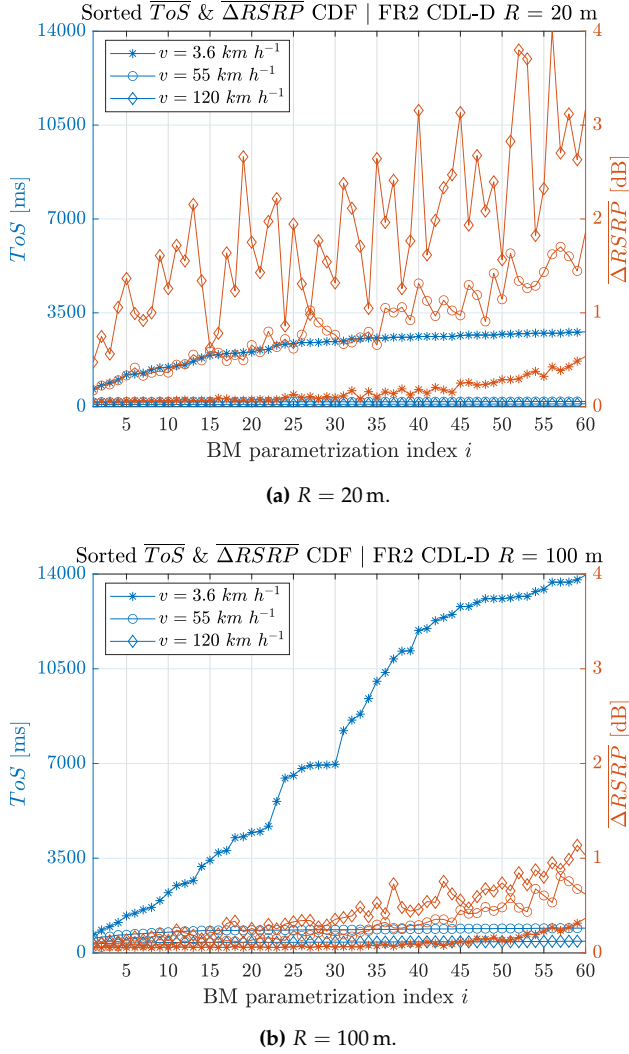


Fig. A.5: \overline{ToS} and $\overline{\Delta RSRP}$ sensitivity to BM parametrization.

Table A.2 and Table A.3 display, respectively, a summary representation of these six scenarios' results for FR2 and BFR2. Moreover, 12 extra scenarios are analyzed, pertaining to the same (R, v) combinations simulated with CDL-D3 and CDL-D5 profiles. These tables provide information on two different fronts. The Range Assessment quantifies how much the KPIs vary with parametrization and the Magnitude Assessment focuses on the order of magnitude of a scenario's maximum attainable \overline{ToS} , $\overline{ToS}_{i_{SC}=60}$, and its corresponding $\overline{\Delta RSRP}_{i_{SC}=60}$.

The tabled values show that \overline{ToS} can be quite influenced by parametrization. In Table A.2, $RG_{\overline{ToS}}$ can take values from 27.26 ms up to 13.29 s. Choosing an improper parametrization can lead a \overline{ToS} to be perceived as 27.26 ms to 13.29 s shorter, potentially compromising the BM procedure.

For all profiles, in both FR2 and BFR2, at higher angular speeds, $RG_{\overline{ToS}}$ decreases, since the smaller N lacks the resolution to differentiate the nuances created by each parametrization. $RG_{\overline{\Delta RSRP}}$ becomes wider since this sample resolution also leads to significant power losses.

Both FR2 and BFR2 magnitude results for CDL-D3 and CDL-D5 reflect the same behavior displayed in Fig. A.5 for CDL-D. Moreover, in FR2, as angular spread increases from CDL-D to CDL-D3 and CDL-D5, for the same (R, v) combination, $\overline{ToS}_{i_{SC}=60}$ decreases. However, for BFR2, based on the juxtaposition of SC3, SC9 and SC15 in Table A.3, \overline{ToS} appears to no longer decrease for higher angular spreads. However, these inconsistent values are associated with unacceptably high $\overline{\Delta RSRP}$ levels. In these types of scenarios, one should settle for a parametrization that offers lower \overline{ToS} in exchange for better link quality.

Moreover, for the same (R, v) in CDL-D, as frequency increases, \overline{ToS} decreases. In BFR2, the growth in the number of antenna elements at the gNodeB leads to narrower beams, resulting in shorter \overline{ToS} . However, this uniformity is lost once the multi-dominant cluster profiles are considered. While CDL-D3 mostly follows the expected trend, CDL-D5 displays improved \overline{ToS} when compared to FR2. Results seem to depend on cluster positioning and the multipath created. If a beam's sidelobe aligns with the clusters, it loses its narrow shape and impacts negatively the \overline{ToS} . However, narrower beams can more easily avoid unwanted alignment with clusters, inadvertently improving BM robustness.

To summarize, parametrization choice has a significant impact on \overline{ToS} and $\overline{\Delta RSRP}$, potentially compromising the 3GPP-defined BM procedure. Since optimal parametrization varies between propagation scenarios, employing a default suboptimal parametrization is not a viable solution. Even when considering an optimal parametrization, the KPIs degrade as angular speed and angular spread increase. However, the narrow beams associated with BFR2, despite degrading \overline{ToS} with angular speed, appear to be more likely to avoid cluster alignment, alleviating the angular spread effect. Finally, although only a subset of scenarios is displayed, the conclusions drawn are supported by all 300 simulated scenarios.

BM Boundary Scenarios

This part of the study is meant to visually pinpoint, within all scenarios simulated, when does the 3GPP defined BM procedure break. To do so, two

5. Results and Discussion

Table A.2: FR2 BM Parametrization Assessment.

CDL	SC	R [m]	v [km h ⁻¹]	Range Assessment		Magnitude Assessment	
				$RG_{\overline{ToS}}$ [ms]	$RG_{\overline{\Delta RSRP}}$ [dB]	$\overline{ToS}_{i_{SC}=60}$ [ms]	$\overline{\Delta RSRP}_{i_{SC}=60}$ [dB]
D	1	20	3.6	2140	0.48	2790	0.54
	2		55	32.46	1.69	195.71	1.86
	3		120	27.26	3.55	109.76	3.17
	4	100	3.6	13290	0.31	13900	0.37
	5		55	385.82	0.75	915.83	0.62
	6		120	106.95	1.04	432.0	1.03
D3	7	20	3.6	1320	0.26	1380	1.83
	8		55	141.25	1.60	197.75	3.50
	9		120	87.68	2.24	138.50	4.32
	10	100	3.6	3970	0.37	4040	1.52
	11		55	567.43	0.52	627.55	2.31
	12		120	298.21	0.84	357.34	2.66
D5	13	20	3.6	436.87	1.09	484.27	3.24
	14		55	141.74	2.02	189.52	4.28
	15		120	82.92	2.53	129.31	5.14
	16	100	3.6	564.45	1.03	611.77	3.03
	17		55	271.16	1.28	318.49	3.63
	18		120	190.73	1.65	236.70	3.93

\overline{ToS} requirements are set, 500 ms and 1 s, under which a scenario is not able to complete the BM procedure. These values are estimated as a lower and upper bound considering typical BM assumptions such as eighth UE beams, no-repetition CSI-RS transmission with 10 ms periodicity and three UE beam sweeps during its refinement stage, to smooth fast fading. Moreover, a limit $\overline{\Delta RSRP}$ is set to 4 dB, over which extending ToS through parametrization would lead to significant performance loss. Values above this are typically linked with inappropriate filtering that excessively flattens RSRP curves and large thr values that skew the beam choice and compromise the link's quality.

The results are presented as boundary plots, displayed in Fig. A.6, where v is plotted against R . Each color represents a different channel profile and the shaded areas encapsulate the (R, v) combinations that meet \overline{ToS} and $\overline{\Delta RSRP}$ requirements. Conversely, the non-shaded areas portray the scenarios where a broad UE beam must be kept, potentially sacrificing BM performance to the point of RLF. The boundary curves are computed with each scenario's optimized parametrization that maximizes \overline{ToS} while maintaining $\overline{\Delta RSRP} \leq 4$ dB. Fig. A.6a and Fig. A.6b are dedicated to the FR2 results, while Fig. A.6c and Fig. A.6d depict BFR2 results.

As angular spread increases, the \overline{ToS} requirements seem to become harder to meet. The shaded area of CDL-D is larger than CDL-D3, which in turn is larger than CDL-D5. Also, as v increases, the time requirement can only be met for higher R values. Moreover, higher \overline{ToS} requirements are more

Table A.3: BFR2 BM Parametrization Assessment.

CDL	SC	R [m]	v [km h ⁻¹]	Range Assessment		Magnitude Assessment	
				$RG_{\overline{ToS}}$ [ms]	$RG_{\Delta RSRP}$ [dB]	$ToS_{i_{SC}=60}$ [ms]	$\Delta RSRP_{i_{SC}=60}$ [dB]
D	1	20	3.6	849.59	0.64	1380	0.71
	2		55	23.01	3.57	110.62	2.45
	3		120	29.36	6.62	81.37	5.62
	4	100	3.6	6250	0.42	6850	0.48
	5		55	95.12	1.03	456.23	1.13
	6		120	40.72	1.65	223.61	1.85
D3	7	20	3.6	1200	0.60	1280	1.63
	8		55	52.65	2.99	110.36	4.66
	9		120	34.27	5.45	80.91	7.70
	10	100	3.6	5190	0.52	5270	1.33
	11		55	360.88	0.86	434.85	2.05
	12		120	140.77	1.31	216.88	2.58
D5	13	20	3.6	949.46	0.47	998.49	2.50
	14		55	67.63	2.97	113.68	4.63
	15		120	50.70	4.52	93.48	7.30
	16	100	3.6	3290	0.58	3340	2.09
	17		55	334.93	0.70	383.62	2.97
	18		120	154.69	1.32	201.37	3.78

challenging to fulfill. While in Fig. A.6a, CDL-D5 could guarantee proper BM up to $v = 30$ km h⁻¹, in Fig. A.6b, where the required \overline{ToS} goes up by 500 ms, there is no scenario where BM is not compromised.

As mentioned in section 5.2, BFR2 CDL-D5 BM appears to be more robust to angular spread than FR2 which is represented in Fig. A.6c and Fig. A.6d by the significant increase in the green shaded area. Lastly, the shaded area gap between profiles is less prominent in BFR2 than in FR2. This is most likely due to the fact that narrower beams are less impacted by the effects of clusters, making the boundary curves for each profile closer to the original, mostly unobstructed, LOS profile, CDL-D.

To summarize, results indicate that the increase of angular speed and angular spread negatively impacts the feasibility of the BM procedure under the simulated scenarios. A significant number of the simulated scenarios, unable to meet the KPI requirements, must skip the UE beam refinement in an attempt to carry on with BM, compromising coverage, throughput and risking RLF. Moreover, the BM feasibility gap between profiles appears smaller in BFR2, due to its narrower beams being less likely to be affected by angular spread. Finally, if pathloss were to be included in this evaluation, under a minimum coverage requirement, the boundary curves could be further restricted for higher values of R .

6. Conclusions

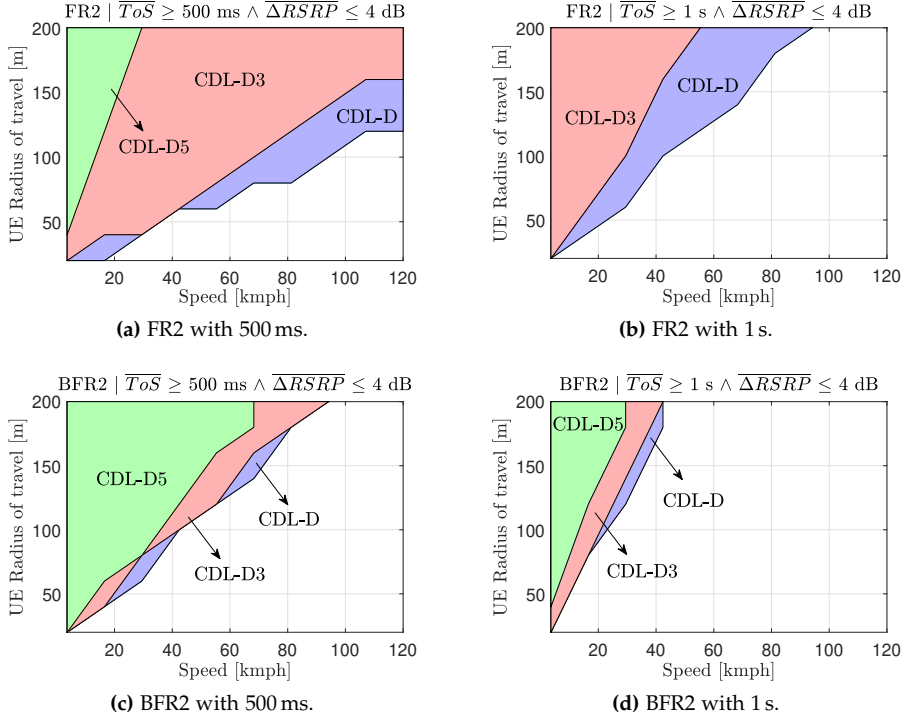


Fig. A.6: \overline{ToS} and $\overline{\Delta RSRP}$ boundary plots.

6 Conclusions

This paper studies the suitability of the current 3GPP BM procedures by performing a sensitivity study on the gNodeB's beam average ToS under challenging operation conditions such as UE mobility, dynamic propagation environments and increasing operational frequencies. Results show that BM parametrization can have a significant impact on the perceived ToS of a beam, risking to compromise the link's quality. Moreover, large angular speed and angular spread can limit the scenarios where the UE beam refinement stage of the BM procedure can occur. Furthermore, BFR2 results show to be less sensitive to cluster positioning, when compared to FR2, likely due to its beams' narrow nature.

This work is focused on intra-cell mobility, in order to grasp a deeper level of complexity on the nuances of the physical layer. However, in future work, an inter-cell scenario should be considered in order to include other challenges such as interference and handover. Additionally, a rule-based or a machine learning algorithm can be pursued to dynamically adapt filter

settings to UE speed, radius of travel and radio channel conditions.

References

- [1] T. S. Rappaport, S. Sun, R. Mayzus, H. Zhao, Y. Azar, K. Wang, G. N. Wong, J. K. Schulz, M. Samimi, and F. Gutierrez. "Millimeter Wave Mobile Communications for 5G cellular: It will work!". *IEEE Access*, 1:335 – 349, 2013.
- [2] 3GPP. NR; Base Station (BS) radio transmission and reception (Release 15). Tech. Spec. 38.104, V1.0.0 2017.
- [3] M. Giordani, M. Mezzavilla, S. Rangan, and M. Zorzi. "Multi-Connectivity in 5G mmWave Cellular Networks". *2016 Mediterranean Ad Hoc Networking Workshop (Med-Hoc-Net)*, pages 1 –7, 2016.
- [4] M. Giordani and M. Zorzi. "Improved User Tracking in 5G Millimeter Wave Mobile Networks via Refinement Operations". *2017 16th Annual Mediterranean Ad Hoc Networking Workshop (Med-Hoc-Net)*, pages 1 – 8, 2017.
- [5] V. Va, H. Vikalo, and R. W. Heath. "Beam Tracking for Mobile Millimeter Wave Communication Systems". *2016 IEEE Global Conference on Signal and Information Processing (GlobalSIP)*, pages 743 – 747, 2016.
- [6] J. Palacios, D. De Donno, and J. Widmer. "Tracking mm-Wave channel dynamics: Fast beam training strategies under mobility". *IEEE INFOCOM 2017 - IEEE Conference on Computer Communications*, pages 1 – 8, 2017.
- [7] S. Jayaprakasam, X. Ma, J. W. Choi, and Member S. Kim. "Robust Beam-Tracking for mmWave Mobile Communications". *IEEE Communications Letters*, 21(12):2654 – 2657, 2017.
- [8] Y. Wang, A. Klautau, M. Ribero, A. C. K. Soong, and R. W. Heath. "MmWave Vehicular Beam Selection With Situational Awareness Using Machine Learning". *IEEE Access*, 7:87479 – 87493, 2019.
- [9] S. Rezaie, C. Navarro Manchón, and E. De Carvalho. "Location- and Orientation-Aided Millimeter Wave Beam Selection Using Deep Learning". *ICC 2020 - 2020 IEEE International Conference on Communications (ICC)*, pages 1 – 6, 2020.
- [10] 3GPP. NR; Medium Access Control (MAC) protocol specification (Release 15). Tech. Spec. 38.321, V15.7.0 2019.

References

- [11] M. Giordani, M. Polese, A. Roy, D. Castor, and M. Zorzi. "A Tutorial on Beam Management for 3GPP NR at mmWave Frequencies". *IEEE Communications Surveys and Tutorials*, 21(1):173 – 196, 2019.
- [12] Y.-N. R. Li, B. Gao, X. Zhang, and K. Huang. "Beam Management in Millimeter-Wave Communications for 5G and Beyond". *IEEE Access*, 8:13282 – 13293, 2020.
- [13] S. S. Kalamkar, F. Baccelli, F. M. Abinader Jr., A. S. Marcano Fani, and L. G. Uzeda Garcia. Stochastic Geometry-Based Modeling and Analysis of Beam Management in 5G, 2020. arXiv:2006.05027v2 [cs.IT].
- [14] 3GPP. Study on requirements for NR beyond 52.6 GHz (Release 16). Tech. Rep. 38.807, V1.0.0 2019.
- [15] 3GPP. Study on new radio access technology Physical layer aspects (Release 14). Tech. Rep. 38.802, V14.2.0 2017.
- [16] 3GPP. "NR; Physical channels and modulation (Release 15)". Tech. Spec. 38.211, V15.3.0 2018.
- [17] 3GPP. Study on channel model for frequencies from 0.5 to 100 GHz (Release 15). Tech. Rep. 38.901, V15.0.0 2018.
- [18] 3GPP. Physical layer; Measurements (Release 16). Tech. Spec. 36.214, V16.1.0 2022.
- [19] 3GPP. NR; NR and NG-RAN Overall Description; Stage 2 (Release 15). Tech. Spec. 38.300, V15.7.0 2019.

Paper B

Improving Beam Management Signalling for 5G NR Systems using Hybrid Beamforming

F. Fernandes, C. Rom, J. Harrebek and C. Navarro Manchón

The paper has been published in the
2022 IEEE Wireless Communications and Networking Conference (WCNC2022)

© 2022 IEEE

The layout has been revised.

Abstract

5th Generation (5G) millimeter wave (mmWave) communications are enabled through directive and narrow beams that mitigate these frequencies' challenging propagation conditions. In the future, 5G-Advanced and 6G will go even higher in the frequency spectrum, to allow for progressively larger bandwidths. The need for a larger number of narrower beams will put a strain in the current analog beamforming (BF) based beam management (BM) framework. This paper proposes an alternative signalling method for BM to parallelize the beam sweeping procedure using a hybrid analog-digital (HAD) BF architecture to enable mmWave signal multiplexing with a manageable overhead. The proposed solution is shown to significantly enhance beam alignment performance while reducing signalling overhead and latency.

1 Introduction

The 5G NR standard supports a range of gNodeB antenna architectures for different frequencies of operation, mainly based on the number of TXRU that these technologies require. Given the poor propagation conditions at mmWave frequencies, large antenna arrays are required but the number of TXRU are not easily scalable. Large bandwidths, characteristic of mmWave, combined with bit resolution requirements makes them a high cost, complexity and power consuming solution. Therefore, fully digital architectures are typically reserved for the lower end of the 5G spectrum [1]. Instead, analog architectures are used for higher frequencies, to avoid the complexity-cost challenges of fully digital beamforming (BF). However, a single TXRU configuration comes with limitations such as the inability to multiplex signals in the spatial dimension.

In the current 5G standard, mmWave communications rely on beam-based operations [1]. This, along with the need for highly directional beams at the receiver and transmitter, prompt the issue of beam alignment that drives BM. This procedure can be described as a set of L1 and layer 2 operations that establish and maintain an optimal beam pair between the gNodeB and the UE, thus ensuring adequate link quality while the UE moves through the cell [2]. Given the importance of this procedure, optimization of BM performance has been extensively pursued in the literature. In [3], a dynamic weight-based algorithm is proposed for initial access (IA) SSB allocation, using static user distribution, to optimize the number of SSBs per sweeping direction. The authors in [4] introduce different beam switching algorithms to improve robustness of BM operations for intra-cell mobility scenarios. A mmWave IA protocol is developed in [5], with a compressive-sensing beam sweeping algorithm that achieves high BF gain, low misdetection probability and reduced search time. Furthermore, [6] employs a machine learning ap-

proach with a deep neural network trained for beam selection using RSRP measurements from standard compliant uplink signals in a high speed train use case, reducing signalling overhead and latency.

Most of these solutions still assume an analog architecture at the gNodeB array for BM. While the standard BM procedure performs adequately for current antenna array configurations, its ability to scale well in future cellular systems, where higher frequencies will be employed, is questionable. Larger antenna arrays will be required to compensate for the high frequency pathloss, making the beams even narrower. To maintain proper coverage, larger codebooks will need to be adopted, which will increase BM overhead, latency and overall complexity [7]. Therefore, the current BM framework must be updated to support a higher number of narrow beams. Hybrid BF architectures, which employ multiple radio frequency (RF) chains with analog phase shifters, can be used at mmWave as a compromise to enable spatial multiplexing while keeping a reduced number of TXRU and a manageable overhead [8].

This paper proposes a signalling scheme that enables the simultaneous transmission of spatially multiplexed SSBs for BM using low cross-correlation signals and a fully-connected HAD architecture. Using Monte-Carlo simulations, it is shown that the proposed signalling scheme is able to reduce overhead and latency of the beam sweeping procedure while improving the overall beam alignment performance when compared to its currently standardized counterpart, particularly for high-speed scenarios.

The remainder of this paper is organized as follows: Section 2 describes the system model, while Section 3 presents the proposed signalling scheme. Section 4 illustrates the performance of the proposed scheme and Section 5 concludes the paper and elaborates on future work.

2 System Model

2.1 Network Layout

A DL single-cell mmWave system is considered, where the gNodeB attempts to achieve beam alignment with a moving UE. A tri-sector cell is assumed, as seen in Fig. B.1, where the UE moves in a linear trajectory with a random direction at speed v in the east sector, bound by mobility ranges r and R . The gNodeB antenna array, standing at height h_{TX} m, is equipped with a ULA panel of patch antennas of size N_{TX} . The UE is modeled as a single isotropic antenna, $N_{RX} = 1$, at a height of h_{RX} m¹.

¹This work focuses on the signalling from the gNodeB side and, as such, this simplifying assumption is taken. Extension of this proposal for multi-antenna UEs is straightforward.

2. System Model

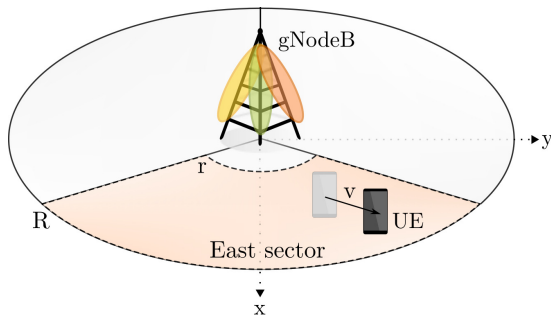


Fig. B.1: Network layout.

2.2 Signal Model

During the beam sweeping stage of BM, the gNodeB transmits several SSBs to determine the best beam to serve each UE. BF is undertaken with an analog or a HAD fully-connected architecture using N_{RF} TXRU, as seen in Fig. B.2 (a) and Fig. B.2 (b), respectively.

The generalized expression for the UE received signal at time-frequency resource k is given by

$$y(k) = \mathbf{h}(k)^\top \mathbf{F}(k) \mathbf{x}(k) + n(k) \quad (\text{B.1})$$

where $\mathbf{h}(k) \in \mathbb{C}^{N_{TX}}$ is the DL channel vector between the UE and the gNodeB in the k th time-frequency resource. These channel coefficients are obtained through a 3D geometry-based stochastic channel model generator, QuaDRiGa, which is compliant with current 3GPP standards for channel modelling [9]. In the gNodeB BF matrix $\mathbf{F}(k) \in \mathbb{C}^{N_{TX} \times N_{RF}}$, each column contains the analog phase shifts $\mathbf{f}_b \in \mathbb{C}^{N_{RF}}$ for a beam b used by a TXRU to transmit an SSB symbol in the k th time-frequency resource. Due to the analog implementation, all entries of $\mathbf{F}(k)$ have a constant modulus of $\frac{1}{\sqrt{N_{TX}}}$. The vector $\mathbf{x}(k) \in \mathbb{C}^{N_{RF}}$ expresses the N_{RF} transmitted SSB symbols in the k th time-frequency resource, with a symbol variance of $\frac{1}{\sqrt{N_{RF}}}$. This signal is generated using the 5G Toolbox[™] from MATLAB[®] [10]. Finally, $n(k) \sim \mathcal{CN}(0, \sigma^2)$ is the receiver's noise in the k th time-frequency resource modeled as a complex AWGN vector. This work assumes perfect subcarrier orthogonality conditions, specifically that the maximum channel delay response is within the cyclic prefix duration and the channel response is constant during a full OFDM symbol.

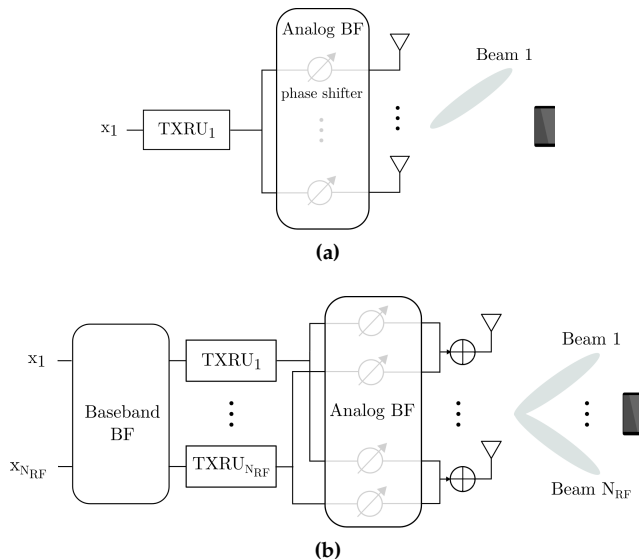


Fig. B.2: BF architectures. (a) Analog array. (b) HAD fully-connected array.

2.3 gNodeB BF Codebook

To perform SSB-based beam sweeping at the gNodeB, a directional BF codebook is adopted, which divides the cell's sector coverage area into separate angular regions. These beams are chosen from a predefined, finite set of N_{SS} vectors $\mathcal{C} = \{f_b | b = 1, \dots, N_{SS}\}$ which is referred henceforth as the codebook. The b th vector of the codebook is chosen as the array steering vector for angle ϕ_b , i.e.

$$f_b = \frac{1}{\sqrt{N_{TX}}} [1, e^{-j\pi \sin \phi_b}, \dots, e^{-j\pi(N_{TX}-1) \sin \phi_b}]^T. \quad (\text{B.2})$$

The angle ϕ_b is the azimuth angle to which the b th beam is pointing, measured on the xy plane with respect to the x axis. The steering angles ϕ_b , are linearly spaced within the angular range of the sector so that

$$\phi_b = -\frac{\pi}{3} + (b-1) \times \frac{2\pi}{3 \times (N_{SS}-1)}, b = 1, 2, \dots, N_{SS}. \quad (\text{B.3})$$

3 Signalling scheme

This section presents the proposed signalling scheme for gNodeB beam selection and how it differs from the current scheme in the standard. SSBs, or

3. Signalling scheme

SS/PBCH blocks, are generally used, among other NR signals, for measurement purposes to ensure proper beam alignment between the gNodeB and the UE. As described in [11], an SSB is grouped into 4 OFDM symbols in time and 240 subcarriers in frequency. It carries a PSS and SSS, for initial synchronization and cell/beam identification, respectively. These signals are pseudo random binary sequences with 127 m-sequence values. Additionally, a PBCH is included, associated with a DMRS. A group of SSBs is identified as an SSBurst, where each SSB is mapped to a different gNodeB beam.

3.1 Current Scheme in 5G NR

In the current NR standard, the SSBurst lasts less than 5 ms and its periodicity T_{ss} varies from 5 ms to 160 ms. All SSBs coming from a common gNodeB share the same PSS and SSS sequences, having the same cell ID. The maximum number of SSBs per SSBurst, N_{max} , as well as its resource mapping, are numerology-dependent [12]. For all numerologies, the SSB pattern always allocates one SSB at a time, as seen in Fig. B.3 (a). The gNodeB performs analog beam sweeping with N_{ss} beams and the UE receives and decodes one SSB at a time. During this process, the signal will be sequentially correlated with known PSS and SSS sequences to recover the physical cell identity of the gNodeB. This information is used to process PBCH-DMRS resources which can be used, together with SSS, to measure L1-RSRP [13]. Finally, the UE stores a subset of the best N RSRP values and reports them back to the gNodeB for beam determination. This study takes the current standardized scheme as a baseline to compare to the proposed scheme in terms of beam alignment performance.

3.2 Proposed Scheme

The proposed scheme employs the capabilities of a fully-connected HAD BF architecture to transmit N_{RF} SSBs in parallel while keeping the same array gain. To distinguish simultaneously transmitted SSBs, each of them must be associated with an unique PSS and SSS combination, exploiting the low cross-correlation nature of these sequences to preserve beam-specific information. Keeping the same SSBurst periodicity and block pattern, SSB groups are transmitted in overlapping time-frequency resources, creating $\frac{N_{SS}}{N_{RF}}$ transmission instances t . The best beam per group is identified during the PSS and SSS decoding stage. In each t , after recovering the correct PSS sequence, the UE searches the time-frequency resources where SSS is allocated, \mathcal{K}_{SSS} , to compute the correlation function between the SSS portion of the received signal, y_{SSS}^t , and all the reference SSS sequences, $r_{SSS,b}$, for each beam b through

$$X_{corr}^t[b] = \frac{1}{|\mathcal{K}_{SSS}|} \left| \sum_{k \in \mathcal{K}_{SSS}} y_{SSS}^t(k) r_{SSS,b}^*(k) \right| \quad (\text{B.4})$$

where $|\mathcal{K}_{SSS}|$ denotes the cardinality of set \mathcal{K}_{SSS} . The strongest correlation peak of each t is stored and reported back to the gNodeB for beam determination. The resources occupied for beam alignment are reduced by $\frac{1}{N_{RF}}$, as represented in Fig. B.3 (b). However, each parallel beam also experiences a scaling in power by the same factor.

3.3 Scheme Comparison

In order to enable the proposed scheme as add-on to the current standard, some requirements must be met. First, the beams assigned to grouped SSBs must be spatially separated to avoid inter-beam interference caused by beam overlap. Their beam indexes, extracted from the codebook \mathcal{C} , should be separated by $\frac{N_{SS}}{N_{RF}}$ positions. Furthermore, the beam indexing information for beams of the same group should be mapped to their unique PSS and SSS combination. Therefore, the PSS and SSS sequences of a group must present low cross-correlation.

4 Results and Discussion

This section details the performance evaluation of the proposed scheme. The KPIs used are detailed in Subsection 4.1. Subsection 4.2 showcases the overhead advantage of the proposed scheme while Subsection 4.3 focuses on the latency benefits for high-speed scenarios. Table B.1 summarizes all the simulation parameters used.

4.1 KPIs

To evaluate beam alignment performance, RSS measurements are performed over the time-frequency resources reserved for data transmission. This study assumes a potential data resource allocation set, \mathcal{K}_{data} , that occupies the whole available bandwidth B and time interval between consecutive SSBursts, as displayed in Fig. B.4 for a generic SSBurst set². The transmission window of one SSBurst and one \mathcal{K}_{data} set is referred to as a measurement period, MP , and lasts for T_{SS} ms. The RSS over \mathcal{K}_{data} for a beam b is defined as

²In a multi-user scenario, the available resource pool needs to be shared among users, resulting in a scaling of the absolute maximum achievable rate per user.

4. Results and Discussion

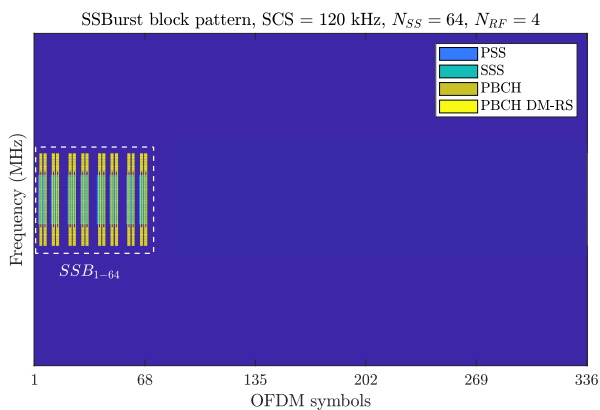
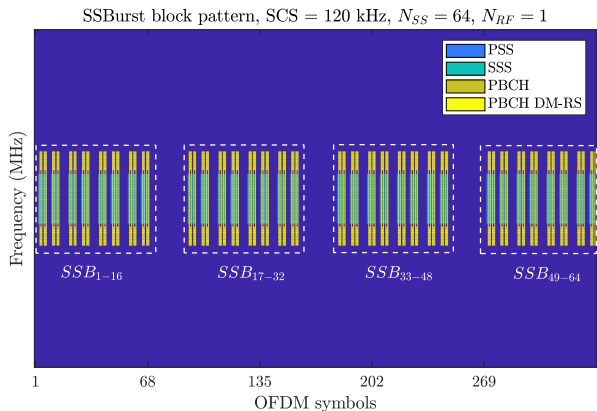


Fig. B.3: SSBurst block pattern for SCS = 120 kHz, $T_{SS} = 20$ ms, $N_{SS} = 64$. (a) Current implementation. (b) Proposed implementation with $N_{RF} = 4$.

$$R[b] = \frac{1}{|\mathcal{K}_{data}|} \sum_{k \in \mathcal{K}_{data}} |\mathbf{h}(k)^\top \mathbf{f}_b|^2 \quad (\text{B.5})$$

where $|\mathcal{K}_{data}|$ denotes the cardinality of set \mathcal{K}_{data} , i.e., the amount of time-frequency resources available for data transmission. For the proposed approach, the best measured beam is dictated by the strongest SSS correlation peak over all different transmission instances t . The corresponding RSS is calculated as

$$R_{meas} = R[\arg \max_b (\max_t X_{corr}^t[b])]. \quad (\text{B.6})$$

To evaluate beam selection accuracy, the measured RSS is compared to a genie beam selection. Considering optimal beam alignment, the maximum

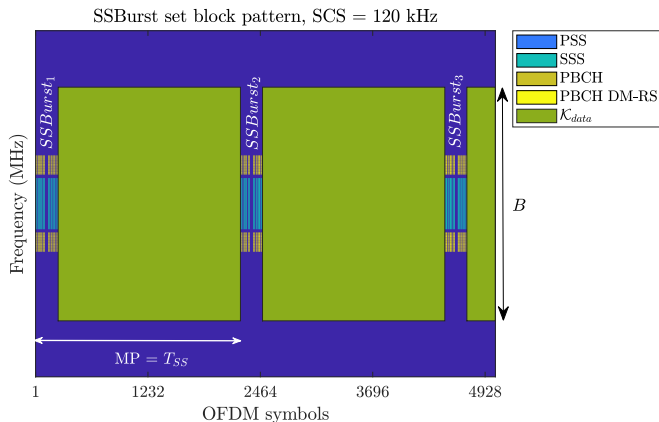


Fig. B.4: Data time-frequency resource allocation.

achievable RSS over all the N_{ss} available beams is determined by

$$R_{genie} = \max_b R[b]. \quad (\text{B.7})$$

Misdetection probability is defined as the probability that the selected best beam does not correspond to the optimal beam, given by

$$P_m = \mathbb{P}[R_{meas} < R_{genie}]. \quad (\text{B.8})$$

The impact of misdetections can vary, depending on how misaligned the measured beam is to the genie beam choice. Therefore, an additional criteria is introduced to quantify the beam misdetection loss, written as

$$\Delta SNR = \frac{R_{genie}}{R_{meas}}. \quad (\text{B.9})$$

To differentiate which misdetections actually jeopardize communications, $P_{m,3dB}$ expresses the probability that the ΔSNR incurred exceeds 3 dB as

$$P_{m,3dB} = \mathbb{P}[\Delta SNR_{dB} \geq 3 \text{ dB}]. \quad (\text{B.10})$$

After beam alignment, the channel's maximum achievable spectral efficiency is calculated as

$$S = \log_2\left(1 + \frac{R_{meas}}{\sigma^2}\right). \quad (\text{B.11})$$

4.2 Comparison of SSB Schemes with Common Overhead

With the proposed scheme, it is possible to support a larger gNodeB array codebook during BM without an overhead increase. This section compares

4. Results and Discussion

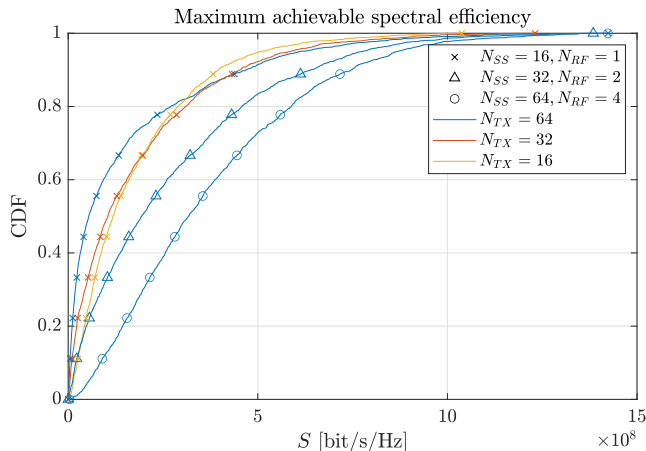
Table B.1: Simulation parameters

Parameter	Notation	Overhead Study	High-speed study
Carrier frequency	f	28 GHz	
Carrier Bandwidth	B	200 MHz	
SCS	SCS	120 kHz	
Maximum SSBs / SSBurst	N_{max}	64	
SSBurst periodicity	T_{SS}	20 ms	
Inner / Outer mobility bound	r / R	15 m / 100 m	15 m / 200 m
Channel model	-	UMi LOS	UMa LOS
gNodeB position	(x, y)	(0, 0)	
gNodeB height	h_{TX}	10 m	25 m
gNodeB TX power	P_{TX}	30 dBm	
UE position	(x, y)	random within east sector	
UE height	h_{RX}	1.5 m	
UE speed	v	60 km h ⁻¹	120 km h ⁻¹
Number of UE trajectories	N_{traj}	2000	
RX Noise Figure	NF	9 dB	
Thermal noise density	N_0	-174 dBm Hz ⁻¹	
gNodeB / UE antenna element	-	patch [14] / isotropic	
gNodeB / UE array size	N_{TX} / N_{RX}	64 / 1	

the BM performance of a UE moving at 60 km h⁻¹ under three different SSB transmission schemes with equal overhead: $N_{SS} = 16$ with $N_{RF} = 1$, $N_{SS} = 32$ with $N_{RF} = 2$ and $N_{SS} = 64$ with $N_{RF} = 4$. Due to the large array size and reduced number of beams, the first SSB transmission scheme is also tested for two smaller array dimensions, to reduce coverage gaps with wider beams. Table B.2 displays the P_m and $P_{m,3dB}$ values for each scheme. From the $N_{TX} = 64$ results, it is clear that beam alignment performance improves with N_{SS} . Since the beams are very narrow, to keep a good coverage level, a larger codebook must be employed. With $N_{SS} = 64$ and $N_{RF} = 4$ it is possible to use four times more beams with the same overhead, which improves coverage significantly. This results in less misdetections, an improved signal-to-noise ratio (SNR) and consequently, enhanced spectral efficiency, as shown in Fig. B.5 and Fig. B.6. However, if the scheme comparison is repeated for $N_{SS} = 16$ with $N_{TX} = 16$, the P_m from the schemes with $N_{RF} > 1$ become larger than the baseline. Since the array size is smaller, the beams lose gain and become wider, covering the sector uniformly. This approach reduces the maximum achievable spectral efficiency of this scheme but also decreases the number of beam misdetections. The increase in misdetections for the proposed scheme are due to inter-beam interference and reduced power levels per beam sent simultaneously. However, the performance of these schemes is still considerably higher compared to the baseline scheme in terms of misdetection loss and spectral efficiency, due to the larger overlap between beams

Table B.2: Detection accuracy

N_{SS}	N_{RF}	N_{TX}	P_m [%]	$P_{m,3dB}$ [%]
16	1	64	16.05	6.30
		32	6.85	2.85
		16	3.25	0.25
32	2	64	6.05	3.05
64	4	64	6.55	0.40

**Fig. B.5:** Maximum achievable spectral efficiency for three SSB schemes with common overhead, UMi LOS, $v = 60 \text{ km h}^{-1}$.

which makes beam misalignment errors less significant. This is evident from the $P_{m,3dB}$ results in Table B.2. Although the number of misdetections is larger, the occurrences where the power loss incurred is large enough to deteriorate communications is greatly reduced, especially for larger codebooks. In conclusion, this signalling scheme may enable the use of larger amounts of beams to improve coverage without overhead or latency costs, provided that adequate beam separation and transmit power are provided.

4.3 Scheme Performance for a High-Speed Scenario

So far, the UE measurement and reporting stage, as well as the gNodeB beam determination process have been considered to have a negligible delay. In reality, besides scheduling and processing delays, the UE may need to scan the gNodeB beams multiple times, either to smooth out fast fading effects or to measure different UE beams, assuming BF on the receiver side. This results in a delay of the beam selection operation. While those delays can be safely overlooked for low and moderate speeds, they can have a significant impact on

4. Results and Discussion

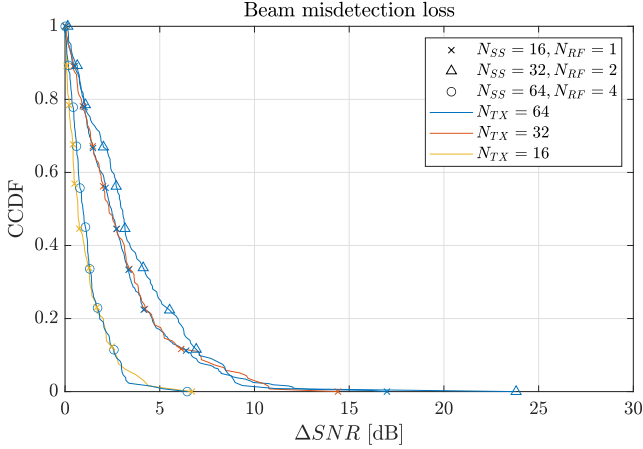
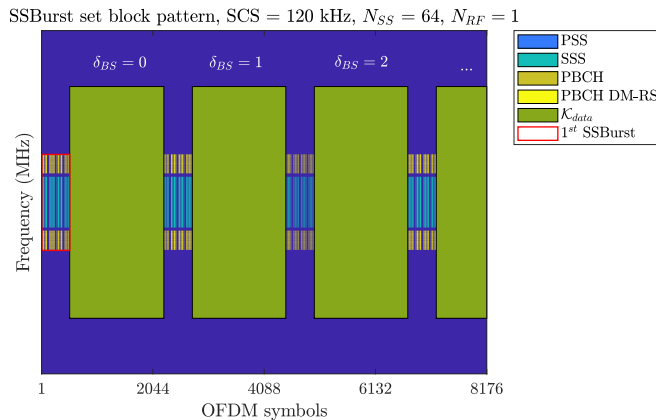


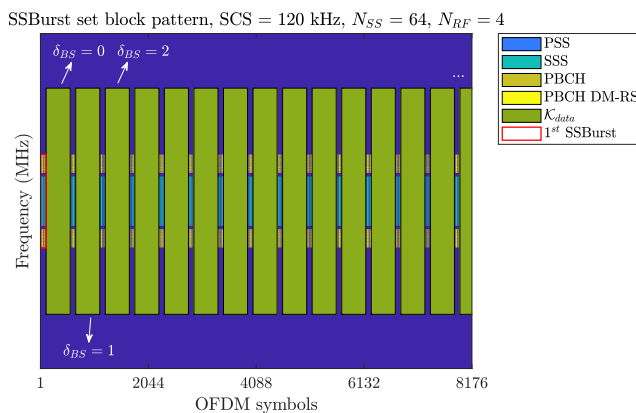
Fig. B.6: Beam misdetection SNR loss for three SSB schemes with common overhead, UMi LOS, $v = 60 \text{ km h}^{-1}$.

beam alignment performance for high mobility UEs, since beam information becomes outdated faster. Fig. B.7 (a) illustrates which \mathcal{K}_{data} period would be the first to employ the beam selection obtained through the measurements collected in the first SSBurst (highlighted in red), for different values of beam selection delay, δ_{BS} . If one MP is considered as the smallest unit of δ_{BS} , an instantaneous beam selection corresponds to $\delta_{BS} = 0$, where the first \mathcal{K}_{data} is transmitted with the beam selected in the same MP . If the delay is now considered to be $\delta_{BS} = 1$, then the beam selected with the measurements from the first SSBurst will only be in effect one MP later, in the second \mathcal{K}_{data} . With the proposed scheme, it is possible to keep the same overhead as in the baseline case and perform more frequent beam updates. Reducing the beam scan latency by a factor of N_{RF} allows for an increased beam scan periodicity, as seen in Fig. B.7 (b). It is assumed that the beam measurement, reporting and determination time constraints mentioned above can be equally compressed with the proposed scheme. The baseline signalling scheme is compared to the proposed scheme, at $v = 120 \text{ km h}^{-1}$, for $\delta_{BS} = 0$, $\delta_{BS} = 1$ and $\delta_{BS} = 3$.

Results in Table B.3 indicate that, as expected, P_m becomes larger when δ_{BS} for the baseline scheme increases, due to high-speed channel variability. This leads to high misdetection loss which deteriorates the maximum achievable spectral efficiency, as shown in Fig. B.8 and Fig. B.9. Employing the proposed solution results in a decrease of P_m which improves misdetection losses and achievable spectral efficiency. The δ_{BS} curves come close to the baseline scheme curve for $\delta_{BS} = 0$. It is worth mentioning that, although improvements for smaller values of δ_{BS} are less significant, this scheme is successful in improving speed robustness for BM without increased signalling



(a)



(b)

Fig. B.7: Selected beam usage for data transmission with different beam selection delays. (a) baseline scheme: $N_{SS} = 64$, $N_{RF} = 1$. (b) proposed scheme: $N_{SS} = 64$, $N_{RF} = 4$.

for lower speeds.

5 Conclusions

This paper proposes an alternative SSB transmission scheme for BM using low cross-correlation signalling and HAD BF in order to improve narrow beam alignment performance with a reduced amount of time-frequency resources. Results show that, with proper beam separation and power levels per beam, this proposal offers a significant improvement of beam detection accuracy and beam sweeping latency without requiring any additional overhead.

5. Conclusions

Table B.3: Detection accuracy

N_{ss}	N_{RF}	δ_{BS}	P_m [%]	$P_{m,3dB}$ [%]
64	1	0	6.45	0.23
		1	17.35	2.27
		3	37.00	9.05
64	4	0	2.00	0.03
		1	5.15	0.12
		3	9.85	0.80

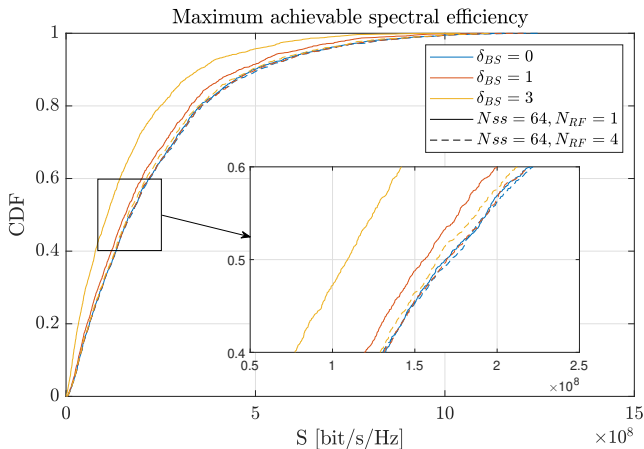


Fig. B.8: Maximum achievable spectral efficiency comparison for the baseline and proposed schemes with different beam selection delays, UMa LOS, $v = 120 \text{ km h}^{-1}$.

This work is meant to be a first step towards evolving the current BM procedure to support the overhead, latency and complexity challenges of future 5G and 6G signalling frameworks for larger antenna arrays. At higher frequencies, cellular systems will require larger BF gains but will also suffer the effects of reduced beamwidths. To guarantee coverage for all users, larger antenna arrays and codebooks will be indispensable. This scheme proposal would enable large codebook sizes of high-gain beams by scaling the signalling required to manage them, all while freeing up resources to improve the system's spectral efficiency. Although HAD BF consumes more energy due to the increase of TXRU, this solution is proposed to be employed on the gNodeB side, where the power cost constraints are less stringent. It boosts considerably the beam alignment performance with a reduced complexity and power consumption when compared to a fully-digital BF architecture. Moreover, to bring the proposed concept to practice, its interaction with time-frequency synchronization procedures will need to be considered, especially for high speed scenarios where perfect orthogonality assumptions may fall

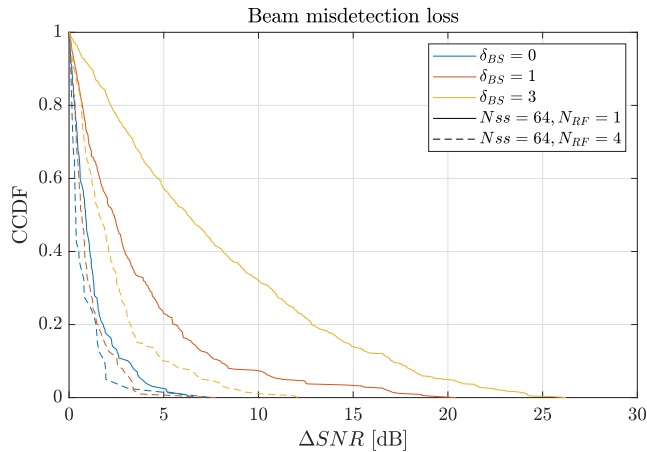


Fig. B.9: Beam misdetection SNR loss comparison for the baseline and proposed schemes with different beam selection delays, UMa LOS, $v = 120 \text{ km h}^{-1}$.

short for proper data decoding; this will be a subject of future research.

References

- [1] M. Enescu, editor. *5G New Radio: A Beam-based Air Interface*. John Wiley & Sons, 1st edition, 2020.
- [2] 3GPP. Study on new radio access technology Physical layer aspects (Release 14). Tech. Rep. 38.802, V14.2.0 2017.
- [3] A. Indika Perera, K. B. Shashika Manosha, N. Rajatheva, and Matti Latva-aho. "An Initial Access Optimization Algorithm for millimeter Wave 5G NR Networks". *2020 IEEE 91st Vehicular Technology Conference (VTC2020-Spring)*, pages 1 – 6, 2020.
- [4] U. B. Elmali, A. Awada, U. Karabulut, and I. Viering. "Analysis and Performance of Beam Management in 5G Networks". *2019 IEEE 30th Annual International Symposium on Personal, Indoor and Mobile Radio Communications (PIMRC)*, pages 1 – 7, 2019.
- [5] I. Ayakin and M. Krunz. "Efficient Beam Sweeping Algorithms and Initial Access Protocols for Millimeter-Wave Networks". *IEEE Transactions on Wireless Communications*, 19(4):2504 – 2514, 2020.
- [6] Y. G. Lim, H. J. Ji, J. H. Park, and Y. S. Kim. "Artificial Intelligence-Based Beam Management for High Speed Applications in mmWave Spectrum". *2020 IEEE Globecom Workshops (GC Wkshps)*, pages 1 – 6, 2020.

References

- [7] Y. Heng, J. G. Andrews, J. Mo, V. Va, A. Ali, B. L. Ng, and J. C. Zhang. "Six Key Challenges for Beam Management in 5.5G and 6G Systems". *IEEE Communications Magazine*, 59(7):74 – 79, 2021.
- [8] H. Yan, S. Ramesh, T. Gallagher, C. Ling, and D. Cabric. "Performance, Power, and Area Design Trade-Offs in Millimeter-Wave Transmitter Beamforming Architectures". *IEEE Circuits and Systems Magazine*, 19(2):33 – 58, 2019.
- [9] S. Jaeckel, L. Raschkowski, K. Börner, and L. Thiele. "QuaDRiGa: A 3-D Multicell Channel Model with Time Evolution for Enabling Virtual Field Trials". *IEEE Transactions on Antennas Propagation*, 62(6):3242 – 3256, 2014.
- [10] MathWorks. 5G Toolbox.
- [11] 3GPP. "NR; Physical channels and modulation (Release 15)". Tech. Spec. 38.211, V15.3.0 2018.
- [12] 3GPP. "NR; Physical layer procedures for control (Release 15)". Tech. Spec. 38.213, V15.12.0 2020.
- [13] 3GPP. NR; Physical layer measurements (Release 15). Tech. Spec. 38.215, V15.6.0 2019.
- [14] 3GPP. Study on channel model for frequencies from 0.5 to 100 GHz (Release 15). Tech. Rep. 38.901, V15.0.0 2018.

Paper C

Hand Blockage Impact on 5G mmWave Beam Management Performance

F. Fernandes, C. Rom, J. Harrebek, Simon Svenden and C.
Navarro Manchón

The paper has been published in
IEEE Access, 2022 Vol. 10, pp.106033 - 106049, 2022

© 2022 IEEE

The layout has been revised.

Abstract

Modelling and managing user-induced rotation and blockage in handheld multi-antenna panel devices are some of the pivotal challenges of future narrow beam millimeter wave (mmWave) communications. While studies have been conducted separately on multi-panel beam management (BM) performance and mmWave user blockage loss, no study has been made to date, to the best of the authors' knowledge, on how hand blockage influences beam alignment accuracy in the context of 5G new radio (NR). This paper presents a link-level evaluation on the impact of user hand grip in BM performance under a 5G NR standard compliant signalling and measurement framework. A high-detail handset model is employed, equipped with multiple panels and different hand grips obtained with CST Microwave Studio, a 3D electromagnetic field simulation tool. Additionally, this study incorporates aspects such as intra-cell mobility, device rotation, hand grip variability and changing propagation conditions. Results show that hand blockage can significantly degrade beam alignment performance, particularly for dual-hand grips in predominantly line-of-sight (LOS) environments. Finally, results suggest that the current blockage model proposed by 3GPP must be further enhanced to account for blockage on a per-panel basis. This would allow a more accurate portrayal of user hand behaviour, which would support the analysis and design of effective solutions to overcome the user's unpredictable shadowing effects at mmWave frequencies.

1 Introduction

While 5G relies on mmWave's large spectrum availability to enable data-hungry applications, its poor propagation conditions require that narrow beams be employed, both on the gNodeB and UE, to improve overall link budget. However, the directional nature of these antennas, along with unpredictable device orientation, create the need for multi-panel integration on the UE side [1]. This adds a higher degree of complexity to the beam alignment procedure, being considered as one of the big challenges for BM in future 5G and 6G releases [2], [3]. Additionally, at these high frequencies, the impact of the user on device performance also extends to self-blockage effects. Besides blockage from surrounding buildings, people or vehicles heightened by the use of narrower beams, the user's body itself will increase impedance mismatch, energy absorption and most significantly, shadowing effects. Therefore, the user's proximity to the device will manifest negatively in the UE's radiation performance, becoming an additional hindrance to the feasibility of mmWave communication systems.

Though both these fronts have been separately investigated, a study is still missing on exploring the BM procedure performance in conjunction with mmWave user blockage. This paper intends to fill this gap in the literature

by assessing the impact of human hand gripping on the performance of link-level mmWave BM. A detailed simulation tool has been created with a multitude of features that aim to recreate realistic scenarios for mmWave communications. These features, which can also be listed as the main contributions of this work, include:

- BM performance evaluation for initial beam alignment based on the 3GPP-defined DL signalling and measurement framework in which future 5G deployments for mmWave will be based on.
- Introduction of intra-cell user mobility, device rotation and variable channel conditions to achieve challenging outdoor simulation environments.
- Design of a multi-panel UE with beamforming capabilities. Most works on multi-panel UEs assume a single wide beam per panel (see Section 1.1). However, future mmWave device implementations will use narrow beams, further complicating the beam alignment process. Therefore, it is important to consider this aspect when evaluating BM performance.
- Usage of a 3D electromagnetic simulation tool to produce a detailed model of the antenna arrays, UE form factor (with a metal chassis, plastic case and glass layers) and the grips used to represent user hand blockage. In this work CST Microwave Studio [4] is employed to capture the effects of the form factor and the user's hand on the radiation performance of mmWave antennas that cause the loss of shape of the original codebook beams. While usually overlooked in the literature, results show that this phenomenon can actually significantly degrade the BM procedure, particularly in LOS environments.
- Adoption of three commonly used hand grips portraying different hand positions and grip tightness levels that could correspond, for example, to a user performing a video call, streaming or gaming on their smartphone. This results in a range of distinct blockage levels over each panel, to ensure that hand blockage is fairly depicted in both optimistic and pessimistic scenarios.
- Incorporation of the 3GPP blockage model in the tool for comparison with the CST model employed regarding their impact on beam alignment accuracy. Through this work it is evident that the 3GPP model leads to an overly pessimistic performance degradation when compared to the CST model, mostly due to its flat attenuation region approach. Results suggest that the introduction of panel-based blockage to the current 3GPP model could be a step towards improving its hand grip blockage characterization.

1. Introduction

In summary, this work focuses on integrating a highly detailed model of the antennas, the smartphone and the user's hand itself in a link-level BM performance analysis. It is important to note that this CST-based model introduces an additional level of complexity that, allied with all the other features mentioned above, provide a level of realism to the system that precludes a theoretical analysis of its performance, hence why Monte Carlo simulations are employed instead. This study is meant to complement other works in the literature such as [5], [6], that employ extensive analytical performance analysis with simplified assumptions on propagation, signalling or handset models.

1.1 Related Works

Extensive work on BM performance assessment has been done incorporating multi-panel UEs. The authors in [7] highlight the performance improvement of mmWave UE multi-panel uplink transmission when compared to its omnidirectional counterpart under 5G-compliant system level simulations. A mmWave system level performance evaluation is conducted in [8] employing 5G NR BM procedures and a proposed UE panel switching mechanism that maintains beam alignment errors low even for higher speeds. In [9] the authors explore the potential vulnerabilities of the multi-panel design for mobility purposes in a scenario where updated beam information might not reach all panels simultaneously. It is worth noting that these studies assume single antenna element panels, without beamforming on the UE side. In [10] a particle filter is used to improve beam alignment performance by combining RSRP measurements for a multi-panel array equipped device with orientation information obtained from inertial measurement unit sensors. A machine learning approach for the same method is proposed in [11] to further boost beam-prediction accuracy. However, the listed works on mmWave BM performance do not factor in user blockage into their studies.

Several works have also been developed to quantify and model human blockage. Some of these approaches include mathematical models where the blockage loss is calculated through the diffracted fields across the body, modeled as a conducting cylinder [12] or a combination of absorbing screens mimicking different body parts [13]. Other papers resort to heuristic models based on electromagnetic simulations and real-life phantom and device measurements that evaluate this blockage in terms of realized gain or equivalent isotropic radiated power-based spherical coverage, as well as RSS through ray-tracing tools for outdoor urban environments [14–18]. Most of these works register full body blockage losses ranging from 20 dB to 35 dB, focusing mostly on the effects of the user's torso with only 2 simplified hand grips: portrait and landscape, depending on the phone's orientations. The large discrepancy in the loss values can be explained by the lack of consistency

within research on antenna types and design, form factor implementation, user stance or gripping assumptions, since there is still no common agreement on how to model all of these complex components. In an attempt to reach a consensus and achieve result replicability, 3GPP proposes a model in [19] that attributes a flat attenuation of 30 dB to a region of the angular space delimited by the phone's orientation. This simplistic modelling has been challenged in works like [20] that propose instead a statistical model to approximate the attenuation of the same self-user blockage loss region to a Gaussian distribution, making the distinction between body and hand grip blockage. In [21] an exhaustive study is conducted to characterize hand and body blockage on a commercial mmWave device that shows blockage is dependent on factors such as antenna type, tightness of hand grip and narrow beams. Based on this, smaller regions of interest are defined in the angular space, based on where significant blockage is experienced, leading the authors to conclude that blockage loss can be considerably lower than claimed in previous papers, registering loss values for hand gripping as low as 5 dB.

1.2 Organization

The remainder of this paper is organized as follows: Section 2 describes the system model, while Section 3 and 4 focus on describing and comparing the two approaches used to model self-blockage in this study. Section 5 illustrates the results of blockage impact on BM performance and Section 6 concludes the paper and reflects on possible solutions to incorporate more detailed representation of self-blockage in current models.

2 System model

Fig. C.1 displays the DL single-cell mmWave system considered in this work, where intra-cell BM operations take place to achieve initial beam alignment between the gNodeB and a moving user. A tri-sector cell is assumed, where the user moves linearly with a fixed orientation and speed v in the east sector, bounded by mobility ranges r and R . The gNodeB, standing at a height of h_t m, is equipped with a UPA of N_t patch antennas. The UE, being held at a height of h_r m, is modeled as a multi-panel device, each panel composed of a ULA of N_r patch antennas. Due to the limited angular coverage of these antennas, its panel placement follows a commonly used edge design [22], with one antenna module on each side of the form factor, as can be seen in Fig. C.2.

The gNodeB and UE positioning can be described according to the GCS represented in Fig. C.1, while their orientation is dictated by their own LCS, expressing any 3D rotation with respect to the GCS. Although the gNodeB is

2. System model

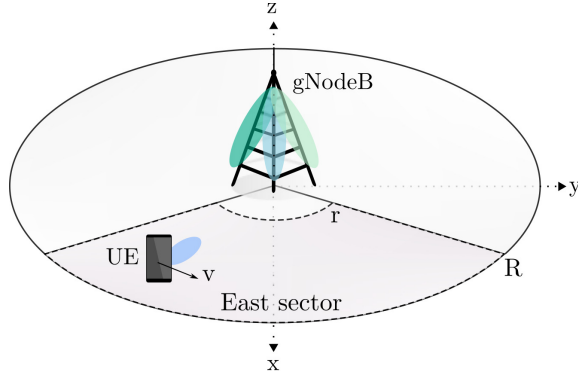


Fig. C.1: Network Layout.

assumed to have a fixed location, with its LCS aligned with the GCS, the UE's orientation varies over the bearing angle α_{UE} , the downtilt angle β_{UE} and the slant angle γ_{UE} . As illustrated in Fig. C.3, this set of angles represents three elemental rotations about the z , y and x axes, respectively [19]. In this work two distinct device orientation modes are considered for the UE: portrait and landscape. Portrait mode takes $\beta_{UE} = 0$ with α_{UE} and γ_{UE} varying randomly according to a uniform distribution in the ranges $\alpha_{UE} \in [0, 2\pi]$ and $\gamma_{UE} \in [0, \frac{\pi}{2}]$. In turn, landscape mode takes $\gamma_{UE} = 0$ with α_{UE} and β_{UE} varying randomly according to a uniform distribution in the ranges $\alpha_{UE} \in [0, 2\pi]$ and $\beta_{UE} \in [-\frac{\pi}{2}, 0]$.

2.1 Channel model

The mmWave DL channel response is obtained for the i th UE panel through QuaDRiGa, a 3GPP compliant, 3D geometry-based stochastic channel model generator [23], modelled in the k th time-frequency resource as

$$\mathbf{H}^i(k) = \sum_{l=1}^L g_l \mathbf{a}_r^i(\theta_{r,l}^i, \phi_{r,l}^i) \mathbf{a}_t^H(\theta_{t,l}, \phi_{t,l}) e^{-j2\pi\tau_l f_k}, \quad (\text{C.1})$$

with L , g_l , τ_l and f_k being the total multipath components of the channel, the path l 's complex gain and delay values and the subcarrier frequency, respectively. Additionally, \mathbf{a}_t and \mathbf{a}_r^i express the transmitter and receiver array responses for a path l 's elevation and azimuth angles of arrival ($\theta_{r,l}^i, \phi_{r,l}^i$), and departure, $(\theta_{t,l}, \phi_{t,l})$ ¹. The array response for a gNodeB or UE array panel of size $N = N_x N_y N_z$ is written as

¹The reader should note that L , g_l , τ_l , departure and arrival angles are considered to be time-varying. However, to simplify notation, the dependency of these channel parameters with the time-frequency index k is omitted in (C.1).

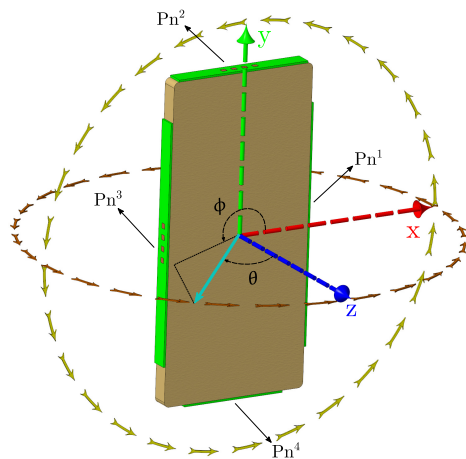


Fig. C.2: UE's LCS, panel placement and spherical coordinates. Pn^i indicates the position of the i th antenna panel.

$$\mathbf{a}(\theta, \phi) = \tilde{\mathbf{a}}(\theta, \phi) \odot \mathbf{g}_{ae}(\theta, \phi), \quad (\text{C.2})$$

where $\mathbf{g}_{ae} \in \mathbb{C}^N$ denotes each antenna element's linear gain, \odot the Hadamard product and $\tilde{\mathbf{a}}$ is described as

$$\tilde{\mathbf{a}}(\theta, \phi) = \frac{1}{\sqrt{N}} \mathbf{a}_z(\theta) \otimes \mathbf{a}_y(\theta, \phi) \otimes \mathbf{a}_x(\theta, \phi), \quad (\text{C.3})$$

where \otimes expresses the Kronecker product, with $\mathbf{a}_x \in \mathbb{C}^{N_x}$, $\mathbf{a}_y \in \mathbb{C}^{N_y}$ and $\mathbf{a}_z \in \mathbb{C}^{N_z}$ given by

$$\mathbf{a}_x(\theta, \phi) = [1, e^{j\pi \sin \theta \cos \phi}, \dots, e^{j\pi(N_x-1) \sin \theta \cos \phi}]^T \quad (\text{C.4})$$

$$\mathbf{a}_y(\theta, \phi) = [1, e^{j\pi \sin \theta \sin \phi}, \dots, e^{j\pi(N_y-1) \sin \theta \sin \phi}]^T \quad (\text{C.5})$$

$$\mathbf{a}_z(\theta) = [1, e^{j\pi \cos \theta}, \dots, e^{j\pi(N_z-1) \cos \theta}]^T. \quad (\text{C.6})$$

2.2 Signal Model

The signal model employed in this paper is based on the current DL signalling proposed by 3GPP for BM, which is described below.

2. System model

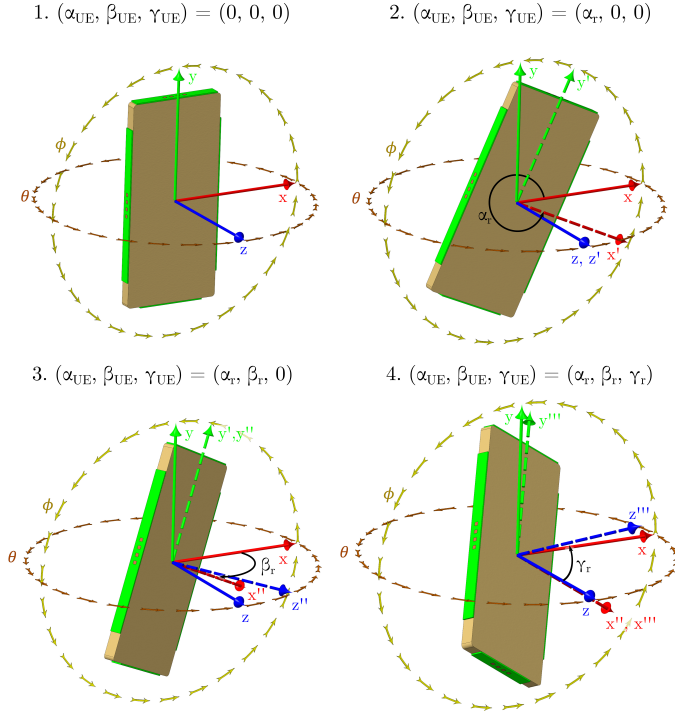


Fig. C.3: LCS (dotted axes) orientation with respect to the GCS (solid axes) through a sequence of 3 rotations: $\alpha_r = \frac{11\pi}{6}$, $\beta_r = -\frac{\pi}{6}$ and $\gamma_r = \frac{\pi}{6}$.

BM procedures - P1, P2 and P3

3GPP's BM framework is described as a set of L1 and L2 procedures that employ beam sweeping, beam measurement, beam determination and beam reporting to achieve and maintain beam alignment between the gNodeB's and the UE's narrow beams [24], [25]. The procedures in question are not specified in the standard but are colloquially referred to as P1, P2 and P3 in technical discussions and reports [24]. P1 refers to the gNodeB beam selection in an IA context where broad beams are typically used to scan the angular space and estimate a coarse serving direction for a user. P2 takes place after P1, where the gNodeB uses narrower beams to refine the former beam selection within the broad beam direction. Finally, P3 occurs after beam selection at the gNodeB side where, with a fixed transmitting beam, the UE can sweep through its beams to find the best beam pair.

It is worth noting that the standard does not mandate that all of these conceptual procedures be instated. Similarly, the beamwidth relationship described above between P1 and P2 beams, despite being a common assumption in the industry, is not specified in the standard. Instead, this should

be scenario-dependent to avoid unnecessary latency and signalling overhead. Therefore, this work employs a variation of these procedures, achieving beam alignment through P1 with narrow beams on the gNodeB side and P3 at the UE, eliminating the need for P2 beam refinement. Two stages are defined for this process: first, a joint gNodeB beam and UE panel selection, followed by a UE panel beam refinement, as detailed in Fig. C.4.

For both P1 and P3, the received signal at any UE panel i in the k th time-frequency resource is given by

$$y^i(k) = \mathbf{w}^{iH} \mathbf{H}^i(k) \mathbf{f} x(k) + \mathbf{w}^{iH} \mathbf{n}^i(k), \quad (\text{C.7})$$

where $\mathbf{H}^i(k) \in \mathbb{C}^{N_r \times N_t}$ denotes the channel matrix for UE panel i as defined in (C.1). $\mathbf{f} \in \mathbb{C}^{N_t}$ is the gNodeB beamforming vector containing the analog phase shifts for a beam, with a constant modulus of $\frac{1}{\sqrt{N_t}}$, that spatially filters the transmitted signal $x(k)$. This signal is received at the UE with a beam defined by the analog phase shifts in the beamforming vector $\mathbf{w}^i \in \mathbb{C}^{N_r}$, with a constant modulus of $\frac{1}{\sqrt{N_r}}$. Finally, $\mathbf{n}^i(k) \in \mathbb{C}^{N_r} \sim \mathcal{CN}(\mathbf{0}, \sigma^2 \mathbf{I})$ is the receiver's noise in the k th time-frequency resource modeled as a complex AWGN vector with variance σ^2 . This work assumes perfect subcarrier orthogonality conditions, where the maximum channel delay response is within the cyclic prefix duration and the channel response remains constant during a full OFDM symbol.

P1 - Joint gNodeB beam and UE panel selection

In this stage, the gNodeB sweeps through N_{ss} narrow beams selected from the gNodeB codebook \mathcal{C}_t (see Section 2.3), each associated with a distinct SSB. SSBs are sets of resources spanning 4 OFDM symbols in time and 240 subcarriers in frequency, generally used for L1-RSRP measurements to determine the best gNodeB serving beam. One or multiple SSBs compose an SSBurst, which is transmitted according to a numerology-dependent transmission pattern [26], [27]. The SSBurst generation is performed through MATLAB[®]'s 5G Toolbox[™] [28]. In P1, the UE activates a single antenna element per panel, receiving and measuring these signals with a wide beam. For this purpose, a broad beam combining vector is employed $\mathbf{w}_{\psi_{r,b}} \in \mathbb{C}^{N_r}$, where all entries are null except for the first one, which takes a unit value. It is assumed that the UE activates all its panels simultaneously for measurement purposes, following 3GPP's "Assumption-2" (MPUE A2) or "Assumption-3" (MPUE A3) [29]. For each received SSB associated to a beam ψ_t , the UE measures its SS-RSRP at each of the panels [30]. This is the linear average over the power contributions (in W) of the resource data set \mathcal{K}_{ss} within that SSB that carries the SS signals. Thus, for panel i and beam ψ_t , the RSRP measurement is computed

2. System model

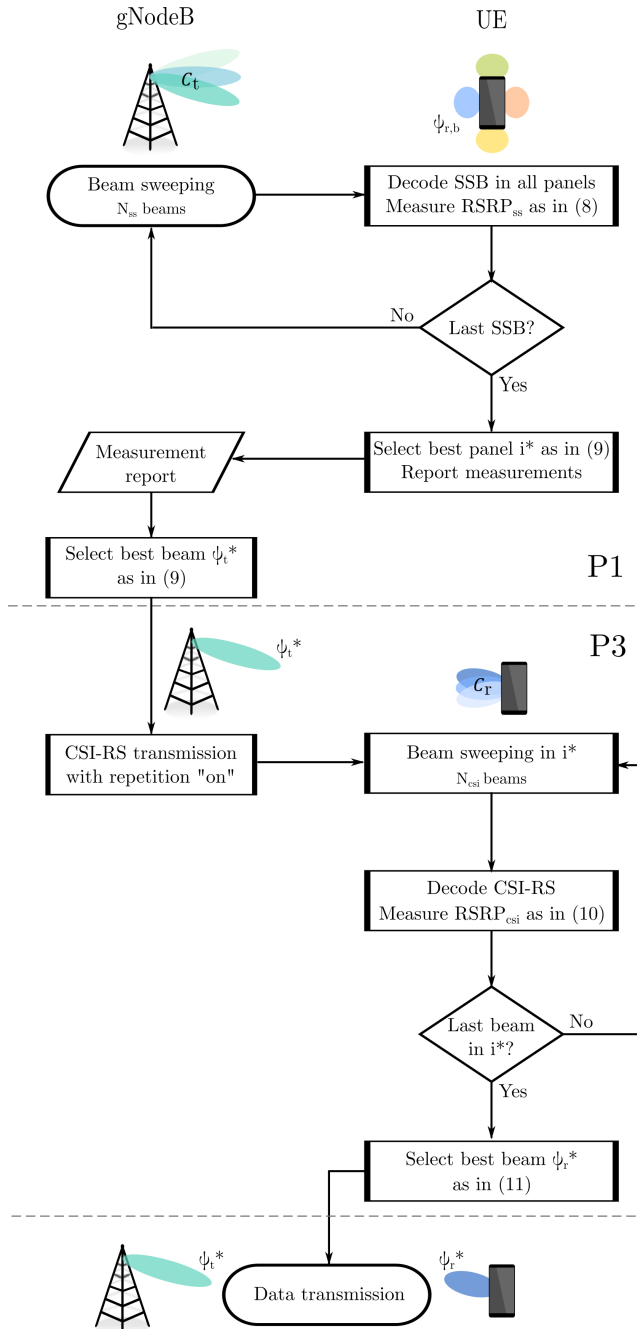


Fig. C.4: Flowchart of adopted 3GPP-based BM process.

as

$$RSRP_{ss}(\psi_t, i) = \frac{1}{|\mathcal{K}_{ss}|} \sum_{k \in \mathcal{K}_{ss}} |\mathbf{w}_{\psi_r, b}^H \mathbf{H}^i(k) \mathbf{f}_{\psi_t} + \mathbf{w}_{\psi_r, b}^H \mathbf{n}^i(k)|^2, \quad (\text{C.8})$$

where $|\mathcal{K}_{ss}|$ refers to the total amount of time-frequency resources from the SSB transmitted by beam ψ_t containing SS signals. After obtaining $RSRP_{ss}$ for all the beams, it is assumed that the UE decides on the best selected panel i^* to keep active for data transmission and reports a subset of the highest power transmit beams back to the gNodeB for selection of the best beam ψ_t^* . This joint gNodeB beam and UE panel selection results thus in

$$(\psi_t^*, i^*) = \arg \max_{\psi_t, i} (RSRP_{ss}(\psi_t, i)). \quad (\text{C.9})$$

P3 - UE beam panel selection

Once ψ_t^* has been determined on the gNodeB side, it is then used to send N_{csi} CSI-RS to the UE, one for each UE beam, to initiate beam refinement on the receiver side. CSI-RS are UE-specific signals transmitted by the gNodeB to monitor radio link channel characteristics for several use cases. These signals have an extremely flexible configuration, tailored to each diverse application. This work focuses on their role for DL BM, to obtain L1-RSRP measurements for UE beam candidate selection [25]. In this particular case, CSI-RS are distinguished with an additional higher layer parameter named "repetition" which has a binary "on" or "off" state. In P3 this parameter is set to "on", meaning that the UE can assume that no sweeping is being done on the gNodeB side and, therefore, can sweep through its own beams in panel i^* , which are selected from the UE codebook \mathcal{C}_r (see Section 2.3). When received at the UE, with a beam ψ_r , its CSI-RSRP is measured, in an analogous process to the one described in (C.8), over the resource elements that carry CSI-RS so that

$$RSRP_{csi}(\psi_r) = \frac{1}{|\mathcal{K}_{csi}|} \sum_{k \in \mathcal{K}_{csi}} |\mathbf{w}_{\psi_r}^H \mathbf{H}^{i^*}(k) \mathbf{f}_{\psi_t^*} + \mathbf{w}_{\psi_r}^H \mathbf{n}(k)|^2. \quad (\text{C.10})$$

This is repeated for all the beams in the panel to allow the UE to complete the beam alignment procedure by selecting the beam with the highest power level, indicated by

$$\psi_r^* = \arg \max_{\psi_r} (RSRP_{csi}(\psi_r)). \quad (\text{C.11})$$

2.3 Beamforming Codebook

2. System model

gNodeB codebook

To ensure sufficient signal strength for any user position, the cell sector's coverage range is divided into two smaller regions, coverage range 1 (CR1) and coverage range 2 (CR2), as seen in Fig. C.5. A user located in CR1 is closer to the gNodeB while a user in CR2 is nearer to cell-edge. The UE's initial position and trajectory direction follow a uniform distribution in the xy plane (since the user's height in the z-axis is kept constant) within the cell sector's area. For the purpose of this study, it is worth highlighting that the UE's mobility is restricted to the bounds of the cell sector r and R , always remaining within the coverage range.

For beam sweeping at the gNodeB, a directional beamforming codebook is adopted, dividing the cell's sector coverage into angular regions in azimuth and elevation. These beams belong to a predefined, finite set of N_{ss} vectors $\mathcal{C}_t = \{\mathbf{f}_{\psi_t} | \psi_t = 1, \dots, N_{ss}\}$ which is referred to henceforth as the gNodeB codebook. The array steering vector for a transmit beam ψ_t pointing towards $(\theta_{\psi_t}, \phi_{\psi_t})$ is defined in the ψ_t^{th} vector of the codebook as

$$\mathbf{f}_{\psi_t} = \mathbf{a}_t(\theta_{\psi_t}, \phi_{\psi_t}). \quad (\text{C.12})$$

In CR1, due to the UE's proximity to the gNodeB, N_{ss}^{CR1} wider beams are employed while users in CR2 require N_{ss}^{CR2} more directive beams to compensate for pathloss. Since these higher gain beams are also narrower, to cover the same angular coverage area, it is assumed that $N_{ss}^{CR1} < N_{ss}^{CR2}$. Therefore, this codebook describes a GoB composed of $N_{ss} = N_{ss}^{CR1} + N_{ss}^{CR2}$ beams. For a given range CR , the azimuth steering angles, $\phi_{\psi_t}^{CR}$, are linearly spaced within the angular range of the sector such that

$$\phi_{\psi_t}^{CR} = -\frac{\pi}{3} + (\psi_t^{CR} - 1) \times \frac{2\pi}{3 \times (N_{ss}^{CR} - 1)}, \psi_t^{CR} = 1, \dots, N_{ss}^{CR}. \quad (\text{C.13})$$

Moreover, all the beams of a common CR share an elevation steering angle, $\theta_{\psi_t}^{CR}$, defined as

$$\theta_{\psi_t}^{CR} = \pi - \arctan\left(\frac{r_{CR}}{h_t - h_r}\right), \quad (\text{C.14})$$

where r_{CR} represents the center of the coverage region's radius. Both regions are assumed to have the same coverage range. The radius of CR1 is given by

$$r_{CR1} = r + \frac{R - r}{4} \quad (\text{C.15})$$

and the radius of CR2 is described as

$$r_{CR2} = r + \frac{3(R - r)}{4}. \quad (\text{C.16})$$

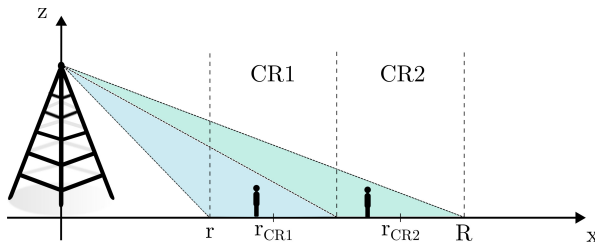


Fig. C.5: Cell coverage regions for gNodeB GoB design.

UE panel codebook

Each panel integrated into the device is considered to have beamforming capabilities for UE beam refinement. Each panel produces a finite set of N_{csi} vectors $\mathcal{C}_r = \{\mathbf{w}_{\psi_r} | \psi_r = 1, \dots, N_{csi}\}$, the UE panel codebook. The array steering vector in any panel for a receive beam ψ_r directed towards $(\frac{\pi}{2}, \phi_{\psi_r})$ is expressed as

$$\mathbf{w}_{\psi_r} = \mathbf{a}_r\left(\frac{\pi}{2}, \phi_{\psi_r}\right). \quad (\text{C.17})$$

Each ULA panel in the UE covers a $\frac{\pi}{2}$ sector of the angular space in the azimuth domain, with linearly spaced steering angles ϕ_r such that

$$\phi_{\psi_r} = -\frac{\pi}{4} + (\psi_r - 1) \times \frac{\pi}{2 \times (N_{csi} - 1)}, \psi_r = 1, \dots, N_{csi}. \quad (\text{C.18})$$

3 Antenna and Hand blockage model

This work focuses on assessing how BM performance is impacted by user hand-grip induced blockage in a multi-panel handset terminal. To achieve this, two models are adopted for human blockage: a simplified model proposed by 3GPP and a highly detailed model of the smartphone antenna integration and hand gripping obtained through CST Microwave Studio [4]. The contrast between these two models comes down to the values that the entries of the vector \mathbf{g}_{ae} take in (C.2), defined in Section 2.1. Both models, linked to a common codebook choice, are compared in Section 4, whereas their influence in BM performance is analyzed in Section 5.

3.1 3GPP model

gNodeB and UE antenna modelling

3GPP defines in [31] a generalized antenna radiation pattern model resembling a patch antenna. Its vertical radiation pattern, in dB, is given by

3. Antenna and Hand blockage model

$$G_{ae,v}(\theta) = -\min\left\{12\left(\frac{\theta - 90^\circ}{\theta_{3\text{dB}}}\right)^2, SLA_v\right\}, \quad (\text{C.19})$$

where $\theta_{3\text{dB}}$ and SLA_v are the vertical half power beamwidth and the side lobe suppression value. Similarly, the horizontal antenna element radiation pattern is expressed in dB as

$$G_{ae,h}(\phi) = -\min\left\{12\left(\frac{\phi}{\phi_{3\text{dB}}}\right)^2, A_m\right\}, \quad (\text{C.20})$$

with $\phi_{3\text{dB}}$ and A_m being the horizontal half power beamwidth and the front to back ratio of the radiation pattern. Finally, the 3D antenna element radiation pattern is computed as

$$G_{ae}(\theta, \phi) = -\min\{-[G_{ae,v}(\theta) + G_{ae,h}(\phi)], A_m\}. \quad (\text{C.21})$$

The same model is considered both at the gNodeB and UE with their own parametrization defined in Table C.1. The antenna arrays are constructed with this model assuming a half-wavelength spacing between antenna elements. For the UE, 4 identical ULA arrays are employed and rotated $90^\circ \times (i - 1)$ degrees, to mimic the relative orientation of a panel Pn^i in the LCS.

Self-blocking model

Two distinct blockage models are detailed in [19], model A and model B. Model A in particular assumes a stochastic approach to characterize human and vehicular blocking, including a self-blocking component. This feature mimics the user's blockage by creating an attenuation region in the UE's LCS for a device oriented in portrait or landscape mode. These self-blocking regions, described in Table C.2, depict a central blockage direction, (θ_{sb}, ϕ_{sb}) , that spans x_{sb} and y_{sb} degrees in azimuth and elevation, respectively. This 3GPP-defined self-blocking model proposes a binary attenuation, where every direction within the self-blocking region suffers a 30 dB loss, while the rest of the angular space remains with 0 dB attenuation, as depicted in Fig. C.6 for each of the UE orientation modes.

3.2 CST model

Form factor modeling

The form factor simulated resembles a commonly adopted wide-body design with a width, length and thickness of 76 mm, 157 mm and 10 mm, respectively. At mmWave frequencies, the performance of smartphone-integrated antennas is much more susceptible to deterioration due to proximity to other

Table C.1: 3GPP gNodeB and UE antenna modelling.

Parameter	gNodeB	UE
$\theta_{3\text{ dB}}$	65°	90°
$\phi_{3\text{ dB}}$		
SLA_v	30 dB	25 dB
A_m		
$\max\{G_{ae}\}$	8 dBi	5 dBi

Table C.2: 3GPP self-blocking region parameters.

Mode	ϕ_{sb}	x_{sb}	θ_{sb}	y_{sb}
Portrait	260°	120°	100°	80°
Landscape	40°	160°	110°	75°

elements contained in the form factor, such as cameras, glass displays or microphones. In order to exclude the impact of design-specific placement of these components to produce a more generic result set, a simplified form factor is considered in Fig. C.7. It is composed of a solid metal chassis surrounded by a 1 mm thick substrate layer and plastic frame, with the front and the back glass components of the device included. These materials' properties, at the operation frequency of 28 GHz, are summarized in Table C.3.

UE antenna modeling

A patch antenna is designed with CST to imitate the 3GPP UE model described in Section 3.1. Each element is simulated as a dual-polarized patch antenna occupying an area of 2.4 mm × 2.4 mm, using the device's chassis as a ground plane and a substrate 1 mm thick. For this study, only one of the polarizations is employed. Assuming a half-wavelength spacing between antenna elements, these patches are simulated as part of 4 distinct ULA arrays integrated at the center of each edge of the form factor, as can be seen in Fig. C.2.

Hand grip modeling

This work considers three representative hand grips for self-blocking, one for the phone in portrait mode and two for the phone in landscape mode. Fig. C.8 represents a right hand grip over the phone in portrait mode. The user's thumb is placed over Pn¹ and three fingers clasp the device in close proximity to Pn³. This position is commonly used during video calls. This study also includes dual-hand grips, since a large number of device applications nowadays require the phone to be used in landscape mode, which, due to

3. Antenna and Hand blockage model

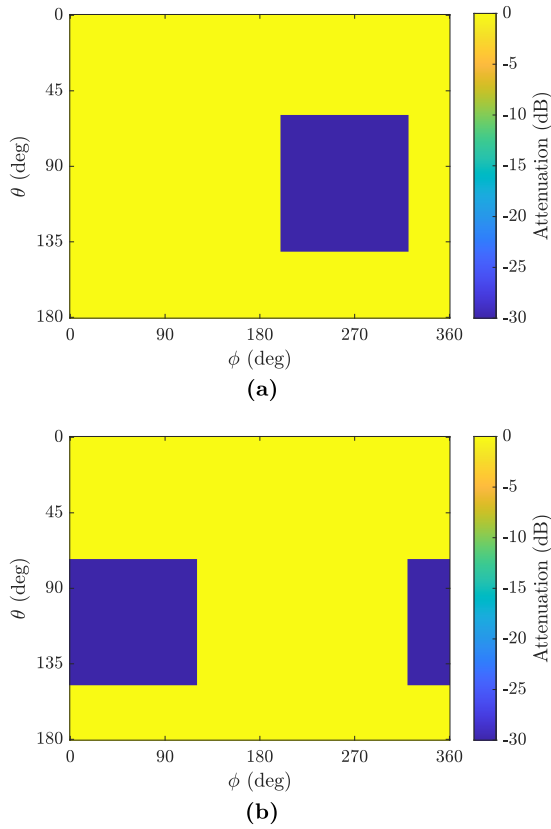


Fig. C.6: Stereographic projection of 3GPP's self-blocking attenuation region. (a) Portrait mode. (b) Landscape mode.

large form factor sizes, is usually done with both hands. Since handling of the phone is subjective to each user, countless grips could be considered. In this paper an attempt to categorize dual hand grips is made by selecting a moderate and severe grip in terms of blockage impact. Fig. C.9 displays dual hand grip model 1, a pessimistic grip where the hands engulf a large area of the smartphone, which can occur when the user is streaming content. Here both Pn^2 and Pn^4 are slightly covered by the users thumbs, while Pn^1 and Pn^3 are partially blocked by the user's fingers and palms, respectively. Dual hand grip model 2 mimics a gaming stance where the user is interacting with the screen, as shown in Fig. C.10. Both Pn^2 and Pn^4 are completely ensnared by the hands, while Pn^1 and Pn^3 remain uncovered. These hand grips are replicated in CST as variations of the Wide Hand Grip CAD model defined and supplied by CTIA [32] with $\epsilon_r = 16.5$ and $\sigma = 25.8 \text{ S m}^{-1}$, as shown in Table C.3 [20].

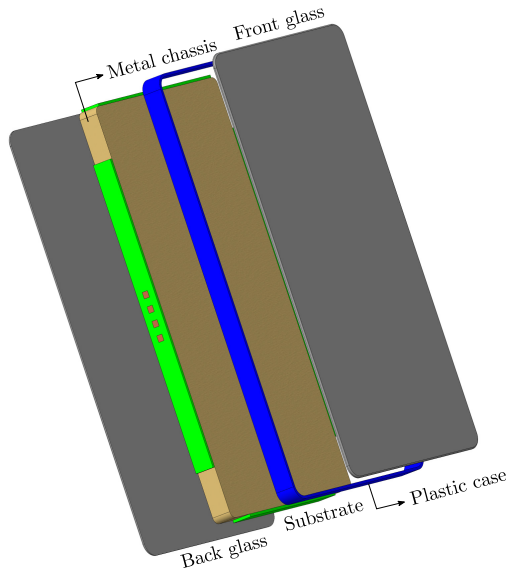


Fig. C.7: CST-modeled form factor.

Table C.3: Dielectric constant (ϵ_r), loss tangent ($\tan \delta$) and electrical conductivity (σ) of the CST model components at 28 GHz.

Component	Material	ϵ_r	$\tan \delta$	σ (S m^{-1})
Chassis	Copper	-	-	5.8
Substrate	Rogers 4003	3.55	0.0027	-
Case	Plastic	2.9	0.0075	-
Glass	-	5.75	0.0036	-
User hand	-	16.5	-	25.8

4 Model comparison

This section highlights the main differences between the 3GPP and CST antenna and user blockage models. While Subsection 4.1 compares the two model approaches on a per-antenna element basis, Subsection 4.2 describes the human blockage model impact on a narrow UE beam codebook.

4.1 Antenna and blockage model comparison

The 3GPP model assumes that all antenna elements in an array share the same radiation pattern, $G_{ae}(\theta, \phi)$, described in Subsection 3.1. In reality, each antenna element's pattern depends on its placement in the form factor. Its proximity to other device components and its coupling to adjacent antennas

4. Model comparison

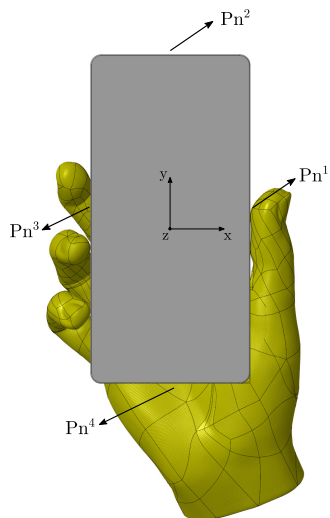


Fig. C.8: Right hand grip model - portrait mode.

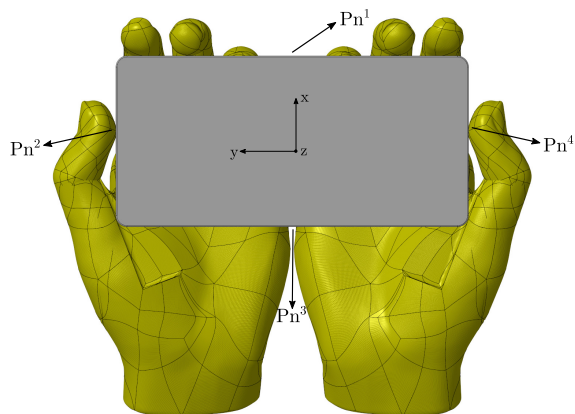


Fig. C.9: Dual hand grip model 1 - landscape mode.

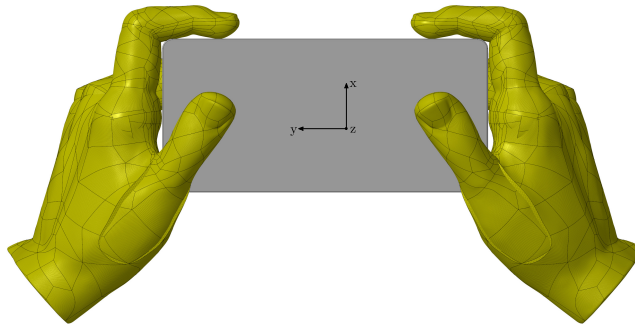


Fig. C.10: Dual hand grip model 2 - landscape mode.

creates a unique radiation pattern for each element, affecting the array's beam shape. This phenomenon is better captured with CST, where it is possible to extract the individual radiation patterns of each antenna in a panel array, resulting in a more realistic combined beam pattern.

However, the repercussions of such a simplification to the model become exacerbated when accounting for the user's self-blockage. In the presence of a hand grip, each antenna in each panel experiences a separate level of blockage, depending on how the hand falls onto the device. It is possible that some antenna elements in a panel are fully or partially covered by a finger while others remain undisturbed. How close together the user's fingers are, as well as their distance to the panel also impacts the performance of each element differently, potentially leading to a complete loss of the original beam shape. However, the current 3GPP model for self-blockage assumes the same blocking region for all panels, with all antennas suffering the same attenuation. Moreover, this model does not account for blockage-induced beam pattern deformation. The beams still resemble the blockage-free scenario except for a fixed attenuation area. The contrast between both models is discernible in Fig. C.11, where the radiation patterns for P_n^1 's antenna element 1 and antenna element 4 are considered under the portrait blockage models. While the radiation patterns of the 3GPP model are indistinguishable, there is a clear discrepancy between the antennas in the CST model. For this grip, as seen in Fig. C.8, the thumb of the user rests over P_n^1 . Although not visible in the illustration, antenna element 1 is the closest to the base of the thumb, being more affected than antenna element 4.

Therefore, 3GPP's approach of keeping the same blockage assumption per panel could lead to misleading results. Instead, CST is closer to reality since it can use CAD models for any user body part, better characterizing the variability of a user's behavior through a wider range of blockage regions. Despite not constituting a generalized model like the ones in [19] or [20],

4. Model comparison

the CST blockage model adopted in this work portrays commonly employed handset designs and user behaviors. Considering that such standardized models are yet to be proposed, these can be used as representative use-cases to complement the simpler blockage model proposed by 3GPP.

4.2 Codebook comparison

In this work, a codebook of 20 narrow UE beams is selected, with $N_{csi} = 5$ beams per panel. These narrow beams are employed during P3 to refine the UE's wide beam of the panel selected in P1. Considering now user shadowing, each blockage scenario will affect the UE's radiation behavior differently, resulting in a unique codebook shape. To evaluate blockage impact, the radiation pattern envelope of all beams is displayed as a stereographic projection in Fig. C.12 for each 3GPP and CST blockage scenario. The plots are organized such that each column represents a panel, from Pn^1 through Pn^4 , and each row one of the considered blockage scenarios. The first three rows represent the codebooks obtained with 3GPP's model. As a baseline, the first row depicts the free space (FS) codebook, to offer a reference of the ideal spatial coverage of the model. The following row depicts the portrait's blockage (BL) codebook followed by the landscape BL codebook in the row below. The same structure is followed for the last four rows, dedicated to the CST model. Here, the last two rows depict the two landscape BL models, models 1 and 2, detailed in Section 3.2².

3GPP model codebook

In free space, 3GPP's codebook presents ideal and symmetrical beam shapes, with a significant gain reduction over the upper and lower bounds of elevation, as seen in the first row of Fig. C.12. This model's portrait blockage, represented in the second row, covers partially Pn^1 and Pn^3 and completely blocks the highest gain region of Pn^4 , leaving Pn^2 unscathed. The blockage for the device in landscape mode, illustrated in the following row, however, reaches out to all the panels, concealing most of Pn^1 and Pn^2 and slightly blocking Pn^3 and Pn^4 .

CST model codebook

CST's free space codebook, displayed in the fourth row of Fig. C.12, despite employing antennas designed to resemble the 3GPP model, produces wider beams with slightly less gain, due to the power dissipating towards the edges of the metallic form factor, providing a more uniform spherical coverage.

²While the color scale in Figure C.12 has been restricted to be between -15 dB and 10 dB for clarity reasons, higher and lower gain values are obtained in some cases.

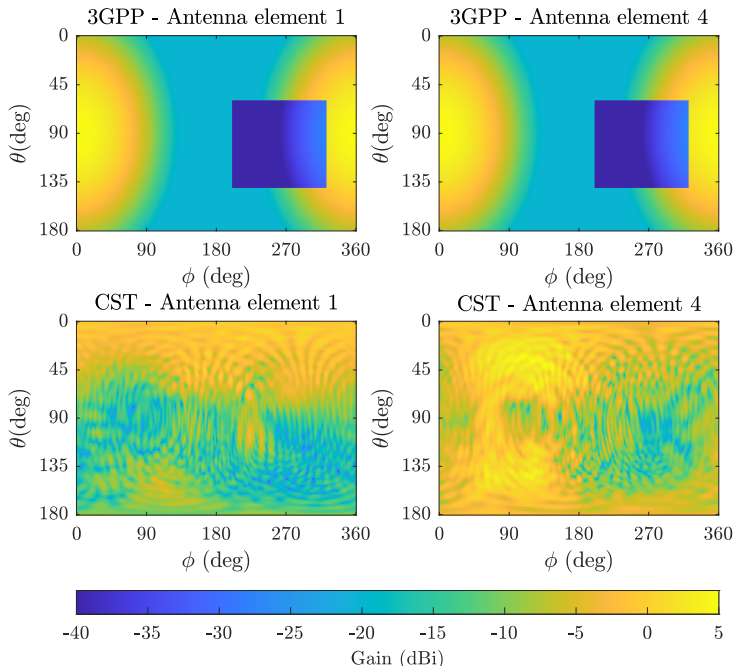


Fig. C.11: Radiation patterns of Pn^1 's antenna elements 1 and 4 for portrait mode blockage - 3GPP and CST models.

However, the proximity of the user to the mmWave antenna arrays integrated in the phone, allied with the glass acting as a wave guide and trapping some of the energy before it bounces around and escapes, can cause standing waves, making the narrow beams lose power and shape with a severity dependent on the grip conditions. Furthermore, the close contact of the panel with the device's metal structure and glass explains the ripple effects observed in the CST radiation patterns, not present in the 3GPP model. The fifth row of Fig. C.12 represents the portrait mode blockage scenario from Fig C.8. Since the user's thumb is pressed against Pn^1 , its codebook becomes severely affected. Pn^2 , on the other hand, barely registers any disturbance, being too far from the hand to produce any significant degradation. Pn^3 is also blocked to some extent but the fingers are quite spaced apart, allowing the panel to conserve part of its beam shape. While it is possible for Pn^3 to radiate almost undisturbed in the top hemisphere of elevation, this does not happen for the bottom hemisphere, where a drastic loss of power takes place in the region of the phone engulfed by the hand. Finally, in Pn^4 , thanks to a small gap between the user's hand and the form factor, the main beams are able to maintain a regular shape and even experience an increase in power due to reflections coming from the user's palm. However, some attenuation

4. Model comparison

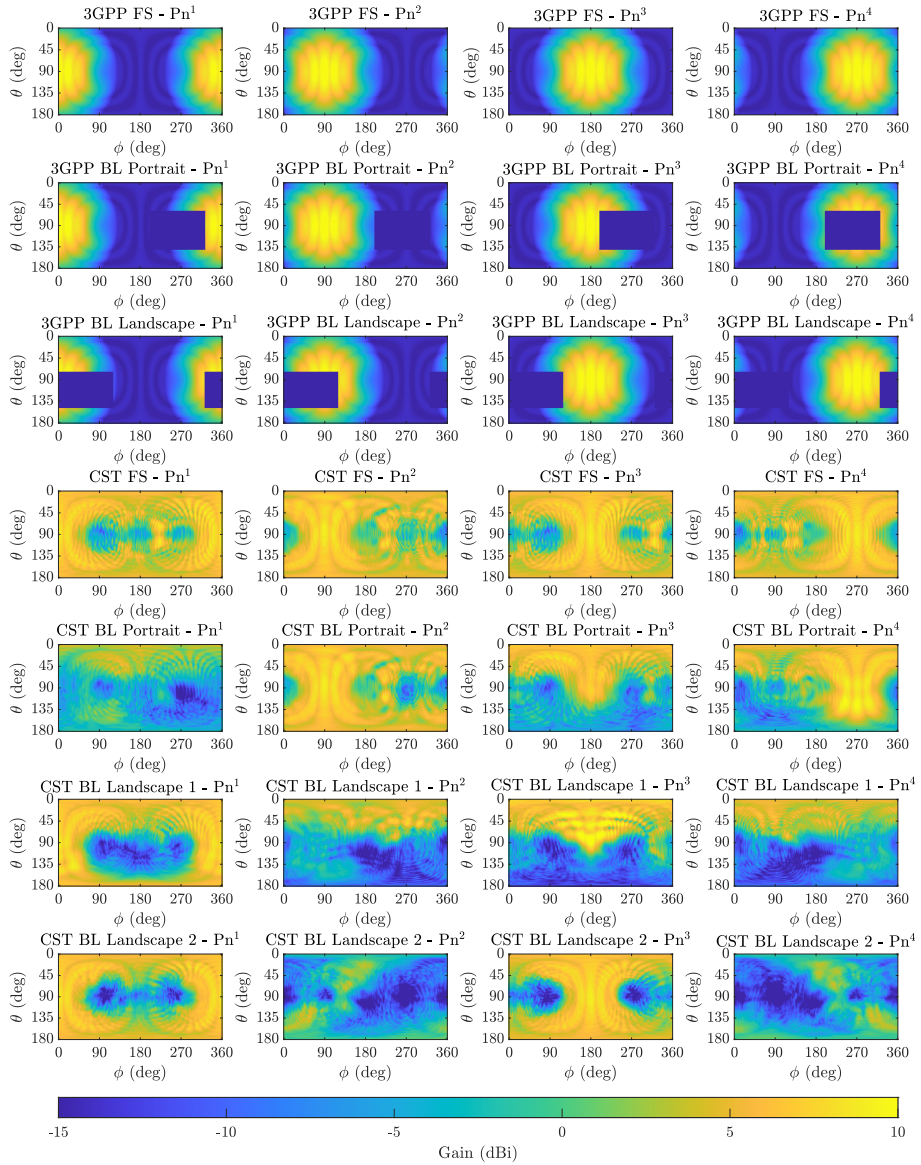


Fig. C.12: 3GPP and CST 5-beam panel codebook envelopes for free space (FS), portrait and landscape blockage (BL).

is still observed in the backlobe region since, at these frequencies, the panel is unable to radiate through the hand cupping the phone. In the following row, landscape grip model 1's codebook from Fig. C.9 can be found. Since both hands are cupping the phone, Pn^2 and Pn^4 patterns are mostly lost for the region above 45° of elevation. Pn^1 beams are able to keep their shape but the backlobes are attenuated due to the hand's position. Pn^3 suffers a similar effect to Pn^4 in portrait mode, where most of its radiation is completely blocked by the user's palms except for the top area of elevation where some reflections are recorded. Finally, the last row displays the codebook for the landscape grip model 2 depicted in Fig. C.10. The attenuation experienced in Pn^2 and Pn^4 is further aggravated, with the beam shapes almost lost in their entirety. This new grip places the user's hands near the top and bottom of the phone, freeing up Pn^1 and Pn^3 to radiate very similarly to the free space scenario. For reference in the studies that follow, Table C.4 details which panels are affected by human blockage and to what extent they are blocked relative to the remaining panels in each blockage scenario.

In summary, the main contrast between the models is how user blockage is characterized:

- The 3GPP model adopts the same blockage region and attenuation values in all panels, resulting in harsher losses over a limited angular region, while the remaining angular space is unaltered when compared to free space.
- In the CST model, where each panel is affected differently by the hand positioning, the hand grip blockage manifests as a disturbance along the entire angular range but rarely displays as drastic attenuation values as its 3GPP counterpart.

5 BM performance evaluation

This section explores the impact of self-blockage in the link-level performance of BM. The KPIs used are defined in Subsection 5.1. Subsection 5.2 and Subsection 5.3 showcase how RSS and beam detection accuracy are influenced by CST and 3GPP's user grip models. Finally, Subsection 5.4 evaluates how the channel's LOS conditions can affect blockage impact perception. Table C.5 summarizes all the simulation parameters used. This study is conducted at $f_c = 28$ GHz with a bandwidth of $B = 104$ MHz. Using an 8×8 UPA at the gNodeB side, BM performance is evaluated over a UMi channel model with a distance dependent LOS probability [19].

5. BM performance evaluation

Table C.4: Panel blockage.

Blockage scenario	Most affected panels
3GPP BL portrait	$Pn^4 > Pn^3 > Pn^1 > Pn^2$
3GPP BL landscape	$Pn^1 > Pn^2 > Pn^4 > Pn^3$
CST BL portrait	$Pn^1 > Pn^3 > Pn^4 > Pn^2$
CST BL landscape 1	$Pn^2, Pn^4 > Pn^3 > Pn^1$
CST BL landscape 2	$Pn^2, Pn^4 > Pn^1, Pn^3$

Table C.5: Simulation parameters.

Parameter	Notation	Value
Carrier frequency	f_c	28 GHz
Carrier bandwidth	B	104 MHz
Subcarrier spacing	Δf	120 kHz
RX noise figure	NF	9 dB
Thermal noise density	N_0	-174 dBm Hz^{-1}
SSB configuration		
SSBurst size	N_{ss}	12
SSBurst periodicity	T_{ss}	20 ms
SSBs for CR1	N_{ss}^{CR1}	4
SSBs for CR2	N_{ss}^{CR2}	8
CSI-RS configuration		
Resources	N_{csi}	5
Configuration row	-	1
Type	-	NZP
Resource bandwidth	-	72 PRB
density	ρ	3
Layout configuration		
Inner mobility bound	r	15 m
Outer mobility bound	R	100 m
Channel model	-	UMi LOS probability
gNodeB position	(x, y)	$(0, 0)$
gNodeB height	h_t	10 m
gNodeB array size	N_t	8×8
UE initial position	(x, y)	uniformly distributed
UE height	h_r	1.5 m
UE panels	I	4
UE panel size	N_r	1×4
UE speed	v	3 km h^{-1}
UE trajectories	-	800

5.1 KPIs

To evaluate BM performance, RSS measurements are performed over the time-frequency resources reserved for data transmission. This work assumes a data resource allocation set, \mathcal{K}_{data} , to occupy, in the frequency domain, all the available bandwidth B , and, in the time domain, the interval that follows the last CSI-RS transmission from P3 and the following SSburst, as displayed in Fig. C.13. The RSS over \mathcal{K}_{data} for a gNodeB beam ψ_t and a UE beam ψ_r at panel i is defined as

$$R(\psi_t, i, \psi_r) = \frac{1}{|\mathcal{K}_{data}|} \sum_{k \in \mathcal{K}_{data}} |\mathbf{w}_{\psi_r}^i \mathbf{H}^i(k)^\top \mathbf{f}_{\psi_t}|^2, \quad (\text{C.22})$$

where $|\mathcal{K}_{data}|$ denotes the cardinality of set \mathcal{K}_{data} , i.e., the amount of time-frequency resources available for data transmission. The best measurement-based beam pair is defined by the gNodeB and UE panel beam combination that offers the highest L1-RSRP levels, given by

$$R_{meas} = R(\psi_t^*, i^*, \psi_r^*), \quad (\text{C.23})$$

where ψ_t^* , i^* and ψ_r^* are determined through the P1 and P3 procedures detailed in Subsection 2.2. To evaluate beam selection accuracy, the measured RSS is compared to a genie-aided beam selection. Considering optimal beam alignment, the maximum achievable RSS over all the $N_{ss} \times I \times N_{csi}$ available beam pairs is determined by

$$R_{genie} = \max_{\psi_t, i, \psi_r} R(\psi_t, i, \psi_r). \quad (\text{C.24})$$

It is considered that a beam misdetection occurs when the measurement selected gNodeB beam, UE panel or UE panel beam stray from the genie selection, based on optimal RSS results. Misdetection probability is then defined as

$$P_m = \mathbb{P}[R_{meas} < R_{genie}]. \quad (\text{C.25})$$

The impact of misdetections can vary, depending on the degree of misalignment between the measured beam pair and the genie solution. An additional criterion is introduced to quantify the beam misdetection loss, given by

$$\Delta SNR = \frac{R_{genie}}{R_{meas}}. \quad (\text{C.26})$$

To distinguish which misdetections risk jeopardizing communications, $P_{m_{thr dB}}$ expresses the probability that the ΔSNR incurred exceeds a threshold thr dB as

$$P_{m_{thr dB}} = \mathbb{P}[\Delta SNR_{dB} \geq thr]. \quad (\text{C.27})$$

5. BM performance evaluation

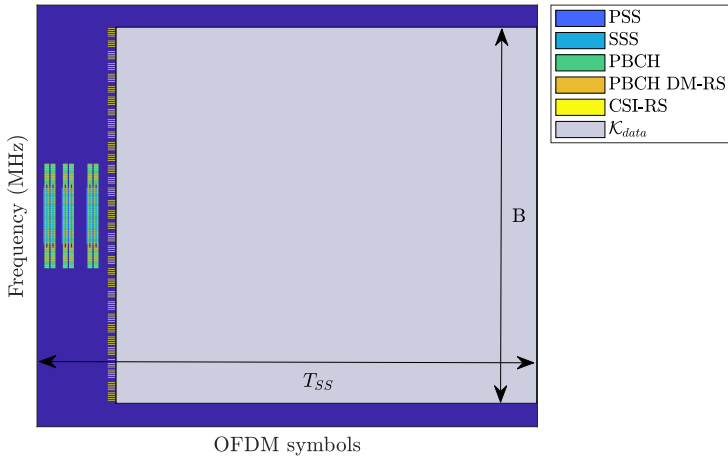


Fig. C.13: Data time-frequency allocation.

5.2 Hand grip impact

It has been established in Section 4.2 that a user's hand gripping can largely impact the beam shapes of a UE codebook. It remains now to be investigated to which extent this will degrade the BM performance. Considering each blockage scenario as a distinct codebook to be compared against the one originally designed for free space, Fig. C.14 shows the resulting RSS obtained for each codebook after measurement-based beam alignment, under 3GPP and CST modelling assumptions. The free space scenario is characterized by two distinct curves, one for the device in portrait mode and another for the device in landscape mode, due to the different rotations introduced to the UE in each mode. To ease interpretation, Table C.6 pinpoints the most significant values on the 10th, 50th and 90th percentiles. For free space, the 3GPP and CST models produce quite similar results, which is to be expected considering these models should match. It is noticeable that the 3GPP portrait blockage curve does not stray too far from the baseline, despite being characterized by such a substantial attenuation. This can be explained by how often each UE panel is selected. Fig. C.15 and Table C.7 indicate, for each blockage scenario, a visual and tabular representation of the selection percentage of each panel. An increased frequency of use for a panel is indicative of its role in achieving the best possible performance.

Results show that, for free space in portrait mode, Pn^1 and Pn^3 are selected more than 60% of the time. Fortunately, the panel most affected by 3GPP's portrait blockage is Pn^4 , which bears the lowest usage percentage in free space. Since Pn^3 is also partially blocked, its usage drops around 2%, but is compensated by the second and third most used panels, Pn^1 and

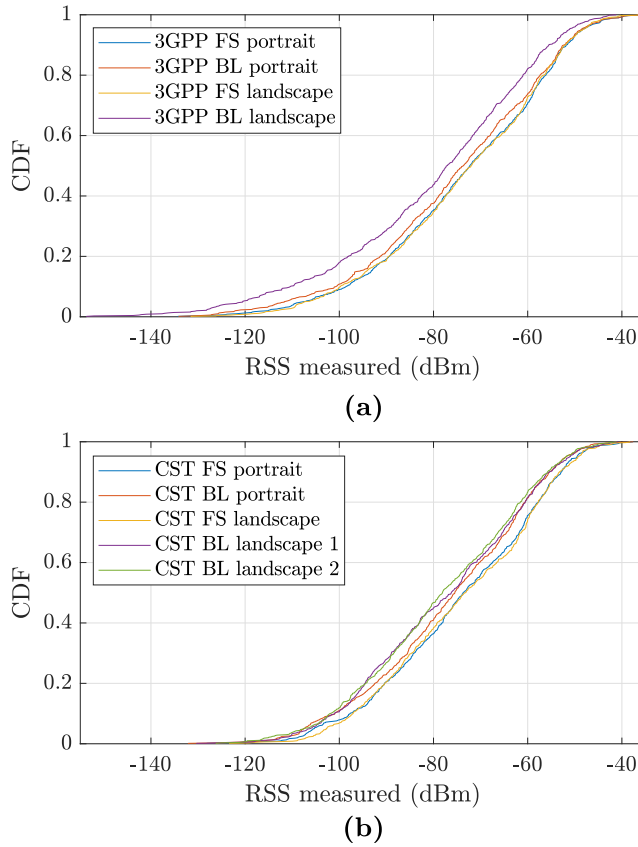


Fig. C.14: Measurement-based RSS (R_{meas}). (a) 3GPP model. (b) CST model.

Table C.6: R_{meas} values in dBm for the 10th, 50th and 90th percentiles.

Blockage scenario	Percentile		
	10 th	50 th	90 th
3GPP FS portrait	-98.6	-72.3	-51.5
3GPP BL portrait	-100.7	-73.7	-52.3
3GPP FS landscape	-99.7	-72.0	-52.0
3GPP BL landscape	-110.4	-77.2	-55.5
CST FS portrait	-97.1	-73.2	-52.9
CST BL portrait	-101	-75.5	-55.4
CST FS landscape	-97.1	-73.2	-53.2
CST BL landscape 1	-101	-76.2	-55.5
CST BL landscape 2	-102	-78.1	-55.8

5. BM performance evaluation

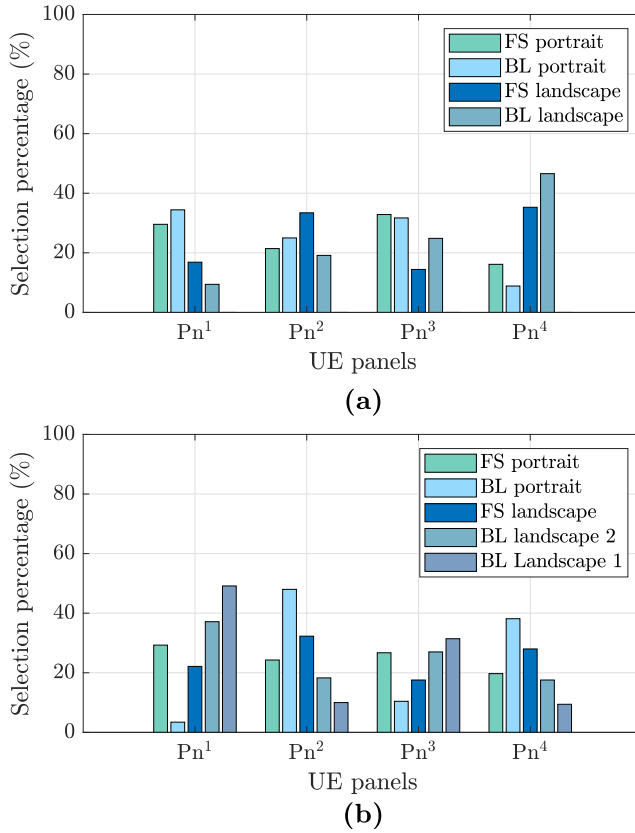


Fig. C.15: Panel selection frequency for all blockage scenarios. (a) 3GPP model. (b) CST model.

Pn², which justifies the small but visible performance deterioration. In landscape mode, however, the blockage impact is a lot more flagrant. The panels blocked more critically are Pn¹ and Pn², the latter being one of the most frequently employed panel in free space. As a result, the usage of these two panels is significantly reduced and substituted by an increase of activity in Pn⁴, the most used panel in free space, and Pn¹, the least resorted to panel in the list, causing the performance degradation observable in Fig. C.14 a).

Since CST in free space offers a more uniform coverage, the distribution of the panel selection is more balanced. Pn¹ and Pn³ still remain as the most used panels but only by a smaller margin. Due to being largely blocked, Pn¹ is selected nearly ten times less than in the baseline. The same behavior is noticeable for Pn³, recording a 17% drop in its usage. The least utilized panels, Pn² and Pn⁴ emerge as the available alternatives, which explains the deterioration of the signal. For free space landscape mode, Pn² and Pn⁴ are chosen the most. However, for both CST landscape blockage grips, these

Table C.7: Panel selection frequency for all blockage scenarios.

		Selection percentage (%)			
		Portrait		Landscape	
		FS	BL	FS	BL 1 / BL 2
Pn¹	3GPP	30.9	34.4	17.1	9.7
	CST	29.6	3.2	22	37.1 / 49.1
Pn²	3GPP	21.1	24.7	33.1	19.3
	CST	23.5	47.1	31.9	18.3 / 10
Pn³	3GPP	33.3	31.5	15.2	24.5
	CST	27.5	10.3	17.9	27.1 / 31.4
Pn⁴	3GPP	14.7	7.5	34.7	46.3
	CST	19.5	39.5	28.3	17.6 / 9.4

are also the two most blocked panels, with a different level of blockage for each grip. Since the best panels are blocked, the remaining less optimal ones are selected more often instead, bringing about the observed loss in power. The performance for hand grip model 2 is even inferior to hand grip model 1 due to the extreme blockage that the gaming grip inflicts on Pn² and Pn⁴, rendering these panels almost unusable. This reduces even further their usage percentage, resulting in higher RSS losses. It is also noteworthy that, even when largely blocked, some panels can still be selected, instead of being discarded from the candidate list, which is a common strategy adopted in prior work.

Overall, the 3GPP blockage model results in a more significant performance degradation in the worst case scenarios, represented by the lowest percentiles in Fig. C.14 a). CST's model, however, leads to a more homogeneous degradation across the RSS range, as depicted in Fig. C.14 b). In summary, hand grip blockage does impact negatively the performance of mmWave BM and should not be disregarded when designing such solutions for user handled devices.

While the current BM procedure appears somewhat resilient to codebook distortions introduced by blockage, it is important to note that the current implementation of this procedure is based on an exhaustive approach, where all panels and a large number of beams are measured, leaving less room for mistakes, under the limitations of our set-up. In future 5G and 6G releases, where the inevitable transition to the higher frequency spectrum will call for larger codebooks of narrower beams, such a strategy may become much less viable [2]. If more sophisticated grip-aware solutions were to be developed for BM that relied, for example, on identifying blocked panels for optimal beam selection such as [33], the variability of the user grips would make this process more prone to mistakes. Moreover, if these algorithms were to

5. BM performance evaluation

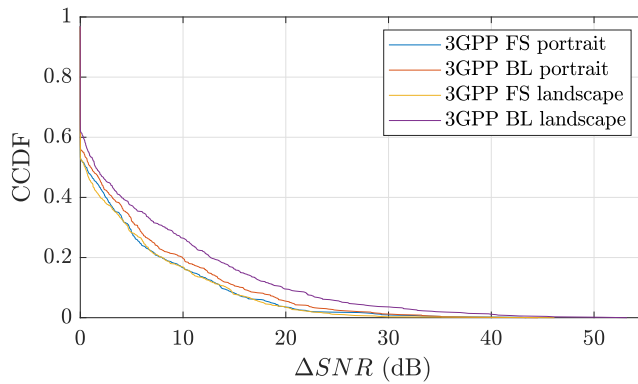
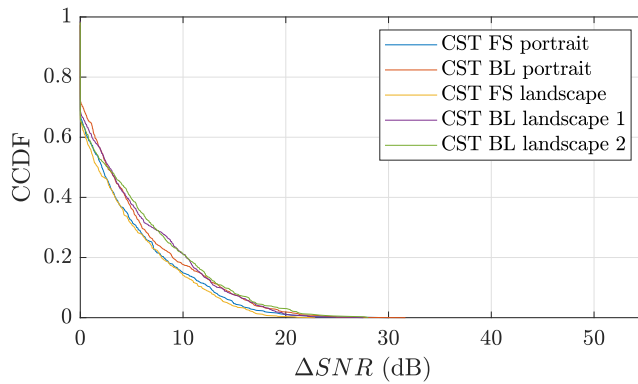
be developed under the current 3GPP blockage model assumptions, due to the lack of nuance of attenuation values and shadowing regions for different grips, it is likely that such solutions would not perform as expected in real-life scenarios. Therefore, it is necessary to consider more accurate blockage models in order to effectively counteract the impact of user influence in mmWave communications.

5.3 Beam detection accuracy

The previous results show the performance of measurement-based beam selection. This selection process, however, is always vulnerable to mistakes that can occur during the BM procedure. In this context, a misdetection can take place when either a non-ideal gNodeB beam, UE panel or UE panel beam are selected. It is then worth to investigate how often these misdetections occur, what is the loss incurred for such mishaps and how user blockage influences these results. Table C.8 contains the P_m , $P_{m,3dB}$ and $P_{m,10dB}$ obtained for each blockage scenario. Overall, P_m results show that misdetections occur quite regularly. This is partly due to the fact that narrow beams are being considered on both the gNodeB and UE sides, making the criteria for optimal beam selection increasingly stringent. Moreover, this surprisingly large number of misdetections is also caused by the usage of a distance-dependent UMi LOS channel model. Due to users' position being uniformly distributed in the cell area, it is more likely for users to be further away from the gNodeB than closer. As users with larger distance to the gNodeB have larger probability of being in NLOS conditions, this is the predominant condition in the simulation, thus increasing the chances for a misdetection. However, the percentage of misdetections that actually lead to a sub-optimal link with a half-power degradation is much lower, as seen by the values registered for $P_{m,3dB}$. It is also noticeable that the CST model is more susceptible to misdetections than 3GPP's, which might be attributed to the nuances between their codebooks. It has been established that, due to the presence of the form factor in free space and the user's hand grip, beams become slightly warped, due to the redirection and absorption of the radiated power, creating a codebook of beams with less gain but more coverage. Therefore, since the power is better distributed over the angular space, it is more likely that there are more beams offering similar power levels, leading to misdetections. The 3GPP codebook retains its ideal shape, even when blockage is considered, only suffering a flat attenuation in a pre-determined region. However, the values in $P_{m,10dB}$ seem to suggest a conflicting trend, where 3GPP performs worse. To explore this further, Fig. C.16 represents the misdetection-induced SNR losses for each blockage scenario. Despite suffering fewer misdetections, 3GPP's SNR loss range is much larger than CST's. This is due in part to the ideal shape of 3GPP beams in free space, having no backlobes and very low power in the

Table C.8: Mis-detection probability for all blockage scenarios under different loss thresholds.

Blockage scenario	P_m (%)	$P_{m_{3dB}}$ (%)	$P_{m_{10dB}}$ (%)
3GPP FS portrait	74.4	37.3	16.7
3GPP BL portrait	76.1	40.6	19.9
3GPP FS landscape	72.9	36.9	17
3GPP BL landscape	77.3	44	26.6
CST FS portrait	81.1	42.7	15
CST BL portrait	84.7	48.4	17.7
CST FS landscape	80.6	42.9	14.1
CST BL landscape 1	83.9	49.3	21.3
CST BL landscape 2	81.7	48.6	21.1

**(a)****(b)****Fig. C.16:** SNR loss for all blockage scenarios. (a) 3GPP models. (b) CST models.

upper and lower bounds of elevation, as opposed to CST. This, combined with the considered blockage model, can produce large power losses when a

5. BM performance evaluation

mis-detection takes place, bringing to light the main drawback of this model's over-pessimistic depiction of attenuation. Therefore, even though mis-detections are rarer under 3GPP modelling, these become considerably more significant than in CST, potentially triggering unnecessary radio link failures. Finally, it is abundantly clear that, for both models, mis-detections tend to increase with the amount of blockage incorporated, which further demonstrates how user blockage must be considered when assessing mmWave BM performance.

5.4 Channel model impact

So far, results have been computed using the 3GPP-defined UMi channel model with a LOS probability dependent on the UE's distance to the gNodeB. This would resemble a more realistic urban environment where users closer to the gNodeB would be more likely to find an unobstructed link than users placed further away in the cell. However, comparing this channel model with a strict LOS or NLOS UMi channel can provide some insightful information on how blockage is perceived in different channel models. This study focuses solely on CST grips since they are deemed in this paper as the most appropriate method to gauge user blockage impact. Fig. C.17 displays the measured RSS for free space, portrait blockage and landscape blockage 1 over each channel model, having NLOS described by dotted-dashed lines, LOS probability with solid lines and finally LOS with dashed lines. The most striking observation lies in the fact that UMi with LOS probability curves share their lower bounds with UMi NLOS and upper bounds with UMi LOS, indicating that having a cluster rich environment negatively impacts BM performance. This is further corroborated by the P_m values in Table C.9, where the mis-detection probability increases significantly as the channel model transitions from a dominant LOS path channel to an obstacle rich one. This trend holds true for ΔSNR as well, as seen in Fig. C.18.

Furthermore, the influence of user blockage is more visible in LOS than for the other two channel models, since in this environment there are fewer reflections to rely on once a panel is blocked. Therefore, opting for an alternative beam pair link when the optimal one is blocked results in a larger degradation than in NLOS, where a signal is already weak, even without the blockage effect.

It is important to note that, besides LOS conditions, the blockage impact assessment results are also dependent on factors such as gNodeB height and device rotation in the 3D space, since these would also alter the angles of arrival of the signal. Another factor that was not explored in this work but could also be important to consider in future studies, depending on the user's body orientation relative to the gNodeB, would be the blockage from the user's torso.

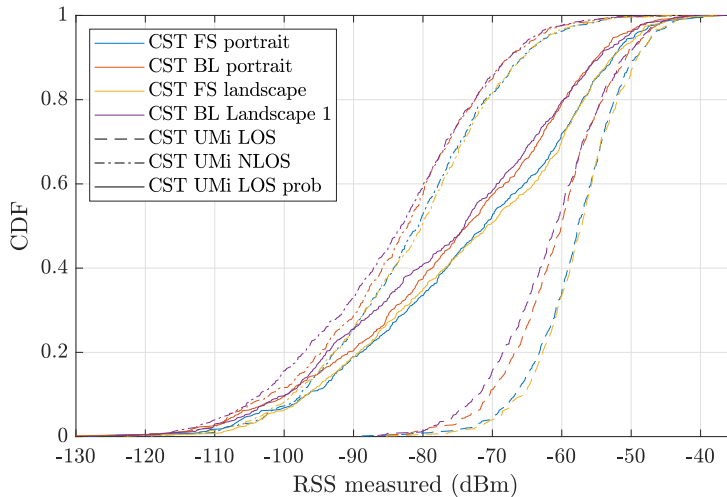


Fig. C.17: Measurement-based RSS (R_{meas}) for all UMi channel models.

Table C.9: Misdetecion probability for all UMi channel models.

Blockage scenario	$P_m(\%)$		
	LOS	LOS prob	NLOS
CST FS portrait	67.5	80.5	90.8
CST BL portrait	73.7	84.6	90.2
CST FS landscape	68	79.5	90
CST BL landscape 1	73.2	82.8	91.6

6 Conclusion

This work has presented a link-level analysis of the impact of high-detail hand grip blockage in mmWave BM performance of handheld devices. Results showed that hand grip type, UE orientation, panel distribution in the form factor, channel conditions and network layout are all determining factors to gauge the severity of a user’s blockage effect and must be carefully modeled when designing solutions to counteract hand blockage and assessing the viability of mmWave communications. While it has been shown that hand blockage noticeably degrades the BM procedure, the current 5G system signaling mechanisms are robust enough to provide sub optimal, yet acceptable, link level performance, even without any proactive measures to mitigate it. However, in future 5G and 6G releases, larger codebooks with narrower beams will likely be employed to handle the transition to higher frequencies, making sweeping-based beam selection implementations impractical. Smarter hand grip and terminal housing-aware mechanisms, such as those

6. Conclusion

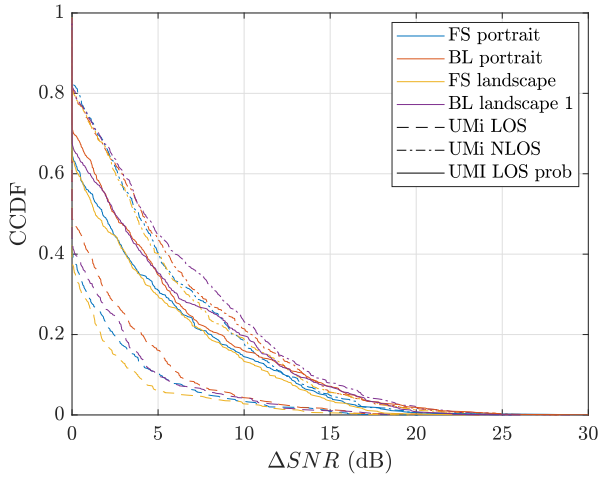


Fig. C.18: SNR loss for all UMi channel models.

in [33–35], should be adopted to create robust solutions to realistic mmWave propagation challenges. In order to enable such approaches, adequate blockage models must be agreed upon to capture the signal’s absorption, reflection and diffraction effects.

6.1 Outlook

This study’s results further suggest that the current stochastic 3GPP self-blockage model [19], perhaps sufficient for system-level evaluations, lacks detail to properly portray user hand grip effects on a link-level basis, leading to an overly pessimist performance degradation. While beyond the intended scope of this work, the task of proposing a simple yet realistic hand-grip induced blockage model would be the next logical step for future work. The CST model employed in this work is quite useful to numerically assess specific UE designs and hand grip modes but lacks the generality to become a viable model for algorithm design. A CST-based approach could still be used to create a more realistic blockage model than 3GPP’s, since it is able to simulate the human body and its behavior with a remarkable level of detail. However, it would require countless computationally heavy simulations to recreate different body blockage scenarios and capture the nuances of the user’s behavior in the antenna performance, which can be deemed as an impractical method. Alternatively, an improvement to the current flat 30 dB attenuation model could be envisioned to establish a standard form factor design and panel placement, as the one considered in this paper, but with a statistical attenuation model instead, as introduced in [20] or [21], on a per panel-basis.

References

- [1] Y.-N. R. Li, B. Gao, X. Zhang, and K. Huang. "Beam Management in Millimeter-Wave Communications for 5G and Beyond". *IEEE Access*, 8:13282 – 13293, 2020.
- [2] Y. Heng, J. G. Andrews, J. Mo, V. Va, A. Ali, B. L. Ng, and J. C. Zhang. "Six Key Challenges for Beam Management in 5.5G and 6G Systems". *IEEE Communications Magazine*, 59(7):74 – 79, 2021.
- [3] Y. Huang, Y. Li, H. Ren, J. Lu, and W. Zhang. "Multi-Panel MIMO in 5G". *IEEE Communications Magazine*, 56(3):56 – 61, 2018.
- [4] Dassault Systemes. CST Microwave Studio.
- [5] Y. Li, J. G. Andrews, F. Baccelli, T. D. Novlan, and C. J. Zhang. "Design and Analysis of Initial Access in Millimeter Wave Cellular Networks". *IEEE Transactions on Wireless Communications*, 16(10):6409 – 6425, 2017.
- [6] M. Rebato, J. Park, P. Popovski, E. De Carvalho, and M. Zorzi. "Stochastic Geometric Coverage Analysis in mmWave Cellular Networks With Realistic Channel and Antenna Radiation Models". *IEEE Transactions on Communications*, 67(5):3736 – 3752, 2019.
- [7] A. Karimi and K. Pedersen. "5G System-Level Performance Analysis of Uplink Multi-Panel Transmission in mm-Wave Frequencies". *2021 IEEE 94th Vehicular Technology Conference (VTC2021-Fall)*, pages 1 – 6, 2021.
- [8] F. Abinader, C. Rom, K. Pedersen, S. Hailu, and N. Kolehmainen. "System-Level Analysis of mmWave 5G Systems with Different Multi-Panel Antenna Device Models". *2021 IEEE 93rd Vehicular Technology Conference (VTC2021-Spring)*, pages 1 – 6, 2021.
- [9] S. B. Iqbal, A. Awada, U. Karabulut, I. Viering, P. Schulz, and G. P. Fettweis. Analysis and Performance Evaluation of Mobility for Multi-Panel User Equipment in 5G Networks, 2022. arXiv:2203.14763v2 [cs.NI].
- [10] A. Ali, J. Mo, B. L. Ng, V. Va, and J. C. Zhang. "Orientation-Assisted Beam Management for Beyond 5G Systems". *IEEE Access*, 9:51832 – 51846, 2021.
- [11] K. N. Nguyen, A. Ali, J. Mo, B. L. Ng, V. Va, and J. C. Zhang. Beam Management with Orientation and RSRP using Deep Learning for Beyond 5G Systems, 2022. arXiv:2202.02247v1 [eess.SP].

References

- [12] M. Peter, M. Wisotzki, M. Raceala-Motoc, W. Keusgen, R. Felbecker, M. Jacob, S. Priebe, and T. Kürner. "Analyzing human body shadowing at 60 GHz: Systematic wideband MIMO measurements and modeling approaches". *2012 6th European Conference on Antennas and Propagation (EUCAP)*, pages 468 – 472, 2012.
- [13] U. T. Virk and K. Haneda. "Modeling Human Blockage at 5G Millimeter-Wave Frequencies". *IEEE Transactions on Antennas and Propagation*, 68(3):2256 – 2266, 2020.
- [14] K. Zhao, J. Helander, D. Sjoberg, S. He, T. Bolin, and Z. Ying. "User Body Effect on Phased Array in User Equipment for the 5G mmWave Communication System". *IEEE Antennas and Wireless Propagation Letters*, 16:864 – 867, 2016.
- [15] K. Zhao, C. Gustafson, Q. Liao, S. Zhang, T. Bolin, Z. Ying, and S. He. "Channel Characteristics and User Body Effects in an Outdoor Urban Scenario at 15 and 28 GHz". *IEEE Transactions on Antennas and Propagation*, 65(12):6534 – 6548, 2017.
- [16] K. Zhao, S. Zhang, Z. Ho, O. Zander, T. Bolin, Z. Ying, and G. F. Pedersen. "Spherical Coverage Characterization of 5G Millimeter Wave User Equipment With 3GPP Specifications". *IEEE Access*, 7:4442 – 4452, 2018.
- [17] C. Ballesteros, L. Vähä-Savo, K. Haneda, C. Icheln, J. Romeu, and L. Jofre. "Assessment of mmWave Handset Arrays in the Presence of the User Body". *IEEE Transactions on Antennas and Propagation*, 20(9):1736 – 1740, 2021.
- [18] L. Vähä-Savo, C. Cziezerski, M. Heino, K. Haneda, C. Icheln, A. Hazmi, and R. Tian. "Empirical Evaluation of a 28 GHz Antenna Array on a 5G Mobile Phone Using a Body Phantom". *IEEE Transactions on Antennas and Propagation*, 69(11):7476 – 7485, 2021.
- [19] 3GPP. Study on channel model for frequencies from 0.5 to 100 GHz (Release 17). Tech. Rep. 38.901, V17.0.0 2022.
- [20] V. Raghavan, L. Akhoondzadeh-Asl, V. Podshivalov, J. Hulten, M. A. Tassoudji, O. H. Koymen, A. Sampath, and J. Li. "Statistical Blockage Modeling and Robustness of Beamforming in Millimeter-Wave Systems". *IEEE Transactions on Microwave Theory and Techniques*, 67(7):3010 – 3024, 2019.
- [21] V. Raghavan, S. Noimanivone, S. K. Rho, B. Farin, P. Connor, R. A. Motos, Y. C. Ou, K. Ravid, M. A. Tassoudji, O. H. Koymen, and J. Li. "Hand and Body Blockage Measurements With Form-Factor User Equipment at 28

- GHz". *IEEE Transactions on Antennas and Propagation*, 70(1):607 – 620, 2022.
- [22] V. Raghavan, M.-L. Chi, M. A. Tassoudji, O. H. Koymen, and J. Li. "Antenna Placement and Performance Tradeoffs With Hand Blockage in Millimeter Wave Systems". *IEEE Transactions on Communications*, 67(4):3082 – 3096, 2019.
- [23] S. Jaeckel, L. Raschkowski, K. Börner, and L. Thiele. "QuaDRiGa: A 3-D Multicell Channel Model with Time Evolution for Enabling Virtual Field Trials". *IEEE Transactions on Antennas Propagation*, 62(6):3242 – 3256, 2014.
- [24] 3GPP. Study on new radio access technology Physical layer aspects (Release 14). Tech. Rep. 38.802, V14.2.0 2017.
- [25] M. Enescu, editor. *5G New Radio: A Beam-based Air Interface*. John Wiley & Sons, 1st edition, 2020.
- [26] 3GPP. NR; Physical channels and modulation (Release 17). Tech. Spec. 38.211, V17.2.0 2022.
- [27] 3GPP. "NR; Physical layer procedures for control (Release 17)". Tech. Spec. 38.213, V17.3.0 2022.
- [28] MathWorks. 5G Toolbox.
- [29] "Feature lead summary #3 of Enhancements on Multi-beam Operations". - R1-1907860, 3GPP TSG RAN WG1 Meeting #97, May 2019.
- [30] 3GPP. NR; Physical layer measurements (Release 17). Tech. Spec. 38.215, V17.2.0 2022.
- [31] 3GPP. Study on new radio access technology: Radio Frequency (RF) and co-existence aspects (Release 14). Tech. Rep. 38.803, V14.3.0 2022.
- [32] CTIA. Test Plan for Wireless Device Over-the-Air Performance v3.8.2, 2019.
- [33] A. Alammouri, J. Mo, B. L. Ng, J. C. Zhang, and J. G. Andrews. "Hand Grip Impact on 5G mmWave Mobile Devices". *IEEE Access*, 7:60532 – 60544, 2019.
- [34] J. Mo, B. L. Ng, S. Chang, P. Huang, M. N. Kulkarni, A. Alammouri, J. C. Zhang, J. Lee, and W.-J. Choi. "Beam Codebook Design for 5G mmWave Terminals". *IEEE Access*, 7:98387 – 98404, 2019.
- [35] V. Raghavan, R. A. Motos, M. A. Tassoudji, Y.-C. Ou, O. H. Koymen, and J. Li. "Mitigating Hand Blockage with Non-Directional Beamforming Codebooks", 2021. arXiv:2104.06472v1 [cs.IT].

Paper D

Machine Learning-based Millimeter Wave Beam Management for Dynamic Terminal Orientation

F. Fernandes, S. Rezaie, C. Rom, J. Harrebek and C. Navarro Manchón

The paper has been **submitted to**
IEEE 97th Vehicular Technology Conference: VTC2023-Spring

Abstract

Time-varying terminal orientation is an often overlooked challenge of beam alignment in millimeter wave communications with multi-panel handset terminals. The use of narrow beams, allied with fast and hard to predict device orientation changes, cause the current measurement-based beam management procedure to rely on potentially outdated beam information, degrading its accuracy. This paper explores the capabilities of deep neural networks to improve user equipment (UE) beam selection under dynamic terminal orientation conditions. Contrary to other works, the proposed solution relies solely on reference signal received power beam measurements, without the aid of other context information. Results show that this simple solution can successfully improve beam selection accuracy for fast rotating UEs, especially in line-of-sight scenarios. No-line-of-sight environments however reduce the proposed solution's effectiveness due to low power-levels and increased channel angular spread.

1 Introduction

Current 5G mmWave communications are enabled by large antenna arrays with high beamforming gains [1]. Although achieving unprecedented data rates, the narrow nature of the transmitter and receiver beams causes a link to become more directional and, consequently, vulnerable to disruptions. This prompted 3GPP to define a set of L1 and L2 operations, namely beam management, to acquire and maintain beam alignment between the gNodeB and the UE beams [2]. Since the current beam management procedure is based on a simplistic approach of beam sweeping, measurement and reporting, extensive research has been conducted in works such as [3–6] to strengthen its robustness against dynamic channel conditions. Concurrently, 3GPP is currently investigating beam management enhancements for Release 18 based on ML [7].

Most of these studies consider the UE to be modeled as a single panel with an isotropic or directional antenna array. In reality, devices must be equipped with multiple directional antenna array panels to be able to offer adequate spherical coverage. The performance benefits of multi-panel UE design are highlighted in [8] where a panel switching mechanism is introduced based on RSRP. This work, along with [9], further elaborate on practical aspects such as the impact of sequential and simultaneous panel activation on beam management performance for distinct mobility scenarios. Furthermore, [10] proposes to use context information, specifically location and orientation data, for a ML beam selection method. This approach recommends a subset of candidate beams/panels to be tested, reducing the beam acquisition overhead and improving the device's power efficiency by deactivating

unused panels.

However, these works assume a time-static orientation for the UE thus concealing an additional challenge for beam alignment: device orientation tracking. Under the current beam management framework, beam selection relies on measurements collected over a span of time. A device whose orientation is shifting, while simultaneously moving through the cell, may cause measurements to become outdated, leading to erroneous beam selection and, ultimately, link performance degradation. This is particularly challenging for handset terminal use cases, where fast and hard to predict orientation changes are common. Therefore, time-varying rotation should be modelled along with other straining factors like user mobility or blockage to truly capture the challenges of beam alignment in multi-panel devices [11]. A few works in the literature have tackled this issue through the use of orientation data obtained from the device's sensors. By employing a particle filter in [12] and a recurrent neural network in [13], the authors show that leveraging this information, along with RSRP measurements, outperforms the current procedure, particularly in scenarios where fast and abrupt device rotation is experienced. However it is worth mentioning that both these approaches require a significant number of samples to be implemented. The particle filter method can not be trained in advance and requires a high number of samples to accomplish its prediction tasks, which can result in a high computation load for the UE. Moreover, while the type of ML model pursued can be trained offline, obtaining a large enough dataset size to train it can be difficult.

Contrary to [12] and [13], this paper explores the feasibility of handling time-varying terminal rotation without resorting to context information sources. A ML solution is proposed based solely on information available to the UE through the current beam management procedure: RSRP measurements. Results show that this information, even if outdated, can be used by a simple NN to infer the UE's orientation pattern and therefore predict the best beam in dynamic orientation scenarios. The proposed solution's performance is compared to a 3GPP-based beam management procedure and its suitability is tested for different usage scenarios based on propagation environment, user speed and time-dynamic device rotation.

The remainder of this paper is organized as follows: Section 2 details the study's system model and Section 3 describes both the 3GPP-based and the ML-based solutions for UE beam selection. Section 4 presents the comparative performance results and Section 5 concludes the paper.

2 System model

Fig. D.1 illustrates a DL single cell mmWave system, where beam alignment takes place between the gNodeB and a single user. This user moves in a straight line at constant speed through the cell while changing the terminal's orientation along its trajectory. The gNodeB is modelled as a UPA of N_t patch antennas and the UE as a multi-panel device. Each of the $I = 4$ panels at the UE is equipped with a ULA module of N_r patch antennas and placed on each side of the form factor according to an edge design [14], as seen in Fig. D.2.

2.1 Channel model

The mmWave DL channel response for the i th UE panel is modelled for a frequency-time resource element (s, k) as

$$\mathbf{H}^i(s, k) = \sum_{l=1}^{L(k)} g_l(k) \mathbf{a}_r^i(\boldsymbol{\varphi}_{r,l}^i(k)) \mathbf{a}_t^H(\boldsymbol{\varphi}_{t,l}(k)) e^{-j2\pi\tau_l(k)f(s)}, \quad (\text{D.1})$$

where $L(k)$, $g_l(k)$, $\tau_l(k)$ are the time-varying total multipath components of the channel, the path l 's complex gain and its delay values at time k , respectively. These are obtained with QuaDRiGa, a 3D geometry-based stochastic channel model generator which enables continuous time evolution of a channel, spatially correlated large and small-scale-fading and a plethora of different 3GPP-compliant propagation scenarios [15]. Additionally, $f(s)$ denotes the s th subcarrier frequency. The transmitter and i th receiver panel array responses are expressed in \mathbf{a}_t and \mathbf{a}_r^i for a path l 's time-varying angles of arrival, $\boldsymbol{\varphi}_{r,l}^i$, and departure, $\boldsymbol{\varphi}_{t,l}$. These angles, expressed in elevation and azimuth (θ, ϕ) , are given by

$$\boldsymbol{\varphi}_{r,l}^i(k) = (\theta_{r,l}^i(k), \phi_{r,l}^i(k)), \quad (\text{D.2})$$

$$\boldsymbol{\varphi}_{t,l}(k) = (\theta_{t,l}(k), \phi_{t,l}(k)). \quad (\text{D.3})$$

The array response for a gNodeB or UE array panel of size $N = N_x N_y N_z$ is written as

$$\mathbf{a}(\theta, \phi) = \frac{1}{\sqrt{N}} g_{ae}(\theta, \phi) \mathbf{a}_z(\theta) \otimes \mathbf{a}_y(\theta, \phi) \otimes \mathbf{a}_x(\theta, \phi) \quad (\text{D.4})$$

where $g_{ae}(\theta, \phi)$ pertains to the antenna element's gain and \otimes expresses the Kronecker product, with $\mathbf{a}_x \in \mathbb{C}^{N_x}$, $\mathbf{a}_y \in \mathbb{C}^{N_y}$ and $\mathbf{a}_z \in \mathbb{C}^{N_z}$ given by

$$\mathbf{a}_x(\theta, \phi) = [1, e^{j\pi \sin \theta \cos \phi}, \dots, e^{j\pi(N_x-1) \sin \theta \cos \phi}]^T \quad (\text{D.5})$$

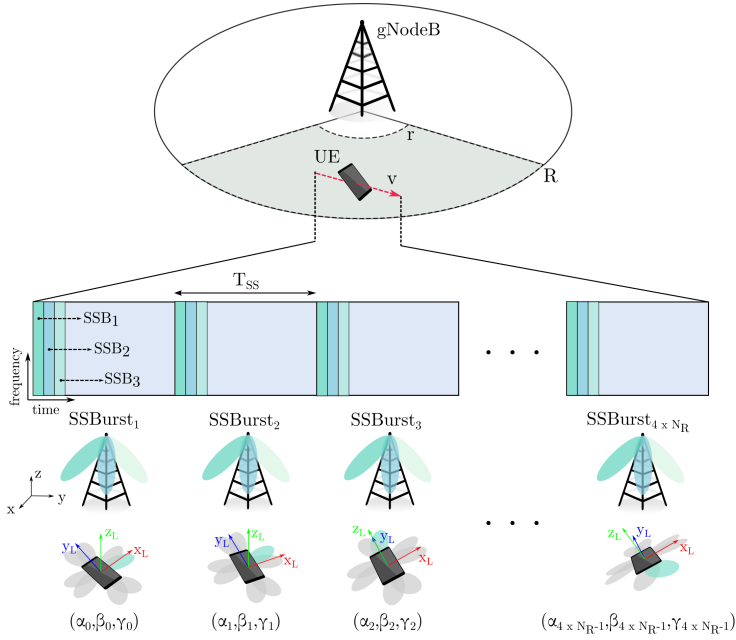


Fig. D.1: Network layout and beam sweeping procedure for $N_T = 3$ and $N_R = 2$. During its trajectory (dashed red), the UE activates one panel beam (highlighted in green) and progressively changes its orientation $(\alpha_t, \beta_t, \gamma_t)$ every T_{SS} ms, as indicated by its LCS (x_L, y_L, z_L) . The gNodeB remains aligned with GCS (x, y, z) .

$$\mathbf{a}_y(\theta, \phi) = [1, e^{j\pi \sin \theta \sin \phi}, \dots, e^{j\pi(N_y-1) \sin \theta \sin \phi}]^T \quad (\text{D.6})$$

$$\mathbf{a}_z(\theta) = [1, e^{j\pi \cos \theta}, \dots, e^{j\pi(N_z-1) \cos \theta}]^T. \quad (\text{D.7})$$

2.2 Signal model

The received signal at any UE panel i in a single frequency-time resource element is given by

$$\mathbf{y}^i(s, k) = \mathbf{w}^H(k) \mathbf{H}^i(s, k) \mathbf{f}(k) x(s, k) + \mathbf{w}^H(k) \mathbf{n}^i(s, k), \quad (\text{D.8})$$

where $\mathbf{H}^i(s, k) \in \mathbb{C}^{N_r \times N_t}$ expresses the channel matrix between the gNodeB and the i th UE panel, as denoted in (D.1). The gNodeB beamforming vector $\mathbf{f}(k) \in \mathbb{C}^{N_t}$ contains a beam's analog phase shifts with a constant modulus of $\frac{1}{\sqrt{N_t}}$. This beam is employed to spatially filter the transmitted signal $x(s, k)$, received at the UE with a beam defined by the analog phase shifts in the

beamforming vector $\mathbf{w}(k) \in \mathbb{C}^{N_r}$ and a constant modulus of $\frac{1}{\sqrt{N_r}}$. The receiver noise is modelled as a complex AWGN vector with variance σ_n^2 and given by $\mathbf{n}^i(s, k) \in \mathbb{C}^{N_r} \sim \mathcal{CN}(\mathbf{0}, \sigma_n^2 \mathbf{I})$.

2.3 Beamforming codebooks

gNodeB codebook

For beam sweeping at the gNodeB, a directional beamforming codebook is adopted, dividing the cell's sector coverage into angular regions. These beams belong to a finite pre-defined set of N_T vectors $\mathcal{C}_t = \{\mathbf{f}_{\psi_t} | \psi_t = 1, \dots, N_T\}$ which is referred to henceforth as the gNodeB codebook. The array steering vector for a transmit beam ψ_t pointing towards $(\theta_{\psi_t}, \phi_{\psi_t})$ is defined in the ψ_t^{th} vector of the codebook as

$$\mathbf{f}_{\psi_t} = \mathbf{a}_t(\theta_{\psi_t}, \phi_{\psi_t}). \quad (\text{D.9})$$

The azimuth steering angles, ϕ_{ψ_t} , are linearly spaced within the angular range of the sector such that

$$\phi_{\psi_t} = -\frac{\pi}{3} + (\psi_t - 1) \times \frac{2\pi}{3 \times (N_T - 1)}, \psi_t = 1, \dots, N_T. \quad (\text{D.10})$$

Moreover, all the beams share the same elevation steering angle, θ_{ψ_t} .

UE panel codebook

Each UE panel produces a finite set of N_R vectors $\mathcal{C}_r^i = \{\mathbf{w}_{\psi_r} | \psi_r = 1, \dots, N_R\}$, constituting the UE panel codebook. In any of the panels the array steering vector for a receive beam ψ_r directed towards $(\frac{\pi}{2}, \phi_{\psi_r})$ is expressed as

$$\mathbf{w}_{\psi_r} = \mathbf{a}_r\left(\frac{\pi}{2}, \phi_{\psi_r}\right). \quad (\text{D.11})$$

Each ULA panel in the UE covers a $\frac{\pi}{2}$ sector of the angular space in the azimuth domain, with linearly spaced steering angles ϕ_r such that

$$\phi_{\psi_r} = -\frac{\pi}{4} + (\psi_r - 1) \times \frac{\pi}{2 \times (N_R - 1)}, \psi_r = 1, \dots, N_R. \quad (\text{D.12})$$

2.4 Beam management model

The gNodeB periodically sweeps N_T beams, where each beam ψ_t is associated to a distinct SSB. SSBs are sets of resources spanning 4 OFDM symbols in

time and 240 subcarriers in frequency employed for power-based measurements that determine the best serving beam pair [16]. An SSBurst is composed of one or multiple SSBs and is transmitted according to a numerology-dependent transmission pattern [17]. The SSBurst generation is performed through MATLAB[®]'s 5G Toolbox[™] [18]. The UE receives each SSB with one of its N_R beams in panel i , ψ_r^i . The received signal is measured for SS-RSRP, defined in [19] as the linear average over the power contributions of the resource elements carrying SS signals. Thus, considering \mathcal{V}_{ss} as a resource data set containing the SS sequence of an SSB, the RSRP measurement for the beam pair (ψ_t, ψ_r^i) is computed as

$$RSRP(\psi_t, \psi_r^i) = \frac{1}{|\mathcal{V}_{ss}|} \sum_{(s,k) \in \mathcal{V}_{ss}} |\mathbf{w}_{\psi_r^i}^H \mathbf{H}^i(s,k) \mathbf{f}_{\psi_t} + \mathbf{w}_{\psi_r^i}^H \mathbf{n}^i(s,k)|^2. \quad (\text{D.13})$$

This work assumes a sequential panel activation at the UE. In other words, as stated by 3GPP's multi-panel "Assumption-1", the UE can only activate one panel at a time for measurement purposes [20]. Moreover, analog beamforming is considered on the panels to reduce power consumption. As a result, the SS-RSRP measurements for all beam pair combinations must be collected at the UE in a round robin fashion: to measure all the beam pair combinations across all panels, $4 \times N_R$ SSBursts must be transmitted during the UE's trajectory, one per UE beam¹. $\mathbf{P}_{meas} \in \mathbb{R}^{4N_R \times N_T}$ stores all measured RSRP values to be used afterwards for beam pair selection.

2.5 Device mobility and rotation model

This work models both time-varying device mobility and device rotation as two independent processes in time. The user moves linearly in the cell sector with constant speed v . The UE's initial position and trajectory direction follow a uniform distribution in the xy plane, with the user's height fixed in the z-axis. Mobility bounds r and R are enforced (see Fig. D.1) where the user is considered to always remain within appropriate coverage range. The UE position is defined according to the GCS represented in black in Fig. D.1. The gNodeB has a fixed orientation coinciding with the GCS (x,y,z) while the UE is considered to experience time-varying rotation over its trajectory. The UE's orientation is dictated by a LCS (x_L, y_L, z_L) , resulting from any 3D rotation with respect to the GCS over three distinct angles: the bearing angle α , the downtilt angle β and the slant angle γ , as shown in Fig. D.2. This set of

¹Although the NR standard supports hierarchical beam sweeping practices, this work opts for a UE with simplistic capabilities in order to highlight a particularly detrimental rotation scenario.

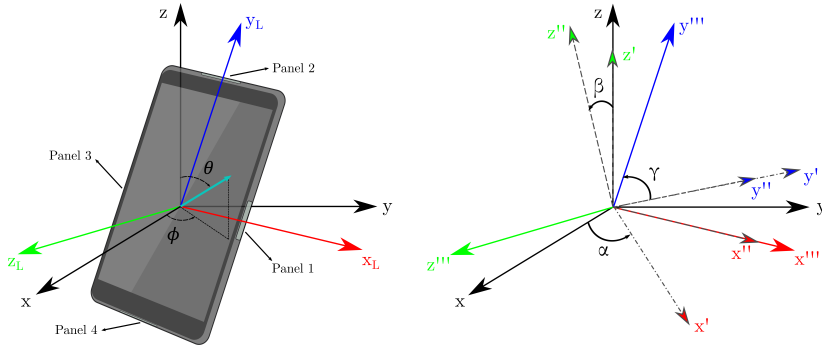


Fig. D.2: Spherical coordinates and LCS transformation (x''', y''', z''') with respect to the GCS (x, y, z) by a sequence of 3 rotations: α, β, γ [21].

angles represents three elemental rotations about the z, y and x axes, respectively [21]. The UE's initial orientation, described as $(\alpha_0, \beta_0, \gamma_0)$, is drawn from an uniform random distribution, taking values between 0° and 360° . The time-varying device rotation is characterized through a filtered random walk model as in [12] and [13]. The process to obtain the UE's orientation for a time sample t is exemplified for α as

$$\bar{\alpha}_t = \bar{\alpha}_{t-1} + \mathcal{N}(0, \sigma^2), \quad (\text{D.14})$$

with σ representing the random walk's standard deviation and $\bar{\alpha}_0 \sim \mathcal{U}[0^\circ, 360^\circ]$. Filtering of the random walk $\bar{\alpha}_t$ is given by

$$\alpha_t = \frac{1}{M} \sum_{m=0}^{M-1} \bar{\alpha}_{t-m}, \quad (\text{D.15})$$

where M is described as the filter's length. The same procedure is applied to obtain β_t and γ_t , with all angles wrapped within $[0^\circ, 360^\circ]$. These values are used to update the $\varphi_{r,l}^i$ values in ((C.1)) over time. This study considers t to match an SSBursts's periodicity T_{SS} . In other words, the device's orientation is assumed to remain constant over each periodic SSBurst transmission and progressively change between consecutive SSBursts as defined in (D.14) and (D.15).

3 UE beam selection

This work focuses on improving UE beam selection in dynamic device rotation scenarios. Overlooking the procedure to select the best gNodeB beam ψ_t^* for a moment, two types of UE beam selection are considered: max-measurement based selection and ML-measurement based selection. Both

methods rely solely on $\mathbf{P}_{meas}^{\psi_r^*} \in \mathbb{R}^{4N_R \times 1}$, i.e. the RSRP measurements obtained with the UE beams across all panels when the gNodeB uses ψ_r^* , collected as described in Section 2.4.

3.1 Max-measurement based beam selection

This method is based on the current beam sweeping and measurement procedure instated by 3GPP. The best UE panel and beam are selected based on a highest instantaneous power metric such that

$$\psi_r^{i*} = \arg \max_{\psi_r^i} (\mathbf{P}_{meas}^{\psi_r^i}(\psi_r^i)). \quad (\text{D.16})$$

Such a solution is prone to errors in a dynamic environment since the beam selection may be based on outdated beam measurements.

3.2 ML-measurement based beam selection

This method uses the same potentially outdated RSRP measurements in an ML context to choose the best UE panel and beam based on its orientation, even if said orientation is never explicitly known. A supervised learning approach is chosen in the form of a feed-forward neural network solving a classification task. The network consists of several dense layers used to process the RSRP measurements for different UE beams. The hidden layers' purpose is to process the RSRP measurements and infer the orientation changes experienced by the UE during the measurement process, thus enabling the network to predict the optimal UE beam at the time of beam selection. During training, each hidden layer is followed by a dropout layer to make the neural network more robust to overfitting. The output layer is made of $4 \times N_R$ neurons, which approximate the optimality probabilities of each of the beams in the UE codebook. Fig. D.3 shows the considered NN structure for UE beam selection, where *tanh* and *softmax* functions are used as non-linear activation functions for the hidden layers and the output layer, respectively.

Each training sample contains $4 \times N_R$ RSRPs, measured along a UE's trajectory in $4 \times N_R$ SSBursts, and the index of the best UE beam for communication at the $4 \times N_R + 1$ SSBurst, which is used as label for training. The categorical cross entropy is used as the loss function of the neural network, i.e.,

$$\mathcal{L} = - \sum_{i=1}^{4 \times N_R} L_i \log(P_i), \quad (\text{D.17})$$

where L_i and P_i denote the label and output of the neural network for the i th UE beam. L is a one-hot vector with 1 at the entry corresponding to the best

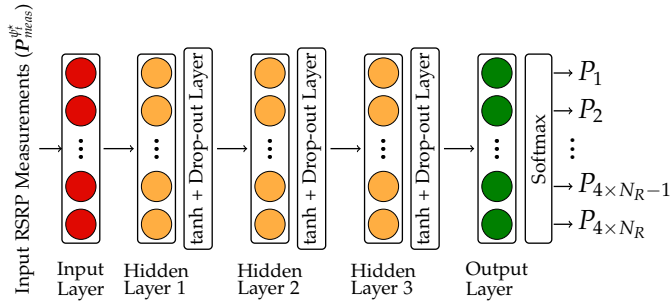


Fig. D.3: The proposed fully connected neural network structure of the ML-measurement based beam selection using RSRPs measured with dynamic terminal orientation.

UE beam at the $4 \times N_R + 1$ SSBurst and 0 in all other entries. This training is UE-specific and done offline, using a 5000-sample dataset size.

4 Results and Discussion

This section assesses the performance of the solutions presented in Section 3 under three distinct factors: user mobility, dynamic device rotation and increasingly challenging propagation conditions. Table D.1 summarizes the simulation parameters used. This study evaluates 2 UE speeds, 2 UE rotation speeds and 3 different propagation environments, resulting in 12 distinct training datasets of 5000 samples for the ML-measurement based solution. Each sample includes the RSRP measurements for all the beam pair combinations in the $4 \times N_R = 12$ SSBursts that constitute the measurement period and the RSS measurements for all those beam pairs at the evaluation period, in the 13th SSBurst window. A neural network architecture is considered, which consists of 5 layers including an input layer with 12 neurons, 3 hidden layers with respectively 120, 120, and 60 neurons, followed by an output layer with 12 neurons. A drop-out rate of 0.3 is used for all the hidden layers. In the training process, an Adam optimizer is used [22] with the learning rate 0.001 and 15 epochs of training with progressively growing minibatch sizes from 4 to 32 samples [23]. The training and test data split is set as 80% and 20%, respectively. The aforementioned parameters have been experimentally tuned according to the dataset sizes and the NN's structure.

4.1 Performance criteria

This work characterizes the beam selection process as consisting of two stages: the measurement period and the evaluation period. The measurement period refers to the SSBurst transmission and measurement stage,

Table D.1: Simulation parameters.

Parameter	Notation	Value
Carrier frequency	f_c	28 GHz
Carrier bandwidth	B	104 MHz
Subcarrier spacing	Δf	120 kHz
RX noise figure	NF	9 dB
Thermal noise density	N_0	-174 dBm Hz^{-1}
Beam sweeping configuration		
SSBurst size	N_T	12
SSBurst periodicity	T_{ss}	20 ms
UE beams per panel	N_R	3
Layout configuration		
Inner mobility bound	r	15 m
Outer mobility bound	R	100 m
Channel model	-	Freespace, UMi LOS, UMi NLOS
gNodeB position	(x, y)	(0,0)
gNodeB height	h_t	10 m
gNodeB codebook elevation	θ_{ψ_t}	103°
gNodeB array size	N_t	8×8
UE initial position	(x, y)	uniformly distributed
UE height	h_r	1.5 m
UE panels	I	4
UE panel size	N_r	1×4
UE speed	v	$3 \text{ km h}^{-1}, 60 \text{ km h}^{-1}$
Number of UE trajectories	-	5000 per dataset
Random walk orientation configuration		
Standard deviation	σ	$1^\circ, 10^\circ$
Filter length	M	21

while the evaluation period pertains to a small time frame following the measurement period where all RSRP values have been collected and beam determination occurs. During the evaluation period, RSS measurements are computed over a set of frequency-time resources, \mathcal{V}_{eval} , for every beam pair combination, (ψ_t, ψ_r^i) , as

$$R(\psi_t, \psi_r^i) = \frac{1}{|\mathcal{V}_{eval}|} \sum_{(s,k) \in \mathcal{V}_{eval}} |w_{\psi_r^i}^i \mathbf{H}^i(s, k)^\top \mathbf{f}_{\psi_t}|^2, \quad (\text{D.18})$$

where $|\mathcal{V}_{eval}|$ denotes the cardinality of \mathcal{V}_{eval} . The RSS value of the selected beam pair is then given by

$$R_{meas} = R(\psi_t^*, \psi_r^{i*}), \quad (\text{D.19})$$

where ψ_t^* and ψ_r^{i*} are determined either through max-measurement beam selection or ML-measurement based selection. To measure beam selection accuracy, a genie-aided solution is considered where optimal beam alignment is always guaranteed. In this case the maximum achievable RSS over all beam pair combinations is described as

$$R_{genie} = \max_{\psi_t, \psi_r^i} R(\psi_t, \psi_r^i). \quad (D.20)$$

The beam selection process occurs successfully when the beam pair selected matches the genie solution. Otherwise, a misdetection takes place. Depending on the degree of misalignment between the selected beam pair and the ideal beam pair, link power loss can be experienced. In such cases, R_{loss} expresses the beam misdetection loss given by

$$R_{loss} = \frac{R_{genie}}{R_{meas}}. \quad (D.21)$$

Therefore, two main performance criteria are considered:

- **Beam selection accuracy (BS_{acc}):** percentage of occasions where the beam pair selection matches the genie-aided selection.
- **Average misdetection loss (\bar{R}_{loss}):** average value of R_{loss} across all samples in dB.

4.2 Beam selection schemes

To properly assess the impact of the proposed solution, distinct gNodeB and UE beam selection schemes are established with an increasing level of realism, summarized in Table D.2:

- **Genie aided beam pair (G-gNB/G-UE):** The best beam pair is chosen based on the highest RSS measured at the evaluation period. This is an ideal, misalignment-free scenario that establishes the upper bound for beam management performance.
- **Genie-aided gnodeB beam and baseline UE beam (G-gNB/B-UE):** This scenario maintains an ideal gNodeB beam selection while the UE beam selection is achieved through the baseline method detailed in 3.1.
- **Genie-aided gNodeB beam and ML-based UE beam (G-gNB/ML-UE):** Similarly, this scenario considers ideal gNodeB beam selection but employs the UE beam selection method from Section 3.2 instead.
- **Baseline beam pair (B-gNB/B-UE):** A more realistic approach is taken based on the current 3GPP procedure where the best beam pair is chosen through the highest RSRP value. This method is taken as the baseline that the proposed solution should outperform.

Table D.2: Beam selection schemes.

Schemes	gNodeB beam	UE beam
G-gNB/G-UE	max RSS	
G-gNB/B-UE	max RSS	max RSRP
G-gNB/ML-UE	max RSS	ML-RSRP
B-gNB/B-UE	max RSRP	
B-gNB/ML-UE	max RSRP	ML-RSRP

- **Baseline gnodeB beam and ML-based UE beam (B-gNB/ML-UE):** This scenario describes the proposed beam management solution presented in this work. The gNodeB beam is selected through the highest RSRP measurement and the UE beam selection follows the ML procedure from Section 3.2.

4.3 Beam management performance - Freespace

Beam management performance is first assessed in Freespace, a simplified propagation scenario portraying free space loss with only one LOS path and no shadow fading. This allows for the evaluation of the proposed solution's potential in a favourable propagation environment, unencumbered by additional effects introduced by complex channel models with several multipath components. The beam selection schemes detailed in Section 4.2 are evaluated for both a low speed, 3 km h^{-1} , and a moderate user speed, 60 km h^{-1} . Additionally two σ values are taken to characterize the rotation of the device, $\sigma = 1^\circ$ and $\sigma = 10^\circ$, which translate into a rotation speed per axis of $6.0422^\circ \text{ s}^{-1}$ in Table D.3 and $60.4218^\circ \text{ s}^{-1}$ in Table D.4, respectively.

BS_{acc} results in Table D.3 show that misalignments can occur fairly frequently for both the proposed solution, B-gNB/ML-UE, and the baseline, B-gNB/B-UE, but lead to almost negligible losses in this slow UE rotation scenario. Furthermore, it is evident that the B-gNB/ML-UE scheme performs marginally worse than the B-gNB/B-UE scheme by less than 0.1 dB, indicating that the proposed solution has no impact on this scenario's beam management performance. For a low UE speed and slow UE rotation, the B-gNB/B-UE scheme performs quite well since the time it takes to collect all the RSRP measurements is short enough to keep up with the UE's mobility and rotation rates. However the beam selection accuracy of the B-gNB/B-UE scheme drops 14.4% when UE speed increases. This performance drop at high speeds is due to misselections of the gNodeB beam: while the G-gNB/B-UE scheme causes a 7% accuracy degradation when compared to the ideal scheme G-gNB/G-UE, the transition to the B-gNB/B-UE scheme results in an additional, more significant, accuracy reduction of 13.8%. Considering

Table D.3: Beam management performance for Freespace, $\sigma = 1^\circ$.

Schemes	BS_{acc} (%)		\bar{R}_{loss} (dB)	
	3 km h^{-1}	60 km h^{-1}	3 km h^{-1}	60 km h^{-1}
G-gNB/G-UE	100	100	0	0
G-gNB/B-UE	94.5	93.0	0.07	0.09
G-gNB/ML-UE	89.3	90.3	0.11	0.12
B-gNB/B-UE	93.6	79.2	0.07	0.28
B-gNB/ML-UE	88.4	76.3	0.12	0.31

Table D.4: Beam management performance for Freespace, $\sigma = 10^\circ$.

Scheme	BS_{acc} (%)		\bar{R}_{loss} (dB)	
	3 km h^{-1}	60 km h^{-1}	3 km h^{-1}	60 km h^{-1}
G-gNB/G-UE	100	100	0	0
G-gNB/B-UE	62.8	61.9	3.75	3.76
G-gNB/ML-UE	75.2	76.0	1.24	1.26
B-gNB/B-UE	62.4	53.4	3.75	3.99
B-gNB/ML-UE	74.9	65.5	1.24	1.41

the source of misalignment in this scenario takes place at the gNodeB side, where ψ_t^* selection is based on a max-RSRP method vulnerable to errors in mobility scenarios, it is unsurprising that the B-gNB/ML-UE scheme fails to offer any benefits, since it employs RSRP measurements from a misselected sub-optimal gNodeB beam.

In Table D.4, where UE rotation is more accentuated ($\sigma = 10^\circ$), it is noticeable that the loss levels experienced are much larger. At $v = 3 \text{ km h}^{-1}$, this additional dynamic factor in the environment warrants an accuracy drop of 37.2% and a loss of 3.75 dB when comparing G-gNB/G-UE to G-gNB/B-UE. This means that significant UE rotation is occurring before it can finish collecting all RSRP measurements, which leads the G-gNB/B-UE scheme to base its beam selection on outdated beam information, resulting in beam misalignment and link performance degradation. The baseline B-gNB/B-UE scheme displays its worst performance at $v = 60 \text{ km h}^{-1}$, since this scenario harbours both the effects of mobility and rotation of the device. This showcases perfectly the impact that lack of device orientation tracking can have on beam management performance.

The B-gNB/ML-UE scheme is shown to successfully improve accuracy and reduce misalignment losses by up to 2.5 dB in this particular scenario. This suggests that, for dynamic terminal orientation scenarios, the NN is able to analyze how the RSRP levels progress over time and infer the UE's orientation changes, allowing it to select the beam that maximizes link performance.

This is something the B-gNB/B-UE scheme cannot achieve, since it chooses the beam with the highest power at the time of measurement, which for UEs with rapidly changing orientation may no longer be the optimal beam at the beam selection stage.

4.4 Beam management performance - realistic propagation scenarios

The Freespace study shows that the B-gNB/ML-UE scheme can improve the current procedure through RSRP measurements alone. However, it remains to be investigated if this approach is still feasible under realistic multipath rich environments. This section focuses on high mobility and high device rotation, since this has been established as the most challenging scenario for the baseline method. The beam management performance of the B-gNB/B-UE and B-gNB/ML-UE schemes are compared in Fig. D.4 under two additional 3GPP-compliant channel environments: UMi LOS and UMi NLOS. These are typically used to portray densely populated urban micro-cell areas with gNodeB deployment below rooftop level [21].

It is clear that the trends observed in Freespace are preserved in the UMi LOS scenario, where the gains of the proposed ML-based method over the baseline are only ever-so-slightly reduced. Results further suggest that the proposed solution's performance is significantly reduced in NLOS, despite still performing marginally better than the current baseline solution. As the environment transitions to a predominantly NLOS environment, propagation conditions progressively worsen: the received signal strength drops considerably and RSRP measurements start to blend together, due to the channel power being more spread in the angular domain. This makes it more challenging for the NN to infer the UE's orientation at the evaluation period, since all measurements have similar low power levels.

In summary, the B-gNB/ML-UE scheme can be leveraged to handle dynamic mobility and rotation scenarios, ultimately improving the robustness of the current beam management procedure, but only in environments with a dominant LOS component.

5 Conclusions

This work focuses on improving multi-panel UE beam selection robustness to mobility and time-varying terminal orientation without relying on context information. The feasibility of an ML solution based solely on RSRP measurements is investigated as an attempt to introduce a simpler alternative to UE beam selection with more manageable training dataset sizes than other context information aided methods in the literature.

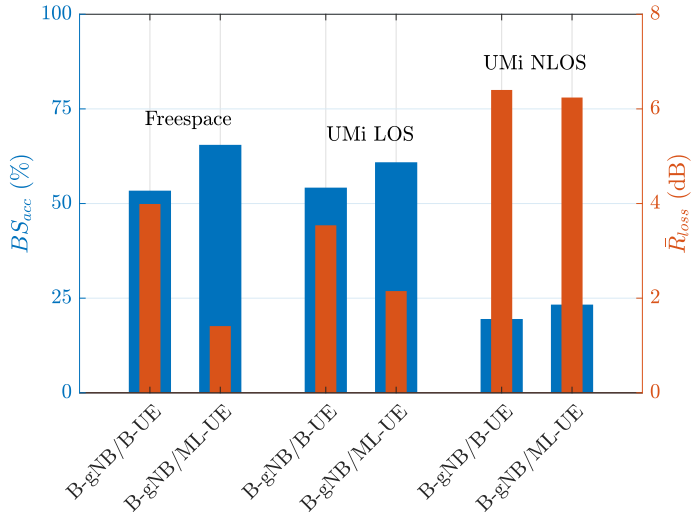


Fig. D.4: Beam management performance comparison of B-gNB/B-UE vs. B-gNB/ML-UE for Freespace, UMi LOS and UMi NLOS at $v = 60 \text{ km h}^{-1}$ and $\sigma = 10^\circ$.

Results indicate that the proposed ML-based scheme does not improve beam management performance for high-speed, slow rotating UEs. Instead, fast UE rotation scenarios respond positively to the proposed solution, showing that, in dominant LOS, outdated RSRP measurements can in fact be explored to successfully infer the UE's rotation pattern to predict its best beam and significantly reduce misdetection losses.

However, this approach's effectiveness suffers in predominantly NLOS environments. The drastically lowered received signal strength levels in these environments, along with the increased angular spread of the channel, cause all RSRP measurements to deteriorate to a point where the ML model struggles to extract the UE's rotation pattern, reducing its accuracy margin over the baseline 3GPP-based solution. This seems to indicate that in realistic scenarios with mixed LOS and NLOS conditions, the ML-solution could only be beneficial if LOS probability is high, potentially requiring more sophisticated solutions to mitigate the misdetections that would occur when transitioning to NLOS. An interesting iteration on this study, left for further investigation, is to determine whether a single model trained in mixed LOS/NLOS conditions could also offer robust beam management, maintaining good performance in LOS channels while not performing worse than the baseline method in NLOS conditions.

References

- [1] M. Enescu, editor. *5G New Radio: A Beam-based Air Interface*. John Wiley & Sons, 1st edition, 2020.
- [2] 3GPP. Study on new radio access technology Physical layer aspects (Release 14). Tech. Rep. 38.802, V14.2.0 2017.
- [3] U. B. Elmali, A. Awada, U. Karabulut, and I. Viering. "Analysis and Performance of Beam Management in 5G Networks". *2019 IEEE 30th Annual International Symposium on Personal, Indoor and Mobile Radio Communications (PIMRC)*, pages 1 – 7, 2019.
- [4] I. Ayakin and M. Krunz. "Efficient Beam Sweeping Algorithms and Initial Access Protocols for Millimeter-Wave Networks". *IEEE Transactions on Wireless Communications*, 19(4):2504 – 2514, 2020.
- [5] S. Tomasin, C. Mazzucco, D. De Donno, and F. Cappellaro. "Beam-Sweeping Design Based on Nearest Users Position and Beam in 5G mmWave Networks". *IEEE Access*, 8:124402 – 124413, 2020.
- [6] H. Soleimani, R. Parada, S. Tomasin, and M. Zorzi. "Fast Initial Access for mmWave 5G Systems with Hybrid Beamforming Using On-line Statistics Learning". *IEEE Communications Magazine*, 57(9):132 – 137, 2019.
- [7] "Study on Artificial Intelligence (AI)/Machine Learning (ML) for NR Air Interface". - RP-213599, 3GPP TSG RAN Meeting #94e, May 2022.
- [8] F. Abinader, C. Rom, K. Pedersen, S. Hailu, and N. Kolehmainen. "System-Level Analysis of mmWave 5G Systems with Different Multi-Panel Antenna Device". *2021 IEEE 93rd Vehicular Technology Conference (VTC2021-Spring)*, pages 1 – 6, 2021.
- [9] S. B. Iqbal, A. Awada, U. Karabulut, I. Viering, P. Schulz, and G. P. Fettweis. "Analysis and Performance Evaluation of Mobility for Multi-Panel User Equipment in 5G Networks". *2022 IEEE 95th Vehicular Technology Conference: (VTC2022-Spring)*, pages 1–7, 2022.
- [10] S. Rezaie, J. Morais, E. de Carvalho, A. Alkhateeb, and C. Navarro Manchón. "Location- and Orientation-aware Millimeter Wave Beam Selection for Multi-Panel Antenna Devices". *arXiv:2203.11714v1*, pages 1–5, 2022.
- [11] Y. Heng, J. G. Andrews, J. Mo, V. Va, A. Ali, B. L. Ng, and J. C. Zhang. "Six Key Challenges for Beam Management in 5.5G and 6G Systems". *IEEE Communications Magazine*, 59(7):74 – 79, 2021.

- [12] K. N. Nguyen, A. Ali, J. Mo, B. L. Ng, V. Va, and J. C. Zhang. "Beam Management with Orientation and RSRP using Deep Learning for Beyond 5G Systems". *2022 IEEE International Conference on Communications Workshops (ICC Workshops)*, pages 133 – 138, 2022.
- [13] A. Ali, J. Mo, B. L. Ng, V. Va, and J. C. Zhang. "Orientation-Assisted Beam Management for Beyond 5G Systems". *IEEE Access*, 9:51832 – 51846, 2021.
- [14] V. Raghavan, M.-L. Chi, M. A. Tassoudji, O. H. Koymen, and J. Li. "Antenna Placement and Performance Tradeoffs With Hand Blockage in Millimeter Wave Systems". *IEEE Transactions on Communications*, 67(4):3082 – 3096, 2019.
- [15] S. Jaeckel, L. Raschkowski, K. Börner, and L. Thiele. "QuaDRiGa: A 3-D Multicell Channel Model with Time Evolution for Enabling Virtual Field Trials". *IEEE Transactions on Antennas Propagation*, 62(6):3242 – 3256, 2014.
- [16] 3GPP. NR; Physical channels and modulation (Release 17). Tech. Spec. 38.211, V17.2.0 2022.
- [17] 3GPP. "NR; Physical layer procedures for control (Release 17)". Tech. Spec. 38.213, V17.3.0 2022.
- [18] MathWorks. 5G Toolbox.
- [19] 3GPP. NR; Physical layer measurements (Release 17). Tech. Spec. 38.215, V17.2.0 2022.
- [20] "Feature lead summary #3 of Enhancements on Multi-beam Operations". - R1-1907860, 3GPP TSG RAN WG1 Meeting #97, May 2019.
- [21] 3GPP. Study on channel model for frequencies from 0.5 to 100 GHz (Release 17). Tech. Rep. 38.901, V17.0.0 2022.
- [22] Diederik P. Kingma and Jimmy Ba. Adam: A Method for Stochastic Optimization. In *Proc. Int. Conf. Learn. Representations*, 2015.
- [23] S. Rezaie, C. Navarro Manchón, and E. De Carvalho. "Location- and Orientation-Aided Millimeter Wave Beam Selection Using Deep Learning". *ICC 2020 - 2020 IEEE International Conference on Communications (ICC)*, pages 1 – 6, 2020.

ISSN (online): 2446-1628
ISBN (online): 978-87-7573-749-9

AALBORG UNIVERSITY PRESS